[American Journal of Science, Vol. 317, December, 2017, P. 1049–1094, DOI 10.2475/10.2017.01]

American Journal of Science

DECEMBER 2017

DETRITAL ZIRCON U-Pb GEOCHRONOLOGY OF THE MAGOG GROUP, SOUTHERN QUEBEC – STRATIGRAPHIC AND TECTONIC IMPLICATIONS FOR THE QUEBEC APPALACHIANS

MORGANN PERROT*,†, ALAIN TREMBLAY*, and JEAN DAVID**

ABSTRACT. In the Quebec Appalachians, the Laurentian continental margin (Humber Zone) and adjacent oceanic domain (Dunnage Zone) were amalgamated during the Ordovician Taconian orogeny. The Dunnage Zone includes ophiolites and overlying synorogenic deposits of both the Saint-Daniel Mélange and Magog Group. The latter consists of a ~3 km-thick pile of sandstone, felsic volcaniclastic rocks and graphitic slate at the base (Frontière, Etchemin and Beauceville formations) overlain by a ~7 km-thick turbiditic flysch sequence, constituting the Saint-Victor Formation. The maximum upper age limit of the Magog Group was considered to be Darriwilian based on graptolite fauna. This was proven consistent with a $462^{+5}/_{-4}$ Ma (U-Pb ID-TIMS) from a felsic tuff of the Beauceville Formation, but contradicts a detrital zircon U-Pb age of 424 ± 6 Ma recently measured in the Saint-Victor Formation. A new detrital zircon U-Pb geochronology study (HR-LA-ICP-MS and ID-TIMS), focused on the Saint-Victor Formation, yields young detrital populations that suggest that the Saint-Victor Formation is not exclusively Ordovician and extends into the Silurian, as indicated by a maximum age of sedimentation around 430 Ma. Detrital zircon U-Pb geochronology associated with fossil age constraints and stratigraphic correlations in adjacent areas attest that the Saint-Victor Formation should be considered as an upper Magog Group sequence that is separated from lower units (the Frontière-Etchemin-Beauceville formations) by an unconformity corresponding to a sedimentary hiatus of ≤ 10 m.y. Regional tectonic considerations imply that the Magog Group evolved from a syn-Taconian forearc basin in Middle-Late Ordovician time to a syn-Salinic peri-continental basin in early Silurian time. Several NW and SE erosional sources are invoked for the sedimentation of the Magog Group, evolving from the erosion of both the southern Quebec ophiolites and adjacent sedimentary rocks of the Laurentia margin to the NW, and volcanic arc rocks of the Ascot Complex, Shelbourne Falls and Bronson Hill massifs to the SE. Potential sources for *ca.* 430 Ma zircons found towards the top of the Saint-Victor sequence are the Silurian Frontenac Formation and the East Inlet granitic pluton, both located in the vicinity of the Quebec-Maine border.

Key words: Taconian orogeny, Appalachians, Salinic orogeny, sedimentary basin, Dunnage Zone, Gaspé Belt, detrital zircon-U-Pb geochronology.

INTRODUCTION

Synorogenic sedimentary basins serve as repositories of detritus delivered from actively deforming and eroding orogens and, as such, they record a significant part of the geodynamic evolution of mountain belts. The relationships between sediment sources and these subsiding basins may thus provide critical information regarding

* Université du Québec à Montréal-Geotop, Département des sciences de la Terre et de l'atmosphère, Case postale 8888, Succursale Centre-ville, Montréal, Québec, H3C 3P8, Canada

** Bureau d'Exploration Géologique du Québec-Geotop, Ministère de l'Énergie et des Ressources Naturelles, Université du Québec à Montréal, 201 av Président-Kennedy, Montréal, Québec, H3C 3P8, Canada

† Corresponding author: perrot.morgann@uqam.ca

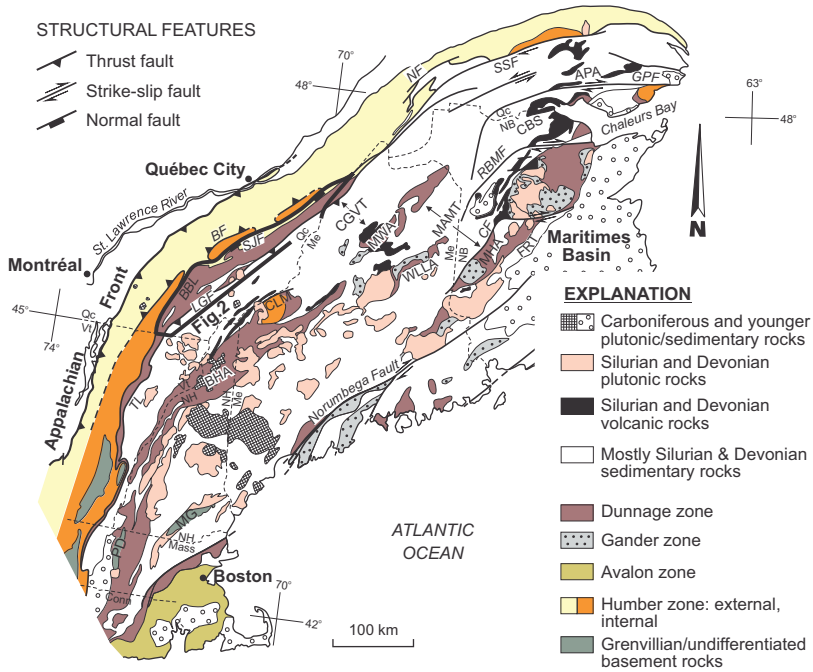

Fig. 1. Simplified lithotectonic map of the Northern Appalachians of mainland Canada and New England (modified from Tremblay and Pinet, 2005; Hibbard and others, 2006). APA – Aroostook–Percé anticlinorium; BBL – Baie Verte-Brompton line; BF – Bennett Fault; BHA – Bronson Hill Anticline; CBS – Chaleurs Bay synclinorium; *CF* – Catamaran fault; CGVT – Connecticut Valley–Gaspé trough; CLM – Chain Lake Massif; FRT – Fredericton trough; GPF – Grand Pabos fault; LGF – La Guadeloupe fault; MAMT – Merrimack, Aroostook–Matapédia trough; MG – Massabesic Gneiss; MHA – Miramichi Highlands Anticline; MWA – Munsungun-Winterville Anticline; NF – Neigette fault; PD – Pelham Dome; RBMF – Rocky Brook–Millstream fault; SJF – Saint-Joseph fault; SSF – Shickshock-Sud fault; TL – Taconic Line; WLLA – Weeksboro–Lunksoos Lake Anticline. State boundaries: Conn – Connecticut; Mass – Massachussets; Me – Maine; NB – New Brunswick; NH – New Hamshire; Qc – Québec; Vt – Vermont.

lithospheric deformation during orogenesis depending on the availability of erosional sources. In the Appalachians of mainland Canada and adjacent New England (fig. 1), the Ordovician Taconian orogeny is attributed to the closure of the Iapetus Ocean due to convergence between Laurentian and Gondwanan tectonic plates (Stanley and Ratcliffe, 1985; van Staal and Barr, 2012; Tremblay and Pinet, 2016). The Taconian orogeny was followed by a Silurian compressive tectonic event known as the Salinic orogeny (for example, van Staal and others, 1998, 2014), which culminated into a period of extensional faulting in the Quebec Appalachians (Tremblay and Castonguay, 2002; Tremblay and Pinet, 2005). In southern Quebec and New England, the time period between the Taconian and Salinic orogenies, represented by a transition from the formation of an onlapping forearc basin during the Ordovician to the development of post-orogenic successor basin(s) in the late Silurian to Early Devonian (for example, Tremblay and Pinet, 2005), is not well constrained in terms of geochronological data.

The Magog Group provides an outstanding opportunity to study the formation and evolution of one of these sedimentary basins. This 10 km-thick flysch-dominated sequence has been interpreted as the vestiges of a forearc basin recording the erosion of Taconian nappes (Cousineau and St-Julien, 1994; de Souza and others, 2014), and historically considered as a typical Middle to Late Ordovician synorogenic sequence

(Cousineau, 1990; Tremblay, 1992a; Cousineau and St-Julien, 1994; Tremblay and others, 1995). Based on graptolite fauna occurrences (St-Julien, 1970; Riva, 1974; St-Julien, 1987), the maximum age limit of the Magog Group is currently considered to be Middle-Late Ordovician, which has been proven to be consistent with a zircon U-Pb age of $462^{+5}/_{-4}$ Ma from a felsic tuff (Marquis and others, 2001). However, a detrital zircon U-Pb age of 424 ± 6 Ma (de Souza and others, 2014), recently measured in the uppermost unit of the Magog Group, suggests that it is possibly younger and extends into the Silurian.

This contribution focuses on the stratigraphy and geochronology of the Magog Group in order to better constrain its age of deposition, to investigate the nature of its sedimentary sources, and its tectonic setting. A detrital zircon U-Pb geochronology study of the Magog Group has been performed in the southern Quebec Appalachians.

There is currently a debate regarding the determination of maximum ages of sedimentation with the U/Pb dating of detrital zircons by HR-LA-ICP-MS analyses. There is agreement on the fact that the age of a single zircon grain cannot be used to define the age of a given sample and that deposition of sedimentary rocks is better defined by the mean age of a detrital grains population, but the question that is usually debated is: how many zircon grains are needed to confidently define a grain population? The ID-TIMS dating method can be useful in order to gain a higher precision on the age of detrital zircons. In this study, ID-TIMS dating has been therefore used as a complementary tool to HR-LA-ICP-MS analyses, in order to better investigate the age of youngest zircon grains. As far as we know, our detrital zircon geochronological study is the first peer-reviewed paper that combines HR-LA-ICP-MS and ID-TIMS analyses on the same grains.

In this paper, we use the International Stratigraphic Chart as proposed by the International Commission on Stratigraphy (Cohen and others, 2013) for the Ordovician and Silurian periods and related stages.

GEOLOGICAL SETTING

In the Quebec Appalachians (fig. 1), three major lithotectonic assemblages are recognized, the Cambrian and Ordovician Humber and Dunnage Zones (Williams, 1979) and the overlying Late Ordovician to Middle Devonian Gaspé Belt (Bourque and others, 2000; Tremblay and Pinet, 2016). The Humber and Dunnage Zones were amalgamated during the Ordovician Taconian orogeny and correspond, respectively, to the remnants of the Laurentian continental margin and its peripheral Iapetan oceanic domain. Most rocks of the Gaspé Belt crop out in the Connecticut Valley-Gaspé trough (figs. 1 and 2; Bourque and others, 2000; Tremblay and Pinet, 2005) but some of them (that is the Saint-Luc, Cranbourne, Lac Aylmer and Lac Lambton formations and the Glenbrooke Group) unconformably overly the Magog Group (fig. 2).

In southern Quebec (figs. 1 and 2), the Humber Zone is subdivided into a lower greenschist to sub-greenschist grade external subzone and an upper greenschist to amphibolite facies internal subzone (Tremblay and Pinet, 2016). To the southeast, the contact of the internal Humber Zone with the Dunnage Zone is marked by the Baie Verte-Brompton line (BBL), which is interpreted as a continent-ocean interface in the Canadian Appalachians (Williams and St-Julien, 1982). In southern Quebec, the BBL is crosscut by a major normal fault known as the St-Joseph Fault (Pinet and others, 1996; Perrot, ms, 2014; Tremblay and Pinet, 2016). The Dunnage Zone occupies the Saint-Victor synclinorium (fig. 2). From base to top, the stratigraphy of the Dunnage Zone includes (1) a series of well-preserved to dismembered ophiolite massifs, (2) the Ascot Complex which represents the remnants of a peri-Laurentian volcanic arc, (3) the Saint-Daniel Mélange which overlies both the ophiolites and the Ascot Complex, and (4) the sedimentary sequence of the Magog Group. The eastern limit of the

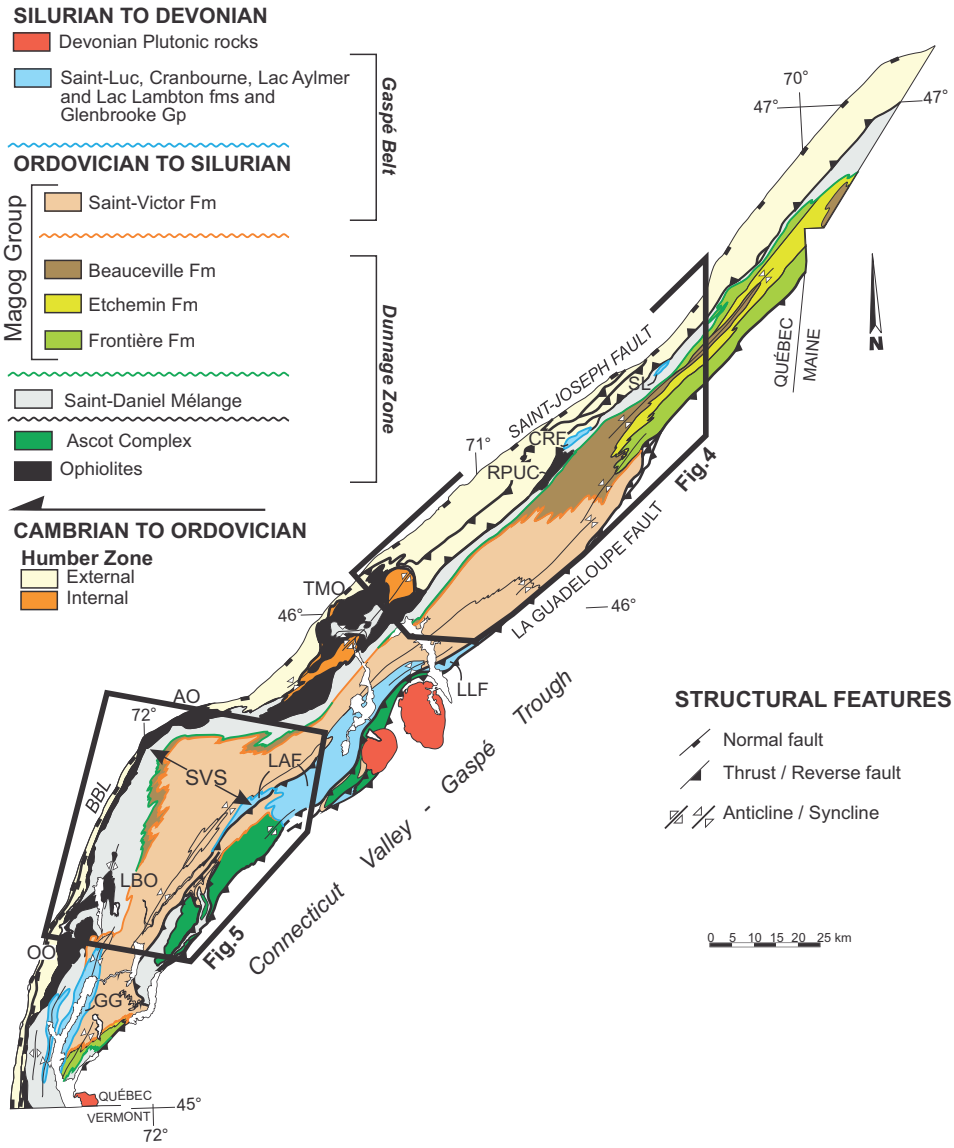

Fig. 2. Geological map of the Dunnage zone of the southern Quebec Appalachians (after Tremblay and others, 2015). AO – Asbestos ophiolite; BBL – Baie Verte-Brompton line; CRF – Cranbourne Formation; GG – Glenbrooke Group; LAF – Lac Aylmer Formation; LBO – Lac-Brompton ophiolite; LLF – Lac Lambton Formation; OO – Mont-Orford ophiolite; RPUC – Rivière-des-Plante ultramafic Complex; SL – Saint-Luc Formation; TMO – Thetford-Mines ophiolite; SVS – Saint-Victor synclinorium. See figure 1 for location.

Dunnage Zone is marked locally by an unconformity but more frequently by the La Guadeloupe fault, a major SE-dipping thrust fault related to the Acadian Orogeny (Tremblay and others, 2000).

The ophiolites comprise the Mont-Orford, Lac-Brompton, Asbestos and Thetford-Mines massifs and the Rivière-des-Plante ultramafic Complex (fig. 2). Plagiogranite bodies of the upper crustal sequence of the Mont-Orford and Thetford-Mines ophio-

lites yielded U-Pb zircon ages of 504 ± 3 Ma and 478 ± 2 to 480 ± 2 Ma, respectively (David and others, 1993; Whitehead and others, 2000). The obduction of these ophiolites onto the Laurentian margin has been constrained by U-Pb zircon ages of syn-obduction anatectic granitoids of the Thetford-Mines ophiolite at 470 ± 3 and 469 ± 4 Ma (Whitehead and others, 2000). These ages are consistent with $^{40}Ar/^{39}Ar$ cooling ages of the infraophiolitic dynamothermal sole and stratigraphic relationships with the overlying Saint-Daniel Mélange, which indicate that ophiolite emplacement occurred, from *ca.* 480 Ma to *ca.* 460 Ma (Schroetter and others, 2006; Tremblay and others, 2011).

The Ascot Complex is a bimodal mafic-felsic volcanic sequence and syn-volcanic granitic intrusion (fig. 2). The volcanic rocks are overlain by, and in fault contact with black and rusty phyllites that have been correlated with those of the Saint-Daniel Mélange (Gauthier and others, 1989; Tremblay and St-Julien, 1990). Felsic volcanic rocks yielded zircon U-Pb ages of 460 ± 3 Ma and $441^{+7}/_{-12}$ Ma (David and Marquis, 1994), whereas the syn-volcanic granitic intrusion yielded a high-temperature ^{40}Ar-^{39}Ar muscovite age of 462 ± 2 Ma (Tremblay and others, 2000).

The Saint-Daniel Mélange (fig. 2) represents the lower part of a syncollisional piggyback sedimentary basin. It consists mainly of basal conglomerates and debris flows that grade up-section into a succession of lithic sandstone and black to greenish shale, and a typical pebbly mudstone unit. Mafic and felsic volcanic rocks, such as the Bolton Igneous Group and the Ware Volcanics (see de Souza and others, 2014), are locally interlayered with the sedimentary rocks. The Ware Volcanics have been recently re-analyzed (sample 08M44 of de Souza and others, 2014) and yielded an age of 468.2 ± 7.7 Ma (J. David, 2016, unpublished data), which is consistent with $^{40}Ar/^{39}Ar$ muscovite ages of mica schist fragments from basal conglomerates of the Saint-Daniel Mélange (467 and 463 Ma, Schroetter and others, 2006; Tremblay and others, 2011).

The Magog Group (fig. 2) occupies the core of the Saint-Victor synclinorium and unconformably overlies the Saint-Daniel Mélange to the NW (Cousineau and St-Julien, 1994; Schroetter and others, 2006) and the Ascot Complex to the SE. It consists of an approximately 3 km-thick section of feldspar-rich sandstone, felsic volcaniclastic rocks and graphitic slate at the base (that is, the Frontière, Etchemin and Beauceville formations of Cousineau, 1990) overlain by a *ca.* 7 km-thick turbiditic flysch sequence of the Saint-Victor Formation (fig. 3, St-Julien, 1987; Tremblay, 1992a; Cousineau and St-Julien, 1994). The Frontière Formation (fig. 4) is made up of mud-slate and greenish-gray volcaniclastic sandstone (Cousineau and St-Julien, 1994). It has been estimated to be approximately 1 km-thick (fig. 3, Cousineau, 1990; Cousineau and St-Julien, 1994). The Etchemin Formation (figs. 3 and 4) is a 1 km-thick succession of purple-greenish mudstone grading into siliceous, quartz-feldspar mudstone and greenish volcaniclastic rocks. It is overlain by a 1 km-thick unit of graphitic and pyritic slates, volcaniclastic sandstones and black mudstones/slates that constitute the Beauceville Formation (figs. 3 and 4). The depositional age of the Frontière and Etchemin formations is unknown. In the vicinity of the Quebec-Vermont international border (fig. 2), the Bunker Hill Sequence has been tentatively correlated with the Frontière-Etchemin formations (Tremblay and others, 2015). Its upper felsic volcaniclastic member yielded a U-Pb zircon age of 455 ± 6 Ma (de Souza and others, 2014). The age of the Beauceville Formation is constrained by the occurrence of *Nemograptus gracil* and *Diplograptus multidens* graptolites fauna (St-Julien, 1970, 1987; Riva, 1974), which correspond to Darriwilian to Sandbian ages (460–449 Ma; Cousineau and St-Julien, 1994). Moreover, a felsic tuff of the Beauceville Formation in the Beauce area yielded a U-Pb zircon crystallization age of $462^{+5}/_{-4}$ Ma (Marquis and others, 2001).

The uppermost stratigraphic unit of the Magog Group, the Saint-Victor Formation, consists of dark-gray, fine- to medium-grained sandstone with minor

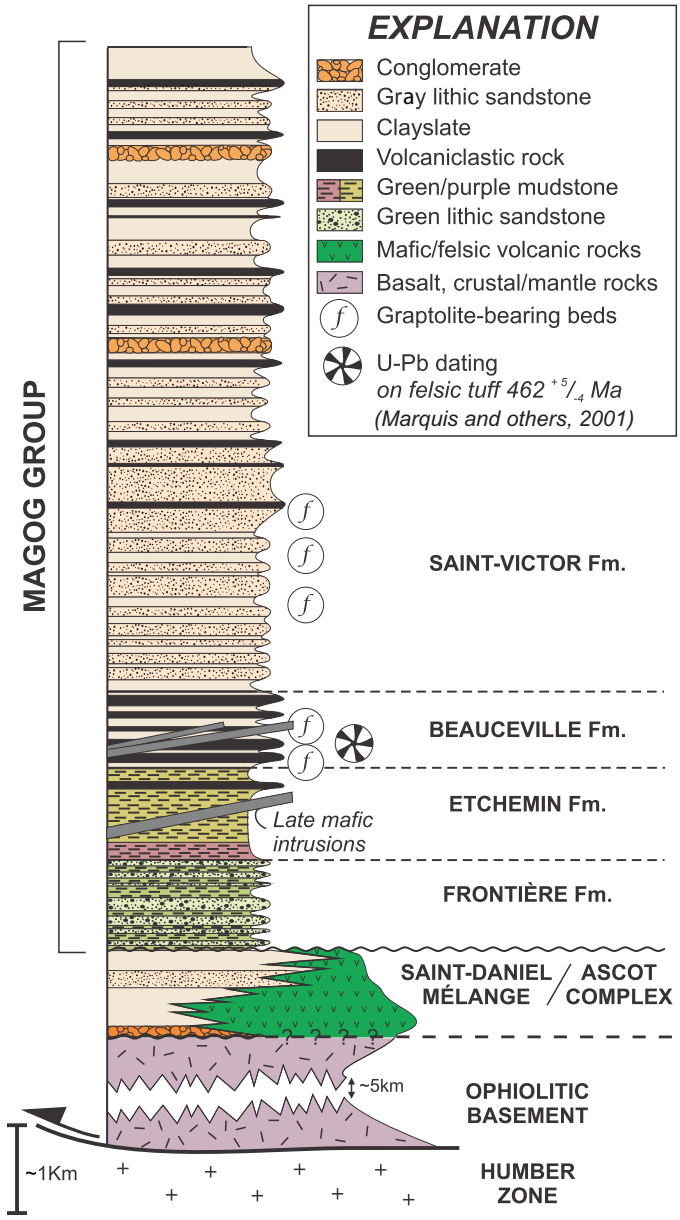

Fig. 3. Stratigraphic column for the Magog Group in the Beauce area according to Cousineau and St-Julien (1994). Fm – Formation.

conglomerate interlayered with mudstone and slate similar to those of the underlying Beauceville Formation. The interlayered sandstone-mudstone sequence forms typical turbidites (Cousineau and St-Julien, 1994). In the Sherbrooke area (fig. 5), this unit is the main target for detrital U-Pb dating results presented in this study, and its geological characteristics and age constraints will be presented in detail below.

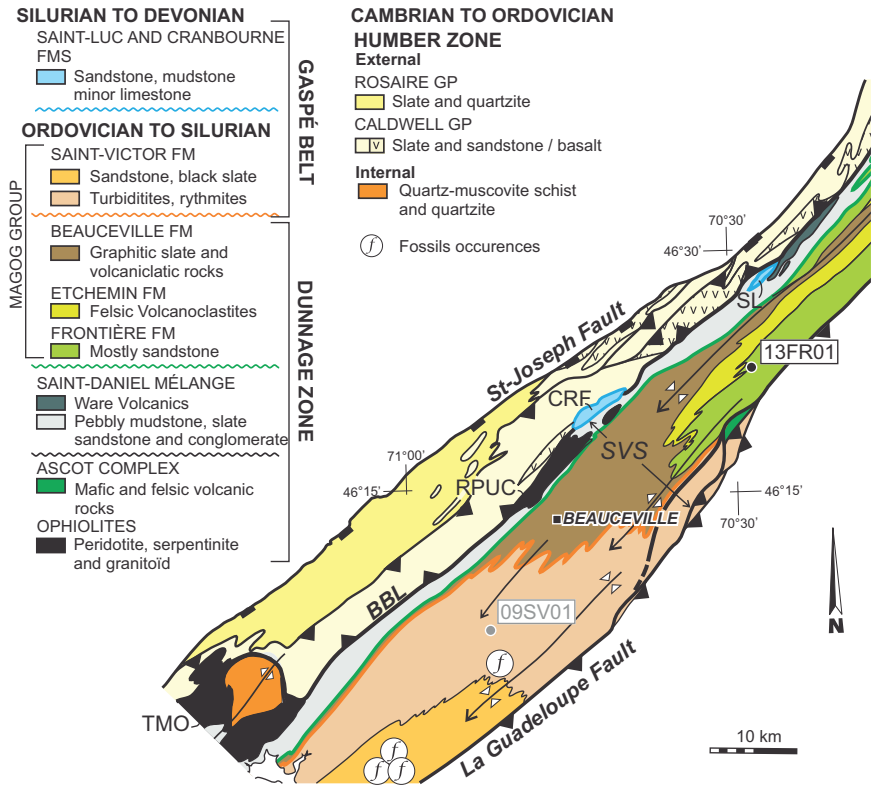

Fig. 4. Geological map of the Beauce area (modified from de Souza and others, 2014). Framed black numbers indicate sample locations, framed gray number indicate sample locations of de Souza and others (2014). See figure 2 for location and the signification of structural features.

Metamorphic and Structural Characteristics of the Dunnage Zone

In the southern Quebec Dunnage Zone, regional deformation and metamorphism are related to the Middle Devonian Acadian orogeny (Tremblay, 1992a; Cousineau and Tremblay, 1993), and correspond to D_4 structures as described by Tremblay and Pinet (2016). Older Taconian and/or Salinic fabrics and structures (that is the D1-2 and D3 events of Tremblay and Pinet, 2016) are, however, locally preserved in the ophiolites, the overlying Saint-Daniel Mélange and, possibly, in the lowermost units of the Magog Group but intense Taconic or Salinic metamorphism is absent except for the infraophiolitic metamorphic sole rocks. Peak Acadian metamorphism varies from greenschist grade (biotite to chlorite zone) in the south (near the Quebec–Vermont border), to prehnite-pumpellyite grade in the Beauce area (fig. 2). $^{40}Ar/^{39}Ar$ dating of greenschist-grade metamorphic rocks of the Ascot Complex yielded 380 to 375 Ma muscovite ages (Tremblay and others, 2000).

The Saint-Victor synclinorium consists of NE- and SW-plunging, open to tight folds, commonly overturned to the NW, which show a regionally-developed axial-planar schistosity or slaty cleavage. From the Quebec-Vermont border to the Beauce area (fig. 2), the La Guadeloupe fault has been recognized as a NW-directed, high-angle reverse fault (Labbé and St-Julien, 1989; Tremblay and others, 1989; Cousineau and Tremblay, 1993), and is associated with greenschist-grade, quartzofeldspathic and calc-silicates mylonites developed in adjacent units. In the

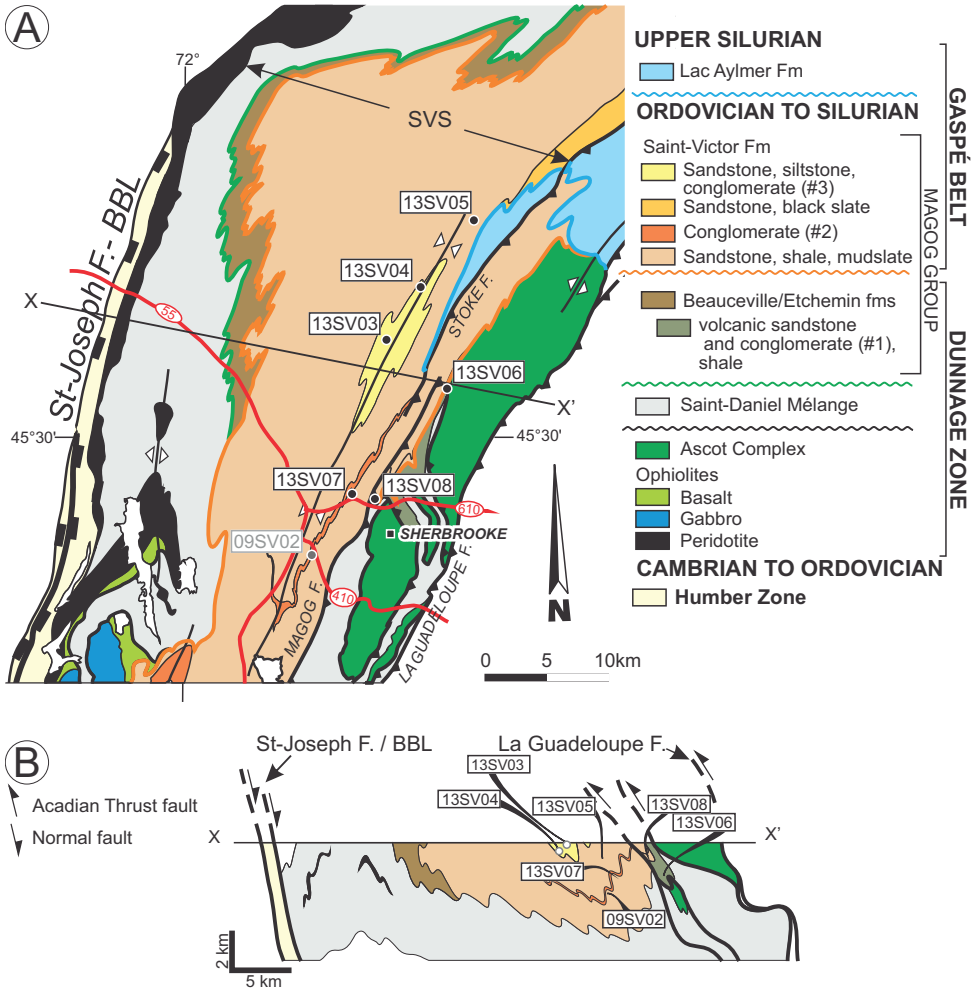

Fig. 5. (A) Geological map of the Sherbrooke-Orford area (modified from Tremblay and others, 2015; Perrot and Tremblay, 2017). (B) Interpretative structural profile X–X'; see figure 3A for location. Framed black numbers indicate sample locations, framed gray number indicate the location of de Souza and others (2014) sample 09SV02. #1, 2 and 3 refer to the three stratigraphic marker horizons of polygenic conglomerate in the Magog Group (numbered as in text). See figure 2 for location and the significance of structural features.

Sherbrooke area (fig. 5), regional folds and faults are overprinted by SE-verging open folds that correlate with the "easterly features" of Osberg (1989) in New England, which are there refolded by late north-trending folds corresponding to a dome-stage regional deformational event (Hatch and Stanley, 1988; Armstrong and others, 1992).

THE SAINT-VICTOR FORMATION

In southern Québec, the Saint-Victor Formation occupies the core of the Saint-Victor synclinorium (fig. 2). Recent geological mapping in the Sherbrooke-Orford area (fig. 5) suggests the occurrence of an unconformity between the Saint-Victor

Formation and underlying rocks of the Ascot Complex, Saint-Daniel Mélange and Beauceville Formation (Tremblay and Pinet, 2016; Perrot and Tremblay, 2017).

In this area, three stratigraphical marker horizons of polygenic conglomerate have been distinguished in the Magog Group (Mercier, ms, 2013). (1) The lowermost horizon (fig. 5) is a volcanic conglomerate with a feldspar-rich sandstone matrix that contains rounded clasts of rhyolite, felsic tuff, hematitic chert, basalt and rare granitic rocks. It was included in the Saint-Victor Formation by Mercier (ms, 2013) but its close association with feldspar-rich, tuffaceous sandstone and rusty black shale suggests that it belongs to the Beauceville Formation instead, as originally suggested by Tremblay (1992a; his M1 unit). (2) The medial horizon of conglomerate (fig. 5) is made up of cm- to meter-size rounded clasts of felsic volcanic and plutonic (rhyolite, granite, granodiorite) and sedimentary rocks in a quartz-feldspar sandstone matrix. It overlies a sandstone-rich turbiditic sequence and is overlain by a sequence of slates interlayered with fine- to medium-grained sandstones (Tremblay, 1992b). This sandstone/wacke turbidites sequence is typical of the Saint-Victor Formation. This conglomerate marker horizon is well-exposed in the Sherbrooke-Orford area (figs. 5 and 6A) and was originally included in the Sherbrooke Formation of St-Julien (ms, 1963). (3) The stratigraphically uppermost horizon of conglomerate is similar in composition to the previous one but is characterized by a more greenish, chlorite-rich sandstone matrix. It clearly overlies the laminated and well-bedded slate-sandstone sequence described above. This conglomerate and associated sandstone and shale were originally attributed to the Upper Silurian Lac Lambton Formation by De Rômer (1985) but are currently considered as part of the Saint-Victor Formation (Mercier, ms, 2013; Tremblay and others, 2015).

The age of the Saint-Victor Formation is essentially based on a few graptolite fauna occurrences. Indeed, in the Beauce and Sherbrooke-Orford areas, Berry (1962), St-Julien (1970) and St-Julien (1987) have described a graptolite fauna of the *Orthograptus truncatus var. intermedius* zone, attributing a Katian age (453–445 Ma) to these rocks. Cousineau and St-Julien (1994) assigned some of these graptolites to the *Diplogratus multidens* zone, rather implying a Darriwilian age (467–458 Ma) to the same rock units. However, these latter graptolite occurrences are doubtful (see Discussion section), and moreover located in the lowermost part of the Saint-Victor Formation (see locations and stratigraphic positions on figs. 3 and 4), they are thus not well suited to constrain the age of the upper part of the sequence. The uppermost part of the Saint-Victor Formation is rather well-exposed in the Sherbrooke-Orford area (fig. 5) where its age remains practically unknown.

Recently, detrital zircon U-Pb dating from a single locality of the Saint-Victor Formation in the Sherbrooke area yielded ages as young as 424 ± 6 Ma (de Souza and others, 2014). The sampling site of the de Souza's and others sample (09SV02; see fig. 5 for location) is stratigraphically located immediately below the medial horizon of conglomerate (#2 on fig. 5) mentioned above, that was attributed to the former Sherbrooke Formation of St-Julien (ms, 1963; fig. 6A). The Sherbrooke Formation was originally considered to unconformably overlie the Magog Group but was later included in the Saint-Victor Formation by St-Julien (1970). According to St-Julien (ms, 1963), this conglomerate horizon contains numerous occurrences of crinoids and fragments of gastropods, cephalopods, corals, brachiopods and bryozoans which yielded inconclusive "Arisaig" (Silurian) age results on the basis of brachiopods fragments (see St-Julien, ms, 1963).

DETRITAL ZIRCON GEOCHRONOLOGY

In order to better constrain the age of the Magog Group, the sampling strategy was oriented towards the control of both spatial and temporal variations. Sandstone samples were taken from the lower and upper parts of the Magog Group. The

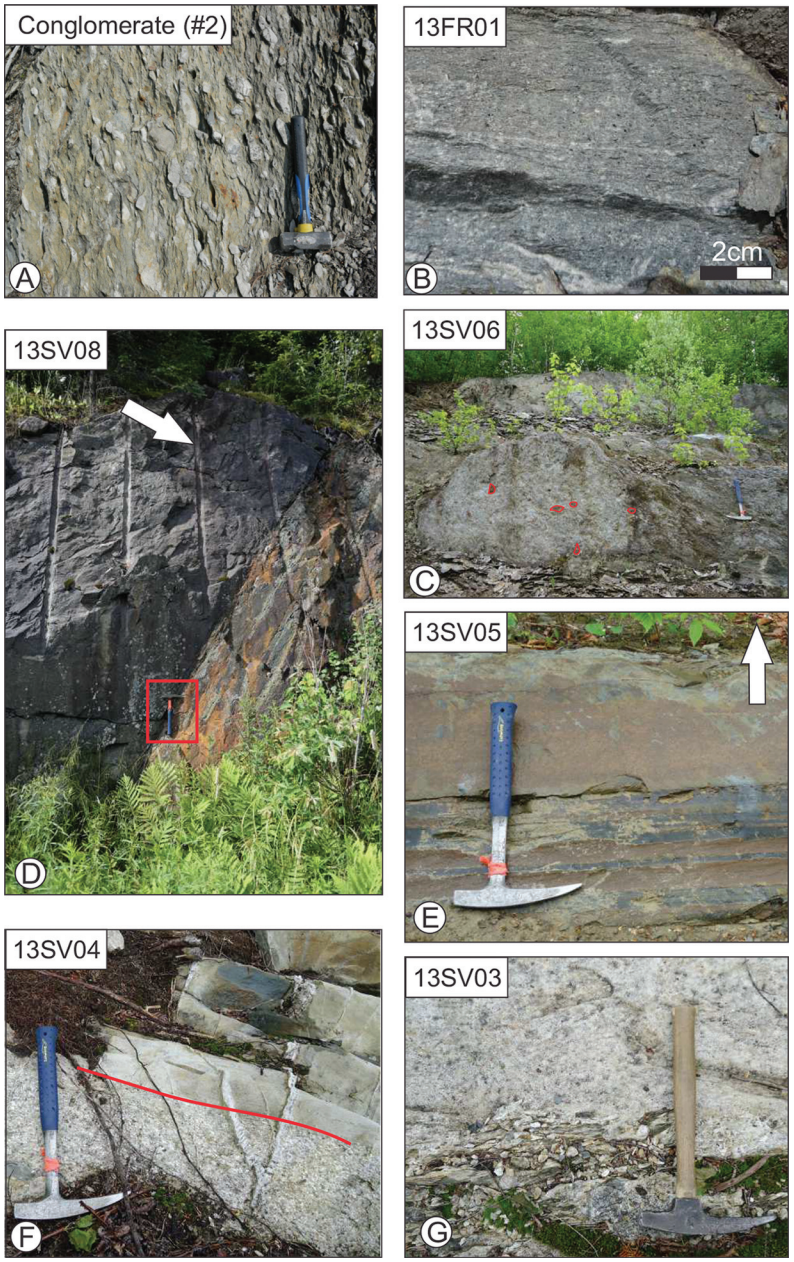

Fig. 6. Field photographs of the Magog Group. (A) Field example of polygenic conglomerate of the former Sherbrooke Formation. (B) Volcaniclastic sandstone sampled for U-Pb dating of detrital zircons of the Frontière Formation (sample 13FR01). (C) Feldspathic sandstone and volcanic conglomerate with chert, tuff, rhyolite clasts of the Beauceville Formation. Some clasts are highlighted by red lines. This outcrop was sampled for U-Pb dating (sample 13SV06). (D) Typical turbidites deposit of the Saint-Victor Formation sampled for U-Pb dating (sample 13SV08). The hammer (red box) show the contact between massif sandstone to the SE and dark shale to the NW; the arrow indicates the stratigraphic top (toward the northwest). (E) Rhythmites of fine- to medium-grained sandstone of the Saint-Victor Formation; the arrow indicates the stratigraphic top. (F) and (G) Polygenic conglomerate with a quartzo-feldspathic sandstone matrix alternating with sandstone beds (the red line highlights the bedding). Sandstone beds were sampled for U-Pb dating (samples 13SV04 and 13SV03). See figures 4 and 5 for location of the samples.

Sherbrooke-Orford (fig. 3) area was chosen as a type locality because the stratigraphy of the Saint-Victor Formation is well-constrained there and most rock exposures are of high quality and easy access. Our unique sample of the Frontière Formation (13FR01) is, however, from the Beauce area (figs. 4 and 6B). In the Sherbrooke-Orford area, sample 13SV06 was taken from the Beauceville Formation (figs. 5 and 6C) and four samples are from the Saint-Victor Formation, 13SV08, 13SV05, 13SV04 and 13SV03, from base to top (figs. 5 and 6D to 6G).

Analytical Procedures

Approximately 10 kg of sandstone was collected at each sampling site. The samples were crushed with a jaw crusher and a disc grinder. A Wilfley table, Frantz magnetic separator and heavy liquids were used to separate the zircons. Hundreds of zircon crystals were randomly extracted from each sample by handpicking under a binocular microscope. The zircon grains were then mounted in epoxy and polished. The cathodoluminescence (CL) imagery of zircons was performed on a scanning electron microscope (SEM) and used to highlight growth zoning within individual grains. Most zircons show oscillatory and sector zoning, some of them showing metamorphic rims overgrowths (fig. 7). U-Pb analyses were conducted by laser ablation (HR-LA-ICP-MS) and isotope dilution thermal ionization mass spectrometry (ID–TIMS) in Geotop laboratories at *Université du Québec à Montréal* (Canada). The core of randomly selected zircons was usually analyzed. Special care has been taken to avoid fractures and inclusions-rich domains within zircon grains.

Laser Ablation (HR-LA-ICP-MS).—Zircon grains were analyzed by a Nu Attom HR-LA-ICP-MS. Metadata are illustrated in Appendix I, as recommended by Horstwood and others (2016). Using the CL images, ablated zones were identified in the cores of zircon grains, and late metamorphic rims and inclusions were avoided when possible. The zircon standard used for calibration of the $^{206}Pb/^{238}U$ ratio was 91500. All data reduction was performed using the Iolite data reduction software (Paton and others, 2011). Analytical data were plotted using Isoplot 4.15 (Ludwig, 2012).

The relative probability density of age distribution diagrams included analyses of zircons that were more or less concordant. Our selected analyses have low error range (<10% at 1-sigma uncertainty in either $^{206}Pb^*/^{238}U$ age or older than *ca.* 1.0 Ga $^{206}Pb^*/^{207}Pb^*$ age). For analyses younger than 800 m.y., those with $^{206}Pb^*/^{238}U$ ages superposed in a 2 sigma error were kept for calculations whereas, for analyses older than 800 m.y., those that are less than 30 percent discordant ($^{206}Pb^*/^{238}U/^{206}Pb^*/^{207}Pb^*$) were kept. Such thresholds were selected to avoid bias in the final set of ages (see Gehrels and others, 2011). All analytical results are shown in Appendix II, and on Pb*/U Concordia and probability density plots (fig. 8).

In order to highlight and better understand the youngest zircon age populations, the results for grains younger than 550 Ma were tested with different modeling methods (fig. 9), namely, (1) a Bayesian mixture modeling method (Jasra and others, 2006) calculated with Isoplot software (Ludwig, 2012), (2) the weighted mean age of youngest cluster method also calculated with Isoplot software from Ludwig (2012), and (3) the Age Pick program of Gehrels (2010). In the probability density distribution diagrams (fig. 8), 2ó error bars are used whereas for the youngest populations highlighted by the Bayesian mixture modeling (fig. 9), the 2ó error bars are statistical errors.

Isotopic dilution (ID–TIMS).—Each zircon showing HR-LA-ICP-MS ages ≤ 430 Ma were extracted from the epoxy and analyzed by ID-TIMS. The procedure we followed for extraction is quite simple; the epoxy paste was soft enough to re-pick the targeted zircon grains with a tweezer. Each grain successfully extracted (approximately 70%) was treated individually or in pairs beginning by high-temperature annealing (*ca.* 50 hours at 900 °C) and chemical abrasion in 48 percent hydrofluoric acid (HF) in Parr

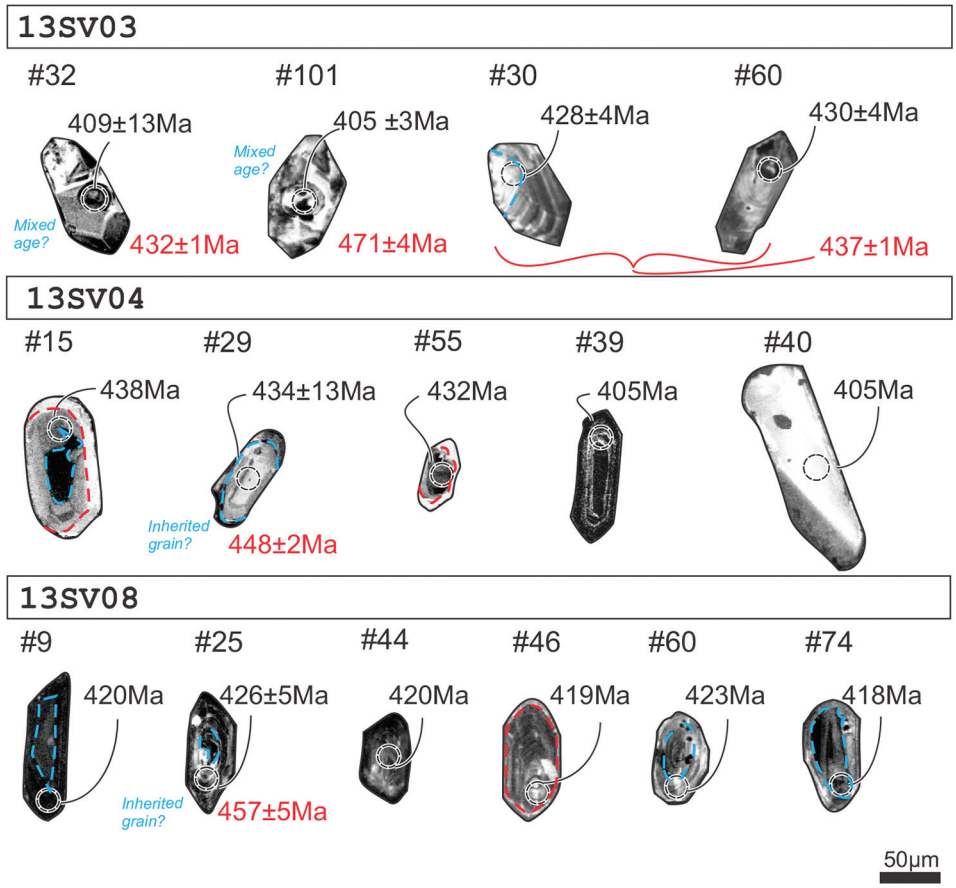

Fig. 7. Cathodoluminescence images for dated zircon from samples 13SV03, 13SV04 and 13SV05. Ages resulting from LA-ICPMS analysis are shown in black, whereas TIMS ages are in red.

liners to remove volumes affected by Pb loss (Mattinson, 2005). The abraded crystals were washed in acetone and H_2O using an ultrasonic bath to remove any contamination. All samples were spiked with a ^{205}Pb-^{233}U-^{235}U-tracer and then dissolved with 20 drops of HF and 2 drops of HNO_3 in pressurized Parr bombs at 195 °C for 3 days. Dissolved zircons were chemically separated and treated according to the method described by Krogh (1973). The U-Pb solutions were dried down and loaded on degassed Re filaments using silica gel and a drop of H_3PO_4 and measured on a VG Sector-54 mass spectrometer. Corrections were made for a 1 pg Pb-blank and a 0.1 pg U-blank. All calculated ages are quoted with a 1 sigma error in Appendix III. Initial common Pb was corrected by using the value from the Pb-evolution model of Stacey and Kramers (1975) at the age of interest. Concordia plots (fig. 10) were drawn with Isoplot 4.2 (Ludwig, 2012), and errors are reported at a 2σ level.

Results

HR-LA-ICP-MS.—Zircon ages obtained from the six samples fall into three broadly-defined age populations: 1) 400 to 550 Ma, 2) 900 to 2000 Ma, and 3) >2.5 Ga (fig. 8, Appendix II). The majority of samples show age distributions characterized by one

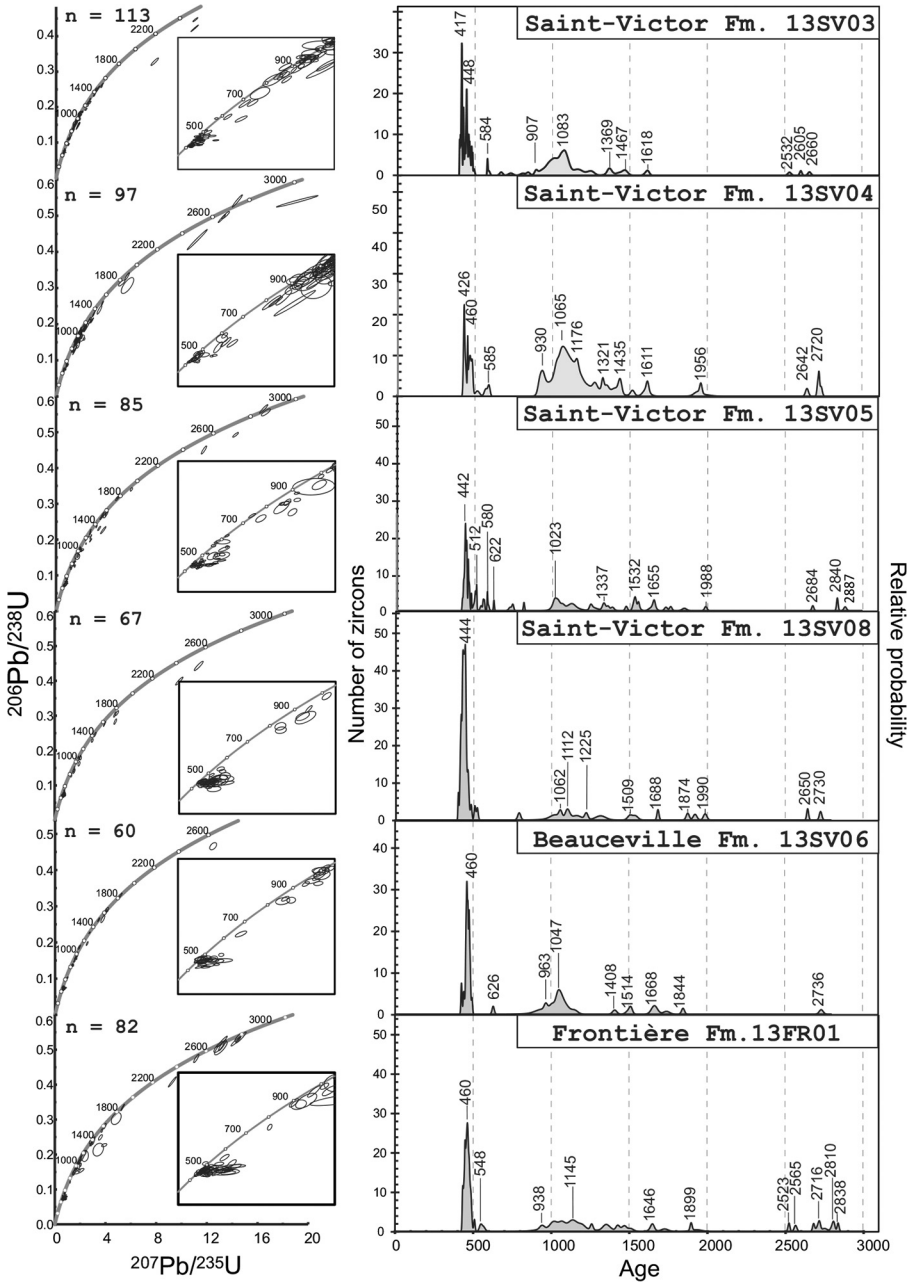

Fig. 8. Global Concordia diagrams and corresponding probability density distribution – frequency diagrams of detrital zircon ages for the analyzed samples. Concordia diagrams shown in the right insets are for youngest ages distributions between 400 Ma and 1000 Ma. All diagrams were generated using Isoplot (Ludwig, 2012).

prominent peak in the Paleozoic and a low proportion of Archean and Proterozoic ages. Samples 13SV04 and 13SV03 yielded a distinctive bimodal distribution, showing age peaks clustering in the Proterozoic and the Paleozoic.

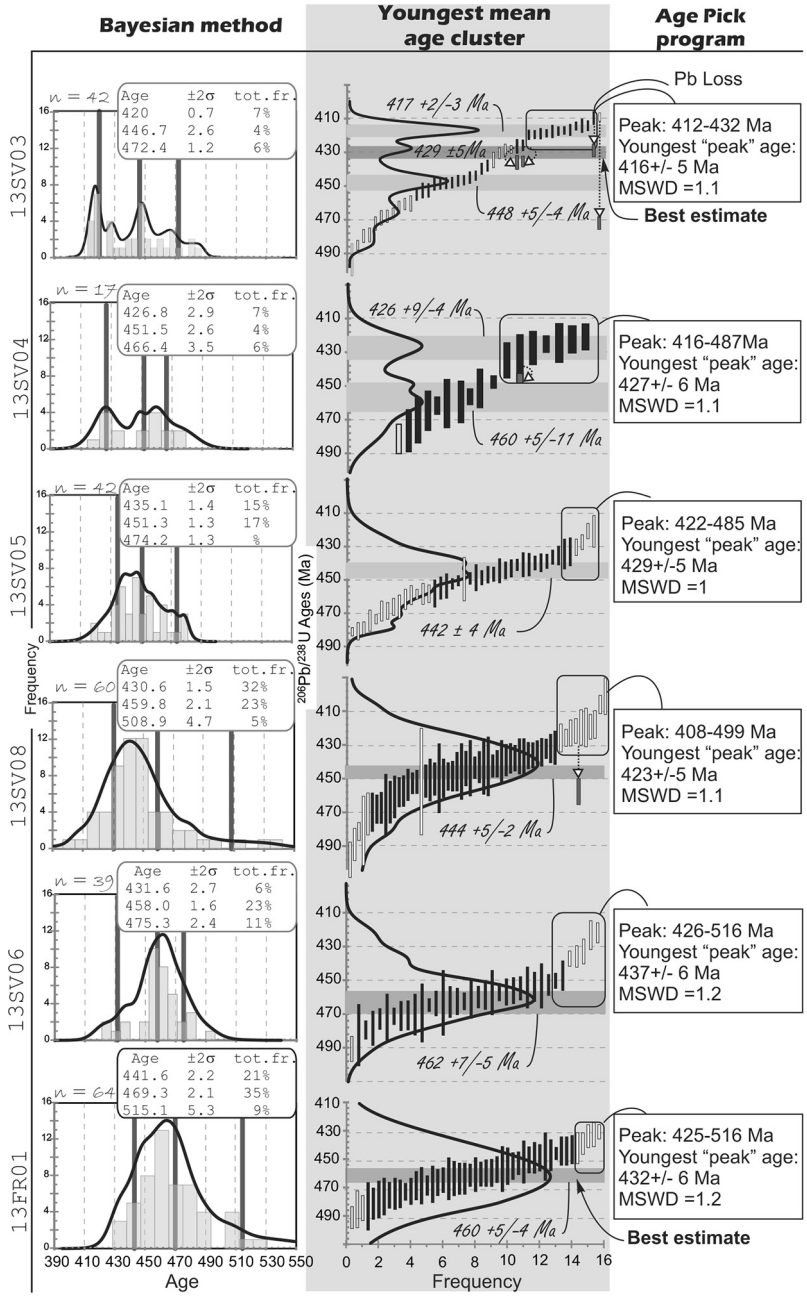

Fig. 9. Illustration of the three different methods of youngest ages calculations by the Bayesian method (left column), the Weighted mean age of youngest clusters (center), and the Age Piks program (right column). Ages corresponding to empty boxes were excluded from mean age calculations. For samples 13SV03, 13SV04 and 13SV08, the dark gray boxes at the end of the arrows correspond to the TIMS ages results. See text for discussion. n – number of zircon grains; MSWD – mean square weighted deviation.

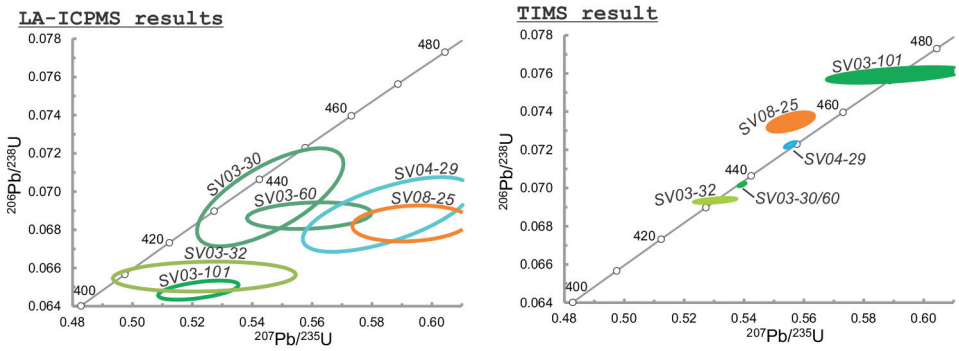

Fig. 10. Comparative concordia diagrams between HR-LA-ICP-MS age results (left diagram; open ellipses) for detrital zircons that have been re-analyzed by ID-TIMS (right diagram; filled circles and ellipses).

The Frontière Formation sample (13FR01), a coarse-grained quartzofeldspathic sandstone (fig. 6B), yielded abundant euhedral, prismatic or elliptical, amber to reddish-brown colored zircon grains showing smooth to sharp edges. 82 results of 118 zircon grains analyzed from this sample were kept (fig. 8). The probability density distribution diagram of this sample highlight (1) a prominent peak around 460 Ma, (2) a broad zircon grains population with ages varying from *ca.* 940 to *ca.* 1500 Ma, and scattered ages around 1646 and 1899 Ma, and (3) some Archean ages (2.5–2.8 Ga).

Sample 13SV06, from the Beauceville Formation, is a feldspar-rich sandstone immediately above the contact with the Ascot Complex (fig. 6C). This sample yielded mostly clear zircon grains showing stalky prismatic shapes with smooth to sharp edges and, for some, a well-rounded shape. 60 results of 87 zircon grains analyzed from this sample were kept (fig. 8). The probability density distribution diagram highlights (1) a dominant peak at *ca.* 460 Ma, and one Neoproterozoic age at *ca.* 626 Ma, (2) a Proterozoic population of *ca.* 960 Ma to *ca.* 1120 Ma and scattered ages of *ca.* 1400 to *ca.* 1845 Ma, and (3) one Archean zircon grain at *ca.* 2736 Ma (fig. 8).

Samples 13SV08 and 13SV05 (figs. 6D-6E) are from coarse-grained sandstone of the Saint-Victor Formation. Sample 13SV08 yielded mostly clear, columnar-shaped zircon grains with smooth edges but also some brownish rounded-shapes, whereas 13SV05 yielded clear-yellowish zircons of stalky to prismatic shapes and pinkish-brownish zircons with elliptic to rounded shapes. For sample 13SV08, 67 results of 84 zircon grains analyzed were kept (fig. 8). The probability density distribution diagram of this sample is characterized by (1) a dominant peak at *ca.* 444 Ma, (2) a Proterozoic population with most ages varying from *ca.* 1000 Ma to *ca.* 1330 Ma and scattered ages between *ca.* 1509 and *ca.* 1990 Ma, and (3) two zircon grains of Archean ages at *ca.* 2650 Ma and *ca.* 2730 Ma (fig. 8). For sample 13SV05, 85 results of 119 zircon grains analysed were kept (fig. 8). The probability density distribution diagram of this sample shows (1) a dominant peak at *ca.* 442 Ma, and two Neoproterozoic ages of *ca.* 580 Ma and *ca.* 622 Ma, (2) a Proterozoic ages population of *ca.* 1000 Ma to *ca.* 1337 Ma with scattered ages from *ca.* 1532 to *ca.* 1990 Ma, and (3) Archean zircon grains between *ca.* 2684 Ma and *ca.* 2887 (fig. 8).

The uppermost samples of the Saint-Victor Formation, 13SV04 and 13SV03 (figs. 6F-6G), yielded mostly clear, orange-to-brownish zircon grains with stalk prismatic to well-rounded shapes and smooth to sharp edges. 96 results of 107 zircon grains analyzed from the sample 13SV04 were kept (fig. 8). The probability density distribution diagram shows a bimodal distribution between Paleozoic and Proterozoic ages

with (1) two dominant peaks at *ca.* 426 Ma and *ca.* 460 Ma and a single zircon with a Ediacaran age of *ca.* 585 Ma, (2) an abundant Proterozoic population with ages varying between *ca.* 930 Ma and *ca.* 1435 Ma, with a peak at *ca.* 1065 Ma and scattered ages around 1611 Ma and 1956 Ma, and (3) two zircon grains older than 2.6 Ma (fig. 8). 113 results of 130 zircon grains analyzed from 13SV03 were kept (fig. 8). The probability density distribution diagram shows an age pattern similar to 13SV04 with (1) two dominant peaks, at *ca.* 417 Ma and *ca.* 448 Ma, and one Ediacaran age at *ca.* 584 Ma, (2) an abundant Proterozoic ages population with some zircons varying from *ca.* 900 Ma to *ca.* 1467 Ma with a peak at *ca.* 1083 Ma and one grain around 1618 Ma, and (3) three scattered ages older than 2.5 Ma (fig. 8).

Youngest HR-LA-ICP-MS detrital ages.—The youngest detrital zircon ages measured in our samples of the Saint-Victor Formation are not consistent with the established chrono-stratigraphic framework of the Magog Group (Cousineau and St-Julien, 1994). A recurring problem in most detrital zircons dating studies is to determine the minimum number of zircon grains that is needed to be representative of a statistically-significant age population (see for example Bradley and O'Sullivan, 2016). Dickinson and Gehrels (2009), for instance, suggested that the youngest zircons age peaks can be defined by three or more coherent zircon grains. If we apply this rule to our U-Pb age results, then all the analyzed samples yield deposition ages much younger than expected for the Magog Group. The use of multiple youngest-age measurements in order to evaluate the youngest detrital zircon ages has been recommended by Dickinson and Gehrels (2009). They argued that the consistency of results obtained with different methods of measurements conduct a greater confidence to the youngest-age analysis whereas strong discrepancies between the various methods may reveal ambiguous U-Pb datasets. Therefore, in order to verify the reproducibility of our U-Pb results and to better constrain the geological significance of youngest ages measurements, we have compared and tested three different methods of calculation (fig. 9):

(1) the Bayesian mixture modeling (BMM, Jasra and others, 2006) proposed in Isoplot (Ludwig, 2012) which allows the identification of ages population mixed with, or hidden by other dominant populations.

(2) a method based on the weighted mean age of youngest clusters calculated with Isoplot (Ludwig, 2012);

(3) the Age Pick program of Gehrels (2010), which can be used to evaluate if U-Pb results have been affected by Pb loss.

Based on the forearc basin setting inferred for the Magog Group (for example Cousineau and St-Julien, 1994; Schroetter and others, 2006), two peaks of detrital zircon ages can be expected: (1) a *ca.* 510 to 470 Ma zircon population that would be related to the possible contribution of the southern Quebec ophiolites and their obduction-related magmatic rocks, and (2) a *ca.* 460 Ma zircon population related to the contribution of the Ascot Complex volcanic arc and correlative rocks. However, youngest detrital zircon ages obtained by de Souza and others (2014) imply the possible contribution of younger sources of *ca.* 430 to 420 Ma. Therefore, for BMM calculations, and in order to evaluate the presence of hidden sources in our data set (fig. 9), we took into account three possible, Ordovician and Silurian, sources of detrital zircons.

In the following, we use the term "maximum age of sedimentation" for the youngest age of sedimentation that can be defined with our analytical results, but it does not mean, however, that we are excluding the fact that the true age of sedimentation cannot be younger.

The Frontière Formation sample (13FR01) shows a well-defined peak of Ordovician age represented by 56 analyses forming a cluster from which was calculated a weighted mean $^{238}U/^{206}Pb$ age of $460^{+5}/_{-4}$ Ma (fig. 8). The youngest age peak

calculated by the Age Pick program and defined by 4 zircon grains is 432 ± 6 Ma whereas the youngest statistical age calculated with the Bayesian mixture modeling is 442 ± 2 Ma (fig. 9). These two younger age results are, however, inconsistent with the U-Pb zircon age of $462^{+4}/_{-5}$ Ma measured in a felsic tuff of the overlying Beauceville Formation (Marquis and others, 2001). Consequently, we consider that the most realistic youngest zircon age population for sample 13FR01 is $460^{+5}/_{-4}$ Ma.

The Beauceville Formation sample (13SV06) shows an Ordovician age peak that is defined by 30 analyses from which was calculated a weighted mean $^{238}U/^{206}Pb$ age of $462^{+7}/_{-5}$ Ma (fig. 9). The youngest peak of ages as calculated with Age Pick program and defined by 7 zircon grains, is 437 ± 6 Ma whereas the statistical Bayesian age analysis of this sample yield results as young as 432 ± 3 Ma (fig. 9). These lower Silurian age results are obviously not consistent with the Marquis's and others (2001) U-Pb crystallization age of $462^{+5}/_{-4}$ Ma. Taking into account the scattering shown by the 7 younger zircon grain ages (ranging from 450–415 Ma), we do not believe that these zircons belong to the same set of population but reflect likely the effect of Pb-loss. The weighted mean age of the youngest cluster at $462^{+7}/_{-5}$ Ma is therefore considered as the best estimate for this sample.

Samples 13SV08 and 13SV05 of the Saint-Victor Formation yielded Ordovician to Silurian overlapping peak ages defined by 57 and 42 analyses, respectively. Among these, 41 and 23 analyses form two $^{238}U/^{206}Pb$ weighted mean age clusters of $444^{+5}/_{-2}$ Ma and 442 ± 4 Ma (fig. 9). The youngest peak of calculated ages by the Age Pick program are 423 ± 5 Ma for 13SV08 (10 zircons) and 429 ± 5 Ma for 13SV05 (6 zircons, fig. 9). For both samples, the Bayesian mixture modeling yields youngest statistical ages of 431 ± 2 Ma and 435 ± 1 Ma, respectively (fig. 9). Based on the weighted mean age clusters of each sample, these results suggest that the maximum age of the youngest erosional source for both samples is approximately 443 Ma. Based on the two other methods, a minimum age of the youngest erosional source can be set around 430 Ma. Regardless of the calculation method, the results are therefore indicative of Hirnantian (Late Ordovician, *ca.* 445–443 Ma) to Wenlockian (middle Silurian, *ca.* 433–427 Ma) epoch of deposition, or younger.

In the uppermost part of the Saint-Victor Formation, for sample 13SV04, the results show two age peaks, defined by 9 and 7 analyses, respectively, yielding weighted mean $^{238}U/^{206}Pb$ ages of $460^{+5}/_{-11}$ Ma and $426^{+9}/_{-4}$ Ma (fig. 9). Sample 13SV03 shows a similar bimodal ages distribution, with 13 analyses forming an age cluster with a calculated weighted mean $^{238}U/^{206}Pb$ age of $448^{+5}/_{-4}$ Ma, and 14 analyses yielding a calculated weighted mean $^{238}U/^{206}Pb$ age of $417^{+2}/_{-3}$ Ma (fig. 9). The youngest age peaks, as calculated by the Age Pick program, are 427 ± 6 Ma (13SV04) and 416 ± 5 Ma (13SV03), defined by 7 and 12 zircons, respectively (fig. 9). These same samples yield statistical Bayesian ages as young as 427 ± 3 Ma and 420 ± 1 Ma. These two samples show less scattering between the different methods of youngest ages calculation, all suggesting a Ludlowian-to-Pridolian, or younger, age of deposition.

ID-TIMS.—ID-TIMS analyses were performed on selected samples in order (1) to evaluate the possible effect of Pb loss or mixed ages on the accuracy of HR-LA-ICP-MS age results and (2) to validate some of the youngest depositional ages obtained by the different methods of calculation, looking for the presence of entirely Silurian magmatic grains.

Zircons from samples of the Saint-Victor Formation that yielded HR-LA-ICP-MS U-Pb ages younger than 430 Ma (34 grains) were extracted from the expoxy pokes for ID-TIMS analyses. Among the 22 zircon grains that have been re-analyzed, 6 zircon grains yielded Ordovician-to-Silurian ages (see fig. 7 for some CL imaging of the grains re-analyzed by ID-TIMS and the corresponding ages, and fig. 10 for a comparison plot for ID-TIMS and HR-LA-ICP-MS results), whereas 18 grains yielded either Grenvillian

ages or unusable results. Grenvillian ages can be explained by the occurrence of zircons with mixed ages, for which chemical abrasion removed the younger rims or domains (see for example Kröner and others, 2014).

In sample 13SV08, zircon grain #25 yielded a ID-TIMS age of 457 ± 5 Ma whereas its U-Pb age measured by HR-LA-ICP-MS is 426 ± 5 Ma (figs. 7 and 10). The ID-TIMS age is grossly consistent with the youngest mean ages cluster obtained for that sample ($444^{+5}/_{-2}$ Ma) as it is included in the main cluster of youngest mean ages (fig. 9), which therefore suggests that deposition is Late Ordovician or younger. If correct, this would imply that younger Silurian ages obtained by HR-LA-ICP-MS for that sample are probably the result of Pb loss. However, on the CL image (fig. 7), the presence of an inherited core in grain #25 cannot be excluded, which would account for the younger age of the laser spot and older age of the inherited part analyzed by TIMS (young domains being annealed by chemical abrasion). Nevertheless, the influence of Pb loss or inherited core suggests a Late Ordovician or younger depositional age as for HR-LA-ICP-MS results of sample 13SV05.

Zircon grain #29 of sample 13SV04 yielded a TIMS age of 448 ± 2 Ma, which is within the error range of the HR-LA-ICP-MS analyses for that sample, at 434 ± 13 Ma (figs. 7 and 10). Zircon grains #32 and #101 (fig. 7) from sample 13SV03, yielded ID-TIMS ages of 432 ± 1 Ma and 471 ± 4 Ma, respectively, whereas their respective HR-LA-ICP-MS ages are 409 ± 13 Ma and 405 ± 3 Ma. Moreover, zircon grains #30 and #60 of sample 13SV03 both yielded a mixed ID-TIMS age of 437 Ma ± 1 Ma whereas the HR-LA-ICP-MS ages of these two grains are 428 ± 4 and 430 ± 4 Ma (figs. 7 and 10). These variations of age results between ID-TIMS and HR-LA-ICP-MS analyses can be attributed to Pb loss affecting the youngest zircon grains or, alternatively, to the presence of an inherited core in grain #29 of sample 13SV04 and of mixed ages in grains #32 and #101 of sample 13SV03 (figs. 7 and 10). However, the TIMS result of 432 ± 1 Ma for grain #32 (sample 13SV03) is consistent with one cluster of mean ages at 429 ± 5 Ma (see fig. 9). Considering all results, HR-LA-ICP-MS and TIMS, the *ca.* 429 Ma mean age cluster can be considered as the most accurate estimation for the maximum age of sedimentation for sample 13SV03, which is consistent with HR-LA-ICP-MS youngest ages between 435 and 422 Ma (fig. 9) obtained with the three different methods of calculation for 13SV04, a sample located at the same stratigraphic position.

In summary, even though our detrital U-Pb age results are, within errors, consistent with the specific stratigraphic position of each sample, ID-TIMS analyses yield results that are ≥ 10 Ma older than the corresponding HR-LA-ICP-MS results, suggesting that some zircon grains of the Saint-Victor Formation may have experienced either mixed ages or Pb-loss. Moreover, anomalously young detrital HR-LA-ICPMS ages possibly reflect post-depositionnal undetected or detected (as metamorphic overgrowth interpreted in grains on fig. 7) metamorphic overgrowth although it is considered unlikely considering the low grade (lower greenschist) of regional metamorphism in the Magog Group. Nevertheless, the detrital zircon age data presented above clearly indicate that sedimentation extends well into the Silurian, which is significantly younger than the current age assignment of the Magog Group.

DISCUSSION

The Magog Group is currently interpreted as the remnant of a forearc basin (Cousineau, 1990; Cousineau and St-Julien, 1994). In most tectonic models, this sedimentary basin was filled by the erosion of metasedimentary and magmatic rock sources located to the NW (that are the ophiolites and underlying/adjacent continental margin rocks of the Taconian orogen), and of felsic-to-mafic volcanic rock sources located to the SE (the Ascot Complex and correlatives). The occurrence of detrital

chromite and the composition of Magog Group sandstones clearly attest for the contribution of NW erosional sources (Cousineau, 1990), whereas the presence of felsic tuffs in the Etchemin and Beauceville formations is consistent with active arc volcanism during sedimentation (the Ascot Complex). Fossils content and zircon U-Pb ages of the Beauceville Formation are also consistent with a forearc basin interpretation, given that it indicates that deposition has been almost coeval with *ca.* 460 Ma volcanic arc rocks of the Ascot Complex.

Our study of U-Pb detrital zircon ages, however, allows us to (1) document the occurrence of detrital ages younger than those expected for these rocks, (2) discuss the nature of along-strike stratigraphic correlations for the Magog Group, (3) propose the existence of alternative erosional sources, and (4) more adequately define the tectonic setting of sedimentation for the Magog Group.

Timing of Deposition for the Saint-Victor Formation and Its Relations with the Beauceville Formation

In the following section, fossils ages and the stratigraphical location and correlations of the different units of the Magog Group are used in order to verify and validate the consistency of the youngest detrital zircon ages.

On the basis of graptolites fauna, the Beauceville Formation can be assigned to a Darriwillian to Sandbian stage (see fig. 11, *ca.* 458 Ma, Riva, 1974; Cousineau and St-Julien, 1994), which is consistent with the $462^{+5}/_{-4}$ Ma U-Pb crystallization age of a Beauceville felsic tuff (David and others, 1993) and with the $462^{+3}/_{-4}$ U-Pb youngest detrital zircon age peak obtained during our study.

Cousineau and St-Julien (1994) suggested that, as for the Beauceville Formation, the Saint-Victor Formation contains a *D. multidens* graptolite fauna in the Beauce area, implying that both units belong, at least partly, to the Sandbian. According to J. Riva (personal communication, 2016), the Beauceville and Saint-Victor formations do not share any graptolite species. Graptolites occurrences in the Saint-Victor Formation in Beauce are found towards its stratigraphical base and belong to the *C. spiniferus*, *C. manitoulinenesis*, and *O. quadrimucronatus* zones (J. Riva, personal communication 2016). This corresponds to the middle and upper parts of the Katian stage (453–445 Ma) of the middle Late Ordovician (Goldman and others, 2007), therefore suggesting the existence of a sedimentary hiatus of a few m.y. (that is corresponding to the top of the Sandbian and the base of the Katian, see fig. 11) between the top of the Beauceville Formation and the base of the Saint-Victor Formation (see Tremblay and Pinet, 2016). In the Sherbrooke-Orford area (fig. 5), our lowermost stratigraphic sample (13SV08) of the Saint-Victor Formation yielded a maximum detrital zircon age of $444^{+5}/_{-2}$ Ma (fig. 11), which is consistent with those fossil age interpretations. Moreover, to the west, the Saint-Victor Formation directly overlies the Saint-Daniel Mélange (fig. 2) in the Lake Memphrémagog area, and contains *O. truncatus intermedius* (Berry, 1962), therefore suggesting, as in Beauce, a Katian age (453–445 Ma) for the lower part of that formation.

Our U-Pb detrital zircon age data suggest that the upper part of the Saint-Victor Formation has a maximum depositional age of *ca.* 429 ± 5 Ma, (fig. 11; sample 13SV03), which corresponds to the Wenlock epoch (433–427 Ma) of the Silurian. Such result, combined with U-Pb detrital ages obtained for other samples during our study (13SV04, 13SV05 and 13SV08) and with U-Pb ages published by de Souza and others (2014), indicates that the current age assignment of the whole sequence of the Magog Group to the Ordovician is not accurate, and that its sedimentation persisted, at least until the Wenlock. Taking into account fossil age constraints for the lower part of the Saint-Victor Formation, this suggests that sedimentation of this important stratigraphic unit of the Magog Group has been

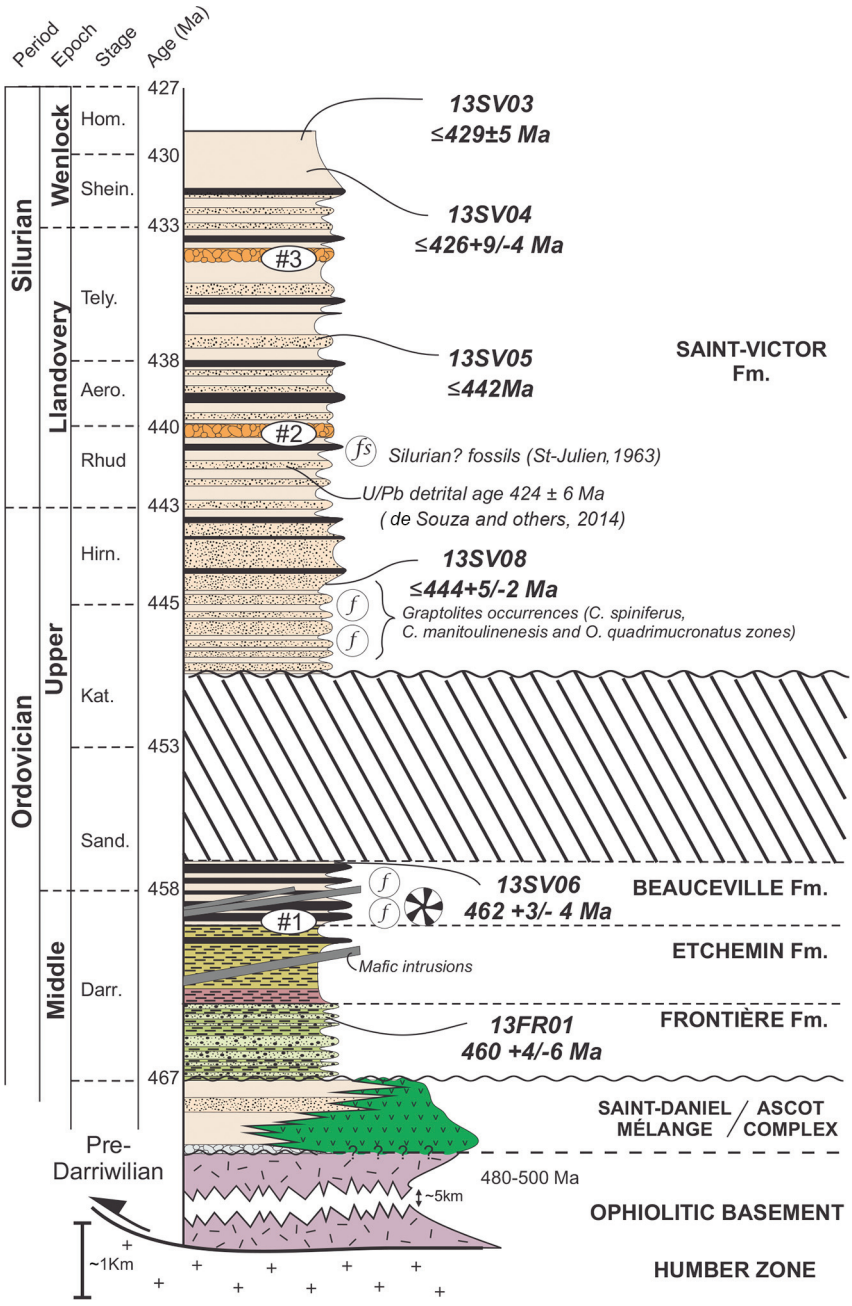

Fig. 11. Revised stratigraphic column for the Magog Group based on this study. Chronostratigraphic limits (in Ma) and subdivisions are from Cohen and others (2013). The diagonal lines pattern refers to sedimentary hiatus. See figure 3 for symbols explanation. As for figure 5, #1, 2 and 3 refer to the three stratigraphical marker horizons of polygenic conglomerate in the Magog Group.

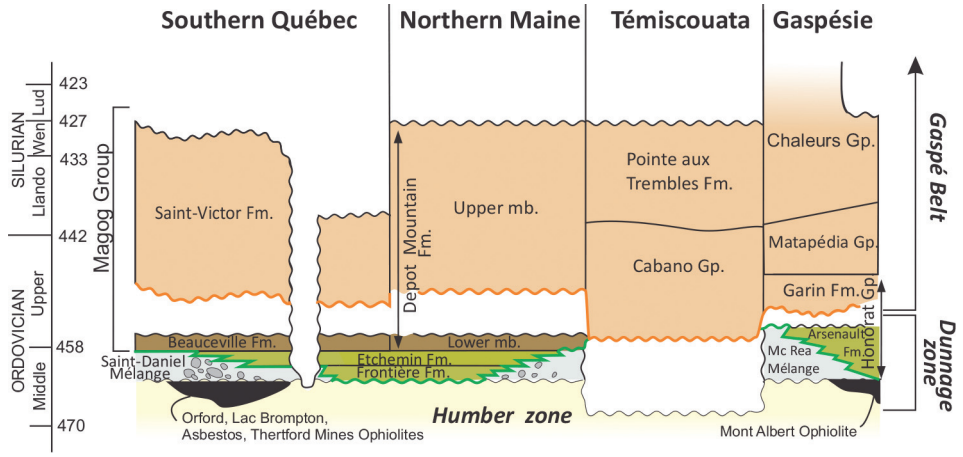

Fig. 12. Stratigraphic correlation chart for sedimentary units of the Magog Group of the Québec Appalachians and relations with underlying units. Green and orange wavy lines represent the base of the Magog Group and the base of the Saint-Victor Formation, respectively.

almost continuous over a time period of 15 to 20 m.y, from middle-upper Katian (*ca.* 450 Ma) to Wenlock times (*ca.* 430 Ma).

Considering that the Saint-Victor Formation is approximately 7 km-thick (Cousineau and St-Julien, 1994), this would correspond to a sedimentation rate of *ca.* 400 meters/m.y. This is lower but comparable to sedimentation rate values suggested, for instance, for the actual Kumano forearc basin of the Japan Sea which vary between 600 and 1300 meters/m.y. (Moore and others, 2015), or those of the Ordovician South Mayo Trough, a 9 km-thick forearc basin sequence of the Irish Caledonides (Dewey and Ryan, 1990; Mange and others, 2010), for which sedimentation rates have been estimated to be approximately 1000 meters/m.y. (Dewey and Mange, 1999).

Stratigraphic Relations and Correlations

The Magog Group does not have any known correlative units south of the Quebec-Vermont border, where only some rock units equivalent to the Saint-Daniel Mélange are preserved (see de Souza and others, 2014 for details).

Towards the NE, the Magog Group extends directly into Maine where it is known as the Depot Mountain Formation (fig. 12) which is divided into a lower and an upper member (Roy, 1989). The lower member consists of dark slates and siltstone, lithic and feldspathic graywackes, felsic tuffs and volcaniclastic conglomerates, and contains a Sandbian graptolites fauna, which indicate that it is equivalent to the lower part of the Magog Group, most likely the Beauceville Formation (Roy, 1989). The upper member of the Depot Mountain Formation consists of unfossiliferous, turbiditic dark slates, lithic graywackes and conglomerates (Roy, 1989) that are lithologically equivalent with the Saint-Victor Formation. The nature of the transition between the lower and upper members of the Depot Mountain Formation is unknown but is believed to be an unconformity (Tremblay and Pinet, 2016).

Northeastward, only the upper member of the Depot Mountain Formation continues in the Temiscouata area, where it merges into the Cabano Group (fig. 12), a sequence of lithic wackes, conglomerates and siltstone-mudstone turbidites (David and others, 1985) that rest unconformably on Cambrian-Ordovician rocks of the Humber Zone (David and others, 1985; Perrot and Tremblay, 2013), without the occurrence of any correlative lithologies with the lower formations of the Magog Group. The Cabano

Group ranges in age from the Sandbian *N. gracilis* zone to Llandoverian C3 (David and others, 1985; Bourque and others, 2000), indicating that its base is, at least in part, time-correlative with the Beauceville Formation and that, as the Saint-Victor Formation, it extends up-section into the Silurian (fig. 12). Consequently, on the basis of these lithological characteristics and available age constraints, both the Cabano Group and the upper member of the Depot Mountain Formation are considered as correlatives to the Saint-Victor Formation.

In Gaspé peninsula, the lower units of the Magog Group (Frontière, Etchemin and Beauceville formations) correlates with the Arsenault Formation of the Honorat Group and the basal unit (Necwick Formation) of the Mictaw Group (fig. 12). These are Darriwilian to Sandbian flysch-dominated turbiditic deposits unconformably overlying the McCrea and Rivière-Port-Daniel mélanges (De Broucker, 1987; Malo and Bourque, 1993; Dupuis and others, 2009), both being correlative with the Saint-Daniel Mélange (Tremblay and Pinet, 2016). In Gaspé, the Saint-Victor Formation correlates with the Garin Formation, the upper part of the Honorat Group, which is an Upper Ordovician turbiditic unit unconformably overlying both the Arsenault Formation and the McCrea mélange (fig. 12, Malo, 1988; Malo and Bourque, 1993), locally marking a sedimentary hiatus of ~10 m.y. Our youngest detrital ages for both the Beauceville-Frontière and the Saint-Victor formations are therefore consistent with their respective stratigraphic position and along-strike correlations from southern Quebec to the Gaspé peninsula.

The detrital zircon U-Pb geochronology results we obtained for the Saint-Victor Formation, combined with its fossil age constraints and inferred stratigraphic correlations in adjacent areas, suggest that there is an orogen-scale sedimentary hiatus of ± 10 m.y. between the top of the Beauceville Formation (Sandbian) and the base of the Saint-Victor Formation (mid-Katian). Recent geological mapping of the Saint-Victor Formation in the Sherbrooke-Orford area (Perrot and Tremblay, 2017) highlights the occurrence of an unconformity at the base of the Saint-Victor Formation (fig. 5). This implies that there are two distinct sedimentary sequences in the Magog Group, a lower part (made up of the Frontière, Etchemin and Beauceville formations) which forms a typical forearc basin sequence, and an upper part (the Saint-Victor Formation) which would be the result of Late Ordovician to Silurian post-Taconian *(sensu stricto)* sedimentation.

Implications for the Nature of Erosional Sources

The U-Pb detrital zircon age data include grains of Archean and Proterozoic ages reflecting rock sources belonging to, or recycled from, the Grenville and Superior provinces. Neoproterozoic to Early Ordovician zircon grains attest for Laurentian crustal material and detrital contributions from low-grade rocks of the Taconian allochtons (Humber Zone). However, the detrital U-Pb data set attest predominantly for the contribution of sources of Ordovician ages, corresponding to Taconian related magmatism, but also of Silurian ages, probably related to Salinic magmatism (see below).

Precambrian sources.—All samples contain Proterozoic zircon grains populations with most ages clustering between *ca.* 900 Ma to *ca.* 1200 Ma with scattered ages between 1300 and 2000 Ma, which obviously correspond to the erosion of Grenvillian source rocks (Rivers, 1997; Chiarenzelli and others, 2015). Neoarchean ages (>2.5 Ga) are also present and correspond to the recycling of crustal material from the Superior Province of the Canadian Shield (for example Percival, 2007).

The uppermost stratigraphic samples of the Saint-Victor Formation are characterized by a typical Precambrian detrital ages signature as compared to the other samples; they show significantly more abundant zircon grains of Late Mesoproterozoic to Neoproterozoic ages. This can be attributed to a more important detrital input of

Grenvillian sources from the Laurentian margin towards the top of the Magog Group, likely reflecting the uplift and erosion of Grenvillian basement rocks as those exposed in the Adirondacks Massif and the Green Mountains anticlinorium of New England, or the erosional recycling of Precambrian zircon grains from Cambrian and early Ordovician siliciclastic rocks of the Humber Zone.

Late Neoproterozoic to Lower Ordovician sources.—Ediacaran ages (*ca.* 635–542 Ma), that would firmly attest for the presence of proximal peri-Gondwanan erosional sources, are only locally found in some samples of the Saint-Victor Formation. This is surprising considering the inferred amalgamation of the peri-Gondwana Moretown Terrane (cropping out just south of the Quebec-Vermont border) during the Taconian orogeny, as proposed by Macdonald and others (2014) on the basis of detrital zircon geochronology. On the other hand, these minor sources of Ediacaran zircons could be explained by erosion of Iapetan rift volcanics on the Laurentian margin (Walsh and Aleinikoff, 1999; Hodych and Cox, 2007). Detrital zircons yielding ages from *ca.* 505 to 475 Ma are however clearly present, and most likely reflect the contribution of magmatic rocks such as those preserved in the southern Quebec ophiolites.

Ordovician and early Silurian sources.—Abundant Ordovician zircon grains of *ca.* 460 Ma are found in the Frontière (13FR01) and Beauceville (13SV06) formations, and in lesser amount in one sample of the St Victor Formation (13SV04). This is attributed to the contribution of proximal volcanic arc rocks such as those preserved in the Ascot Complex (460 Ma ± 3 Ma, David and others, 1993). However, distal sources like the Ammonoosuc volcanic sequence of the Bronson Hill Anticlimorium (*ca.* 469–443 Ma, Moench and Aleinikoff, 2003; Aleinikoff and others, 2011) and of the Shelburne Falls arc (485–470 Ma, Karabinos and others, 1998; Karabinos and Hepburn, 2001) of New England also represent possible erosional sources. Correlative Ordovician volcanic arc rocks are lacking in the Temiscouata and Gaspé Peninsula areas, suggesting that such sedimentary sources were spatially restricted. The possibility that Ordovician arc source rocks are presently buried beneath the Gaspé Belt cannot be ruled out.

Peaks of Late Ordovician to early Silurian zircon ages (from 448–442 Ma) were identified in three samples of the Saint-Victor Formation (13SV08, 05 and 03). Such ages can be interpreted as originating from the erosion of youngest volcanic facies of the Ascot Complex ($441^{+7}/_{-12}$ Ma, David and others, 1993). On the basis of stratigraphic relations between the Ascot Complex phyllites (which correlate with the Saint-Daniel Mélange) and the various assemblages of volcanic rocks in the Ascot Complex, Tremblay and Pinet (2016) have however questioned the geological significance of the latter age range, and stressed that these "younger" volcanic rocks are essentially part of the same volcanic sequence that is stratigraphically located below the Saint-Daniel Mélange and was formed at *ca.* 460 Ma unit. Hence, the contribution of the Ascot Complex remains contentious in terms of possible Late Ordovician source rocks.

Alternative sources for these Late Ordovician-early Silurian zircon grains can be proposed, (1) the early Silurian volcaniclastic rocks of the Pointe-aux-Trembles Formation (*ca.* 437 Ma; David and Gariépy, 1990) in the Témiscouata area, (2) the Attean pluton (*ca.* 443 Ma; Gerbi and others, 2006) in northwestern Maine, (3) the early Silurian volcanic rocks of the Clinton River Formation, and correlative Smalls Falls Formation in New Hampshire, and/or (4) the Lost Nation pluton (*ca.* 442 Ma; Moench and Aleinikoff, 2003) near the New Hampshire-Vermont border. However, considering the volume and the proximity of the Bronson Hill arc volcanic massif, and the age of the Quimby sequence (the youngest volcanic series of Bronson Hill sequence; 454–442 Ma, Stanley and Ratcliffe, 1985; Tucker and Robinson, 1990;

Moench, 1993), this arc sequence is considered here as a major source for Late Ordovician to early Silurian detrital zircons during the deposition of the top of the Magog Group. This hypothesis is moreover supported by the fact that the zircon age distribution of the top samples of the sequence (SV03 and SV04) is similar to those presented by Bradley and O'Sullivan (2016) in their first Acadian detrital zircon cycle of the Central Maine Basin, a sedimentary basin that lies east of Connecticut Valley-Gaspé trough, on the eastern side of the Bronson Hill Anticlinorium, which is considered as its main detrital source (Bradley and O'Sullivan (2016). More distal sources can be also proposed, like the porphyric and dioritic units of the Pumpkin Ground orthogneiss in southwestern Connecticut that yielded a U-Pb zircon ages of 448 ± 3 Ma and 443 ± 2 Ma, which are, however, mantled by overgrowth rims with a mean age of 431 ± 4 Ma (Wathen and others, 2015).

Middle Silurian sources.—Peaks of Wenlock zircon epoch (*ca.* 430 Ma) characterize the two uppermost stratigraphic samples of the Saint-Victor Formation (13SV04 and 03). All potential sources for these zirons are present east of the Saint-Victor Formation. Two potential proximal sources exist in the southern Québec and New Hamphshire, the Frontenac Formation, which has been dated at 432 ± 10 Ma (Moench and others, 1995) and the East Inlet granite which yielded a U-Pb crystallization age of 430 ± 4 Ma (Lyons and others, 1986).

Tectonic Implications for the Quebec Appalachians

Originally, the Quebec Dunnage Zone, including the Magog Group, has been defined as belonging to the Notre-Dame subzone (Tremblay and others, 1995). However, geochronological data and detailed mapping (Schroetter and others, 2006; de Souza and others, 2014, this study) raise problems regarding the inclusion of whole units of the Magog Group into the Dunnage Zone. Tremblay and Pinet (2016) recently proposed to subdivide the Magog Group into lower and upper sequences, and to exclude the upper sequence from the Dunnage Zone and instead include it in the lower part of the Gaspé Belt. Our detrital U-Pb zircon ages results are consistent with this suggestion, as it indicates that the Saint-Victor Formation was mostly deposited during the Late Ordovician and early Silurian on a basement of accreted rocks of the Humber and Dunnage zones, including the lower stratigraphic units (Frontière, Etchemin and Beauceville formations) of the Magog Group.

Detrital zircons U-Pb ages of the Saint-Victor Formation and stratigraphic relationships discussed in this contribution can be reconciled with paleotectonic evolutionary models of the Quebec-New England Appalachians as recently proposed by Tremblay and Pinet (2016). The U-Pb data furnish constraints about the timing of sedimentation and provenance of the lower and the upper Magog Group sequences and allow us to speculate on the tectonic evolution of this sedimentary basin between Middle Ordovician and late Silurian times. The basic assumptions for our tectonic interpretation are the following, (1) the Taconian orogeny started with the Early-to-Middle Ordovician ophiolites emplacement onto Laurentia, and the progressive accretion of peri-Laurentian oceanic terranes during Middle-to-Late Ordovician times (Tremblay and Pinet, 2016 and cited references); (2) the tectonic convergence between Laurentia and outboard oceanic terranes was accommodated by east-dipping (present coordinates) subduction during most of the Ordovician (for example Osberg, 1978; Stanley and Ratcliffe, 1985; Robinson and others, 1998; van Staal and Barr, 2012; Tremblay and Pinet, 2016); (3) the Salinic orogeny is considered as a mid-Silurian (430–422 Ma) collision between Gander (Gondwana) and composite Laurentia following subduction reversal (from SE- to NW-dipping) during the Late Ordovician closure of a Japan Sea-type backarc basin (van Staal and Barr, 2012). In southern Québec, the Salinic includes the hinterland-directed folds, backthrusts and associated retrograde low-grade metamorphism of the Laurentian margin (Tremblay and Pinet, 2016).

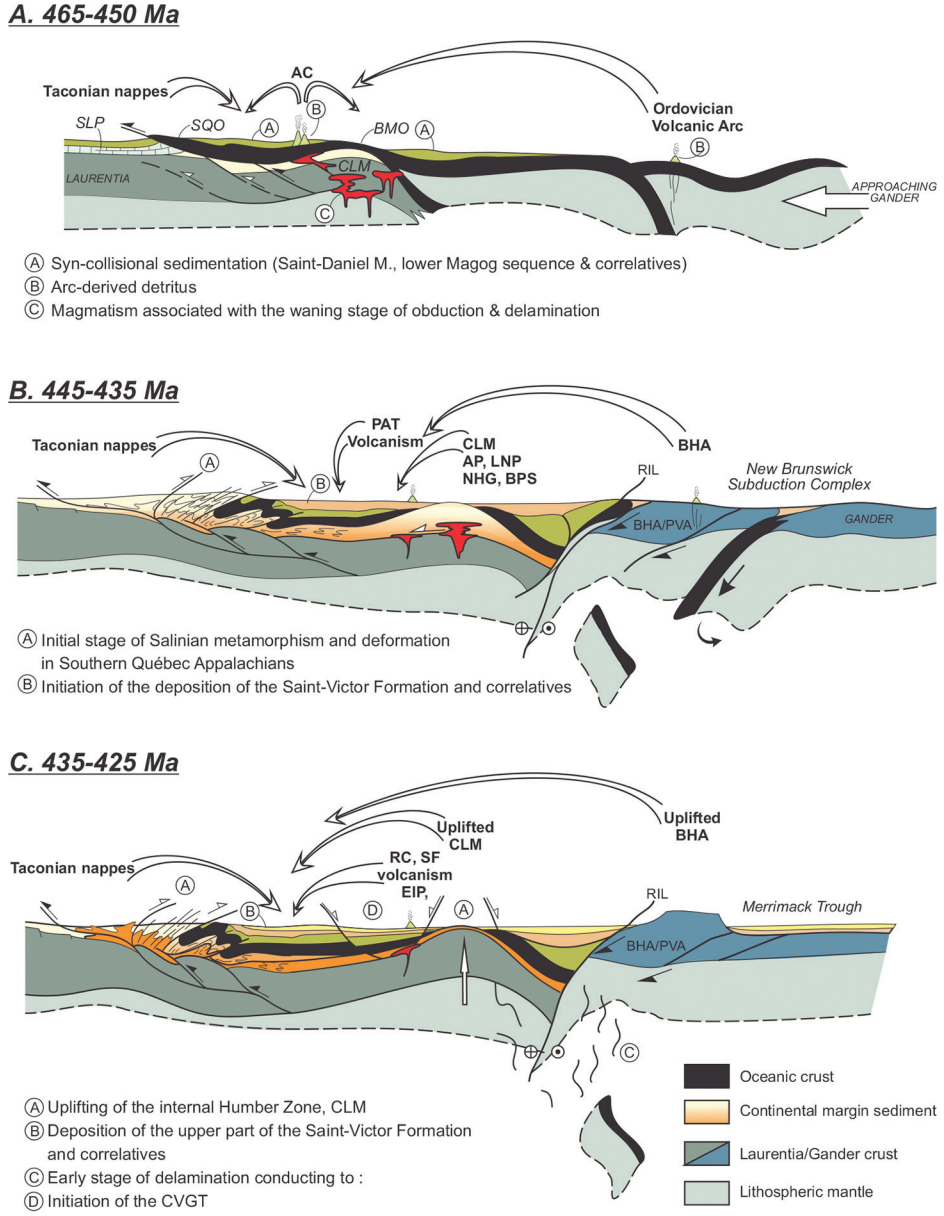

Fig. 13. Schematic model for the tectonostratigraphic and paleogeographic evolution of the southern Quebec Appalachians between Middle Ordovician and upper Silurian time. Modified from Tremblay and Pinet (2016). Zircon detrital record discussed in this study are illustrated by large arrows which show inferred sources. (A) Climax stage of the Taconian orogeny and deposition of the lowermost units of the Magog Group. (B) Initial stage of the Salinic orogeny and onset of sedimentation of the Saint-Victor Formation. (C) Collision between Gander and composite Laurentia during the Salinic orogeny and coeval uplifting of the internal Humber Zone. Age brackets are approximate. AC – Ascot Complex; AP – Attean Pluton; BHA/PVA – Bronson Hill and Popelogan-Victoria arcs; BMO – Boil Moutain ophiolite; BPS – Brookfield plutonic series; CLM – Chain Lakes Massif; CVGT – Connecticut Valley-Gaspé Trough; EIP – East Inlet Pluton; LNP – Lost Nation Pluton; NHG – Newtown and Harrison gneisses; PAT – Pointe-aux-Trembles; RC – Clinton River; RIL – Red Indian Line; SF – Small Falls; SLP – St. Lawrence platform ; SQO – Southern Quebec ophiolite.

In figure 13, we propose a schematic model illustrating the principal tectonic implications for Ordovician-to-Silurian sedimentation of the Magog Group, evolving from a syn-Taconian forearc basin setting for the lower Magog sequence to a syn-Salinic sedimentary basin for the upper Magog sequence.

(1) 465–450 Ma.—The progression of Taconic deformation in the Laurentian margin led to the formation of a piggyback basin represented by the Saint-Daniel Mélange (Schroetter and others, 2006; de Souza and others, 2014) and the deposition of the lowermost units of the Magog Group (fig. 13A). The progressive emplacement of the Iapetan oceanic crust onto Laurentia led to the syncollisionnal exhumation of accreted ophiolites and underlying continental material during the deposition of the lower Magog Group sequence. The Ascot Complex arc volcanism and more distal Ordovician volcanism, as recorded by the Ammonoosuc sequence and the Shelbourn Falls arc in New England, were coeval with sedimentation of this lower sequence.

(2) 445-435 Ma.—By the end of the Ordovician (fig. 13B), the initial stage of the Salinic orogeny has been attributed to subduction reversal (see, for instance, van Staal and Barr, 2012). We believe that this has been related to the onset of sedimentation of the Saint-Victor Formation. In southern Quebec, Salinic deformation is attributed to thick-skin thrusting during which NW-directed thrusts in the Laurentian margin continued to develop synchronously with SE-directed structures associated with the growth and uplift of the internal Humber Zone (Tremblay and Pinet, 2016). Existing geochronological isotopic constraints (summarized in Tremblay and Pinet, 2016) suggest that the earliest stage of Salinic deformation are Llandoverian (445–435 Ma). Such timing is almost perfectly coeval with our detrital U-Pb data for the the Saint-Victor Formation, suggesting that the upper Magog sequence can be interpreted as a synorogenic (syn-Salinic) sedimentary sequence. The main erosional sources available during the onset of sedimentation of the Saint-Victor Formation were Late Ordovician rocks, which are mainly represented by the volcanics of the Pointe-aux-Trembles Formation, the metamorphic and plutonic rocks of the Chain Lakes Massif and of the Attean and Lost Nation plutons, and the youngest volcanic rocks of the Bronson Hill arc (that is the Quimby sequence, see for example, Bradley and O'Sullivan, 2016).

(3) 435–425 Ma.—By mid-Silurian times (fig. 13C), a full collision between Gander and composite Laurentia was initiated. Various breccias and conglomerates towards the upper part of the Saint-Victor Formation (Mercier, ms, 2013) attest for the development of a more tectonically active sedimentary environment. Taking into account a significant increase of 900 to 1950 Ma zircons in the uppermost stratigraphic samples, we propose that, due to active Salinic deformation, clastic detritus were originated from both sides of the Saint-Victor sedimentary basin : the Laurentian margin (Humber Zone) to the NW and uplifted peri-Laurentian (for instance, the Chain Lake Massif) and/or peri-Gondwanan terranes (such as the Bronson Hill Arc) to the SE.

CONCLUSION

This contribution focuses on the stratigraphy and geochronology of the Magog Group to better constrain its depositional ages and investigate the paleogeography and tectonic setting of its stratigraphical formations. Detrital zircon age data for each of the analyzed samples have been interpreted in function of their particular environment, taking into account the occurrence of well-dated fossils occurrences.

The most outstanding result is the relative abundance of Silurian zircons in the stratigraphically uppermost samples. Such young detrital populations indicate that the upper part of the Magog Group, represented by the Saint-Victor Formation, is not exclusively Ordovician and extends from upper Katian (450–445 Ma) to Wenlock times (*ca.* 430 Ma). Combined with fossil age constraints and inferred stratigraphic

correlations in adjacent areas, our detrital zircon U-Pb geochronology study indicate that the Saint-Victor Formation should be considered as a syn-Salinic sequence, separated from the lower Magog Group sequence by an unconformity corresponding to a sedimentary hiatus of $\leq$ 10 m.y. This study also implies that the Saint-Victor Formation should be excluded from the Dunnage Zone and reassigned to the base of the Gaspé Belt sequence. The Magog Group can thus be considered as a syn-Taconian Middle-Late Ordovician forearc basin which has evolved during the Silurian time as a syn-Salinic peri-continental basin, and thus provides the opportunity to study the formation and evolution of a sedimentary basin deposited during the time period between the Taconian and Salinic orogenies in southern Québec.

The evolution of detrital zircon populations of the Magog Group sedimentary sequence reflects a dual source progression between the West and East of the basin. To the NW, the southern Quebec ophiolites and adjacent sedimentary rocks of the Laurentian margin are considered as the main erosional sources for the sedimentation of the Magog Group. To the SE, volcanic arc rocks of the Ascot Complex are considered as a major source, more distal volcanic arc units preserved in the Shelburne Falls and Bronson Hill massifs are considered as potential sources for Late Ordovician to early Silurian detrital zircons, whereas the Frontenac Formation and the East Inlet granitic pluton are currently the two most likely proximal youngest sources for middle Silurian zirons found towards the top of the Saint-Victor Formation. At the scale of the Quebec Appalachians, sedimentary and paleogeographic studies for correlative units in the Temiscouata and Gaspé Peninsula (David and others, 1985; Bourque and others, 2000; Malo, 2004) suggest that the same types of sources were presumably present along the strike of the orogen. At the scale of the Appalachians-Caledonides belt, the Dunnage zone sequences of southern Québec and northwestern New England have been recently compared with the South Mayo Trough of Western Ireland (de Souza and others, 2014); the Ordovician strata of these sequences yielding similar detrital age distributions (see Mange and others, 2010; Yin and others, 2012). However, detrital zircon provenance data are currently lacking in Temiscouata and Gaspé Peninsula areas, as well as in Silurian strata unconformably lying on the South Mayo Trough sequence. A comparative U-Pb geochronological study of the Cabano and Honorat groups in Quebec, as well as in Silurian strata of the South Mayo area, would be usefull to determine the nature of along-strike variations, if any, of erosional source terranes at different scales.

ACKNOWLEDGMENTS

This contribution is part of the first author's Ph. D. thesis at the *University du Québec à Montreal (UQAM)*. Sincere thanks are due to André Poirier for help in using the HR-LA-ICP-MS laboratory. This study was supported by the Natural Sciences and Engineering Research Council of Canada (NSERC) through an operating grant (PG105669) to A. Tremblay, and by a Geotop grant to M. Perrot. J. D. Eusden and G. Walsh are sincerely acknowledged for providing comments and constructive reviews of the manuscript. We also thank H. Dubé-Loubert for the critical reading of an earlier version and M. Valette for providing a field photograph for the Frontière Formation sampling site and her assistance in the field.

APPENDIX I

Data reporting table for LA-ICP-MS U-Pb analyses

Laboratory & Sample Preparation	
Laboratory name	Geotop, University of Quebec in Montreal
Sample type/mineral	Detrital zircons
Sample preparation	Conventional mineral separation, 1 inch resin mount, 1µm polish to finish
Imaging	CL, Centaurus, Hitachi S-3400N SEM
Laser ablation system	
Make, Model and type	Photon-machine G2
Ablation cell and volume	Helex, 2-volume cells with squid smoothing device
Laser wavelength (nm)	193 nm
Pulse width (ns)	4 ns
Fluence ($J.cm^{-2}$)	3 $J.cm^{-2}$
Repetition rate (Hz)	5 Hz
Ablation duration (secs)	40 secs
Ablation pit depth / ablation rate	Not available
Spot diameter (µm) nominal/actual	40 µm / 30 µm
Sampling mode / pattern	Static spot ablation
Carrier gas	100% He in the cell, 35% Ar along the sample transport line to the torch.
Cell carrier gas flow (l/min)	0.7 l/min He in the 1st volume cell 0.5/min He in the 2nd volume cell
ICP-MS Instrument	
Make, Model and type	HR ICP-MS (Atom, Nu Instruments)
Sample introduction	Ablation aerosol from laser to torch
RF power (W)	1375W
Make-up gas flow (l/min)	Sourced from Atom (estimated at 0.7 l/min) Ar.
Detection system	Secondary ion multiplier
Masses measured	202, 204, 206, 207, 208, 232, 235, 238.
Integration time per peak/dwell times (ms)	500ms for each isotope
Total integration time per output datapoint (secs)	~0.6secs
'Sensitivity' as useful yield (%, element)	0.4% U (NIST610 = 500ppm, #atoms sampled: 500ppm*85um*3Hz*3J/cm^2, #ions detected: >25 mcps)
IC Dead time (ns)	20 ns
Gas blank	30 second on-peak zero subtracted
Calibration strategy	91500 used as primary reference material, Ybr377 used as secondaries/validation
Reference Material info	91500 (Wiedenbeck and others, 1995) Ybr377 (David and others, 2010)
Data processing package used / Correction for LIEF	Iolite 2.5 (with Igor Pro 6) and Isoplot 4.1 softwares. laser-induced elemental fractionation correction assumes reference material and samples behave identically.
Mass discrimination	N/A - Down-hole effect with Iolite.
Common-Pb correction, composition and uncertainty	No common-Pb correction applied to the data.
Uncertainty level and propagation	Ages are quoted at 2*s* absolute, propagation is from Iolite software. Reproducibility and age uncertainty of reference material and common-Pb composition uncertainty are propagated where appropriate.
Quality control / Validation	91500. TIMS: 91500 - Weighted average $^{206}Pb/^{238}U$ age 1066.2±0.6 (2s, MSWD=1.14).

APPENDIX II

HR-LA-ICP-MS U-Pb zircon data for rocks of the Magog Group

Sample/grain	Data for Wetherill plot[1]					Data for Tera-Wasserburg plot[1]					Dates[1] (Ma)						Uppm[2]	% conc.[3]
	$\frac{^{207}Pb}{^{235}U}$	2σ abs	$\frac{^{206}Pb}{^{238}U}$	2σ abs	Rho	$\frac{^{238}U}{^{206}Pb}$	2σ abs	$\frac{^{207}Pb}{^{206}Pb}$	2σ abs	Rho	$\frac{^{207}Pb}{^{235}U}$	2σ abs	$\frac{^{206}Pb}{^{238}U}$	2σ abs	$\frac{^{207}Pb}{^{206}Pb}$	2σ abs		
13FR01																		
13FR01_18	0.536	0.013	0.06882	0.00082	0.38	14.53066	0.17313	0.0575	0.0012	0.09	435.2	8.8	429.1	4.9	512	49	45.4	N/A
13FR01_34	0.638	0.024	0.0692	0.0014	0.00	14.45087	0.29236	0.0669	0.0023	0.22	500	15	431.1	8.5	816	74	19.5	N/A
13FR01_69	0.615	0.03	0.0694	0.0013	0.05	14.40922	0.26991	0.0649	0.0034	0.26	485	18	432.3	7.9	730	100	20.6	N/A
13FR01_36	0.656	0.027	0.0703	0.0012	0.61	14.22475	0.24281	0.0674	0.0022	0.26	511	16	437.6	7.5	835	65	84.7	N/A
13FR01_61	0.542	0.016	0.0708	0.0018	0.31	14.12429	0.35909	0.0556	0.0015	0.01	439	10	441	11	423	60	25.5	N/A
13FR01_32	0.728	0.038	0.071	0.0017	0.89	14.08451	0.33723	0.074	0.0025	0.69	557	22	442	10	1053	62	78.4	N/A
13FR01_41	0.571	0.017	0.0711	0.0017	0.44	14.0647	0.33629	0.0592	0.0018	0.27	460	11	443	10	573	62	32.21	N/A
13FR01_65	0.575	0.021	0.0711	0.0017	0.57	14.0647	0.33629	0.0581	0.0015	0.16	461	14	443	10	544	56	32.93	N/A
13FR01_23	0.56	0.014	0.07144	0.00069	0.44	13.99776	0.1352	0.0565	0.0013	0.11	450.9	9	444.8	4.2	472	48	40	N/A
13FR01_75	0.583	0.016	0.0716	0.0018	0.68	13.96648	0.35111	0.0597	0.0013	0.20	468	11	446	11	587	47	47	N/A
13FR01_57	0.637	0.04	0.0718	0.0029	0.27	13.92758	0.56253	0.0628	0.0035	0.33	497	25	447	17	690	110	10.7	N/A
13FR01_101	0.656	0.017	0.072	0.0018	0.58	13.88889	0.34722	0.0664	0.0015	0.39	513	11	448	11	818	45	73.9	N/A
13FR01_50	0.578	0.019	0.0722	0.0015	0.59	13.85042	0.28775	0.0578	0.0015	0.01	462	12	449.4	9.2	532	58	19.47	N/A
13FR01_54	0.81	0.1	0.0726	0.0026	0.31	13.7741	0.49329	0.0759	0.008	0.05	574	45	451	15	970	190	5.53	N/A
13FR01_39	0.588	0.02	0.0726	0.0013	0.33	13.7741	0.24664	0.0588	0.0018	0.02	469	13	451.8	8.1	547	65	34.5	N/A
13FR01_49	0.577	0.018	0.073	0.0016	0.73	13.69863	0.30024	0.0579	0.0011	0.04	462	11	453.9	9.4	522	41	51.5	N/A
13FR01_58	0.588	0.018	0.0731	0.0021	0.60	13.67989	0.39299	0.0582	0.0014	0.12	469	11	454	13	529	54	39.5	N/A
13FR01_85	0.629	0.027	0.0734	0.0026	0.20	13.62398	0.48259	0.0623	0.0028	0.42	494	17	456	16	676	88	14.74	N/A
13FR01_29	0.562	0.019	0.0734	0.0015	0.30	13.62398	0.27842	0.0557	0.0019	0.19	452	13	456.4	9.1	461	77	16.11	N/A
13FR01_109	0.619	0.04	0.0738	0.0016	0.13	13.55014	0.29377	0.0618	0.0041	0.03	486	23	458.8	9.6	620	130	13.8	N/A
13FR01_22	0.698	0.028	0.0739	0.0014	0.17	13.5318	0.25635	0.0692	0.0029	0.32	536	17	459.7	8.4	899	82	17.32	N/A
13FR01_19	0.67	0.061	0.074	0.002	0.65	13.51351	0.36523	0.066	0.0048	0.46	514	35	460	12	770	150	16.17	N/A
13FR01_24	0.6221	0.008	0.0741	0.0013	0.51	13.49528	0.23676	0.06127	0.0007	0.62	491.1	5.1	460.5	7.9	647	24	130.5	N/A
13FR01_12	0.792	0.044	0.0745	0.0021	0.55	13.42282	0.37836	0.0774	0.0037	0.12	594	25	463	12	1118	94	29.67	N/A
13FR01_35	0.587	0.02	0.0745	0.0025	0.80	13.42282	0.45043	0.0576	0.0011	0.08	468	13	463	15	515	44	55.8	N/A
13FR01_45	0.581	0.013	0.0745	0.0018	0.69	13.42282	0.32431	0.05704	0.00093	0.44	464.6	8.6	463	11	497	34	54.9	N/A
13FR01_53	0.792	0.069	0.0745	0.0019	0.36	13.42282	0.34233	0.0755	0.0055	0.14	585	38	463	11	1020	140	51.3	N/A
13FR01_46	0.61	0.023	0.0746	0.0015	0.47	13.40483	0.26953	0.0603	0.0021	0.26	482	15	463.9	8.8	595	75	29.5	N/A
13FR01_15	0.616	0.025	0.0747	0.0015	0.68	13.38688	0.26881	0.0612	0.0022	0.46	486	15	465.7	9.2	630	73	27.7	N/A
13FR01_74	0.654	0.037	0.0752	0.0022	0.72	13.29787	0.38903	0.0624	0.0026	0.25	508	22	467	13	677	90	30.1	69
13FR01_60	0.63	0.028	0.0754	0.0017	0.14	13.2626	0.29902	0.0617	0.0029	0.13	495	17	468	10	636	92	22.69	74
13FR01_84	0.627	0.026	0.0752	0.0022	0.05	13.29787	0.38903	0.0595	0.0028	0.52	493	16	468	13	590	110	18.44	79
13FR01_44	0.74	0.037	0.076	0.0016	0.25	13.15789	0.27701	0.0703	0.0031	0.03	560	22	472.2	9.4	951	91	16.66	50
13FR01_28	0.66	0.031	0.07605	0.00098	0.42	13.14924	0.16944	0.0647	0.0028	0.15	516	18	472.5	5.9	779	76	36.9	61

APPENDIX II

(continued)

Sample/grain	Data for Wetherill plot[1]					Data for Tera-Wasserburg plot[1]					Dates[1] (Ma)						Uppm[2]	% conc.[3]
	$\frac{^{207}Pb}{^{235}U}$	2σ abs	$\frac{^{206}Pb}{^{238}U}$	2σ abs	Rho	$\frac{^{238}U}{^{206}Pb}$	2σ abs	$\frac{^{207}Pb}{^{206}Pb}$	2σ abs	Rho	$\frac{^{207}Pb}{^{235}U}$	2σ abs	$\frac{^{206}Pb}{^{238}U}$	2σ abs	$\frac{^{207}Pb}{^{206}Pb}$	2σ abs		
13FR01																		
13FR01_20	0.632	0.026	0.0763	0.0018	0.63	13.10616	0.30919	0.0596	0.0019	0.06	496	16	474	11	596	69	20.62	80
13FR01_114	0.788	0.057	0.0765	0.0015	0.18	13.0719	0.25631	0.0746	0.0055	0.19	585	30	474.9	9.2	1000	130	20.74	47
13FR01_72	0.633	0.021	0.0767	0.0022	0.27	13.03781	0.37397	0.0604	0.0018	0.29	497	13	476	13	603	66	45.1	79
13FR01_110	0.741	0.075	0.0769	0.0022	0.02	13.0039	0.37202	0.0698	0.0071	0.06	555	39	478	13	820	160	18.08	58
13FR01_77	0.695	0.037	0.0774	0.0019	0.46	12.9199	0.31716	0.065	0.0032	0.19	533	21	481	11	739	99	33.32	65
13FR01_10	0.868	0.067	0.0778	0.0028	0.78	12.85347	0.46259	0.0799	0.0041	0.61	630	36	483	17	1171	98	25.94	41
13FR01_2	0.635	0.024	0.078	0.0015	0.38	12.82051	0.24655	0.0592	0.002	0.07	498	15	484.2	8.8	557	74	16.54	87
13FR01_88	0.674	0.039	0.0782	0.0021	0.03	12.78772	0.3434	0.0629	0.0043	0.44	520	23	485	13	670	130	5.74	72
13FR01_99	0.892	0.079	0.0792	0.0013	0.25	12.62626	0.20725	0.0818	0.007	0.07	639	40	491.1	7.7	1160	150	14.3	42
13FR01_112	0.749	0.034	0.0816	0.0014	0.31	12.2549	0.21026	0.0667	0.0026	0.17	560	14	505.4	8.4	788	63	30.6	64
13FR01_113	0.861	0.035	0.0817	0.0036	0.76	12.2399	0.53933	0.0758	0.0024	0.40	629	19	506	21	1095	63	65.5	46
13FR01_79	0.797	0.034	0.0883	0.0029	0.79	11.32503	0.37194	0.0662	0.0017	0.23	593	20	545	17	822	50	24	66
13FR01_64	0.756	0.035	0.0914	0.0038	0.83	10.94092	0.45487	0.0601	0.0013	0.29	574	22	563	22	601	48	15.9	94
13FR01_87	1.208	0.017	0.1211	0.0026	0.53	8.257638	0.17729	0.0725	0.0013	0.59	804	7.8	737	15	1002	33	75	74
13FR01_14	1.473	0.057	0.1454	0.0042	0.32	6.877579	0.19866	0.0737	0.0026	0.27	920	23	874	24	1030	69	10.16	85
13FR01_33	1.428	0.034	0.1473	0.0037	0.79	6.788866	0.17053	0.07047	0.00098	0.18	899	14	885	21	939	28	34.27	94
13FR01_86	1.54	0.079	0.1496	0.0066	0.64	6.684492	0.2949	0.075	0.003	0.10	942	32	898	37	1079	80	6.87	83
13FR01_42	1.94	0.3	0.1523	0.0065	0.80	6.565988	0.28023	0.0873	0.0082	0.60	1038	70	913	36	1300	140	11.58	70
13FR01_78	1.61	0.047	0.1596	0.005	0.88	6.265664	0.19629	0.0734	0.0012	0.23	972	18	954	28	1022	34	22.75	93
13FR01_47	1.75	0.052	0.1604	0.0044	0.77	6.234414	0.17102	0.0802	0.0015	0.17	1028	19	958	25	1198	38	19.06	80
13FR01_1	1.707	0.031	0.1653	0.0028	0.67	6.049607	0.10247	0.0748	0.0012	0.24	1010	12	986	16	1066	34	9.75	92
13FR01_81	1.85	0.12	0.1693	0.0085	0.19	5.906675	0.29655	0.0807	0.006	0.32	1069	43	1006	47	1170	140	12.11	86
13FR01_71	2.026	0.055	0.1703	0.0043	0.48	5.871991	0.14827	0.0866	0.002	0.21	1129	20	1013	24	1354	46	14.96	75
13FR01	1.851	0.052	0.1756	0.0022	0.66	5.694761	0.07135	0.0774	0.0014	0.03	1062	19	1043	12	1128	38	20.5	92
13FR01_80	1.939	0.079	0.1783	0.0051	0.61	5.608525	0.16042	0.0794	0.0027	0.05	1096	27	1057	28	1178	64	18.61	90
13FR01_97	1.892	0.067	0.1787	0.0058	0.71	5.595971	0.18163	0.0785	0.0021	0.02	1076	23	1059	32	1149	54	13.3	92
13FR01_96	2.004	0.039	0.1887	0.0047	0.55	5.299417	0.13199	0.0779	0.0017	0.60	1116	13	1114	26	1146	44	21.88	97
13FR01_104	2.326	0.038	0.2044	0.0041	0.84	4.892368	0.09813	0.0824	0.00075	0.13	1220	12	1199	22	1258	17	67.1	95
13FR01_13	2.409	0.072	0.2054	0.0057	0.74	4.868549	0.13511	0.0865	0.0016	0.48	1254	19	1204	31	1346	37	12.82	89
13FR01_55	2.903	0.068	0.2299	0.0045	0.78	4.349717	0.08514	0.092	0.0012	0.08	1381	18	1333	24	1470	26	21.8	91
13FR01_9	2.82	0.08	0.2361	0.0047	0.55	4.235493	0.08432	0.0878	0.0024	0.08	1359	21	1366	25	1369	53	5.03	100
13FR01_63	2.97	0.17	0.238	0.011	0.98	4.201681	0.1942	0.091	0.0018	0.45	1389	51	1375	58	1448	39	19.26	95
13FR01_82	3.051	0.083	0.238	0.0076	0.80	4.201681	0.13417	0.0942	0.0018	0.40	1422	22	1375	40	1507	36	12.16	91
13FR01_94	2.973	0.075	0.2404	0.0071	0.88	4.159734	0.12285	0.0898	0.0011	0.35	1402	19	1388	37	1424	22	31.68	97

APPENDIX II

(continued)

Sample/grain	Data for Wetherill plot[1]					Data for Tera-Wasserburg plot[1]					Dates[1] (Ma)						Uppm[2]	% conc.[3]
	$^{207}Pb/^{235}U$	2σ abs	$^{206}Pb/^{238}U$	2σ abs	Rho	$^{238}U/^{206}Pb$	2σ abs	$^{207}Pb/^{206}Pb$	2σ abs	Rho	$^{207}Pb/^{235}U$	2σ abs	$^{206}Pb/^{238}U$	2σ abs	$^{207}Pb/^{206}Pb$	2σ abs		
13FR01																		
13FR01_67	3.6	0.13	0.2491	0.0064	0.74	4.014452	0.10314	0.1056	0.0024	0.23	1546	29	1433	33	1726	43	8.56	83
13FR01_17	3.715	0.057	0.2685	0.0043	0.60	3.724395	0.05965	0.1014	0.0012	0.31	1576	12	1533	22	1648	22	32.4	93
13FR01_66	3.934	0.098	0.2813	0.0068	0.75	3.554924	0.08593	0.1013	0.0018	0.12	1619	21	1597	34	1645	34	15.8	97
13FR01_83	4.85	0.32	0.303	0.014	0.39	3.30033	0.15249	0.1191	0.0043	0.10	1804	48	1704	69	1929	64	8.51	88
13FR01_103	5.36	0.12	0.3349	0.0079	0.96	2.985966	0.07044	0.11605	0.00085	0.22	1876	20	1861	39	1896	13	62.4	98
13FR01_76	9.28	0.26	0.408	0.012	0.97	2.45098	0.07209	0.1667	0.0012	0.26	2363	27	2203	54	2524	12	31.9	87
13FR01_106	11.17	0.17	0.475	0.0099	0.89	2.105263	0.04388	0.1709	0.0018	0.13	2536	15	2504	44	2566	17	24.8	98
13FR01_93	13.11	0.41	0.505	0.016	0.81	1.980198	0.06274	0.1917	0.0043	0.42	2688	30	2633	69	2752	36	5.1	96
13FR01_98	12.96	0.33	0.508	0.013	0.80	1.968504	0.05038	0.1864	0.0022	0.24	2677	25	2646	58	2709	20	9.72	98
13FR01_108	13.23	0.25	0.513	0.013	0.91	1.949318	0.0494	0.1875	0.0016	0.43	2694	19	2667	56	2720	14	26.1	98
13FR01_95	13.2	0.34	0.523	0.013	0.97	1.912046	0.04753	0.1827	0.0015	0.27	2691	25	2709	57	2682	13	17.53	101
13FR01_105	14.3	0.32	0.524	0.011	0.94	1.908397	0.04006	0.1972	0.0024	0.50	2768	22	2716	47	2802	20	8.99	97
13FR01_90	14.51	0.25	0.536	0.01	0.87	1.865672	0.03481	0.1984	0.0018	0.48	2782	17	2767	44	2812	15	14.61	98
13FR01_89	14.7	0.34	0.535	0.013	0.95	1.869159	0.04542	0.2017	0.0015	0.14	2797	22	2771	51	2839	12	22.77	98
13SV06																		
13SV06-49	0.642	0.035	0.06763	0.00097	0.39	14.78634	0.21208	0.0686	0.0033	0.11	502	21	421.8	5.8	880	99	19.48	N/A
13SV06-03	0.6	0.042	0.0679	0.0014	0.83	14.72754	0.30366	0.0656	0.0039	0.65	475	26	423.2	8.4	760	120	22.7	N/A
13SV06-07	0.678	0.038	0.0694	0.0012	0.47	14.40922	0.24915	0.0705	0.0034	0.14	523	23	432.8	7.2	960	100	12.25	N/A
13SV06-21	0.61	0.032	0.0699	0.001	0.35	14.30615	0.20467	0.0641	0.0032	0.02	482	20	435.7	6.2	720	100	20.48	N/A
13SV06-17	0.74	0.022	0.07014	0.00073	0.18	14.2572	0.14839	0.0769	0.0026	0	562	13	437	4.4	1108	67	23.74	N/A
13SV06-41	0.69	0.057	0.0712	0.0018	0.03	14.04494	0.35507	0.069	0.0058	0.16	528	34	443	11	870	160	14.1	N/A
13SV06-63	0.63	0.021	0.07231	0.00073	0.55	13.82935	0.13961	0.0632	0.0018	0.28	495	13	450	4.4	706	60	39.37	N/A
13SV06-47	0.586	0.017	0.0727	0.001	0.37	13.75516	0.1892	0.058	0.0014	0.39	468	11	452.5	6.1	547	45	21.21	N/A
13SV06-57	0.599	0.023	0.0727	0.0022	0.3	13.75516	0.41625	0.06	0.0023	0.25	476	15	453	13	607	74	26.34	N/A
13SV06-55	0.588	0.024	0.0729	0.0014	0.27	13.71742	0.26343	0.0593	0.002	0.18	469	15	453.6	8.5	568	73	22.44	N/A
13SV06-83	0.56	0.017	0.073	0.0011	0.43	13.69863	0.20642	0.0557	0.0014	0.08	456	11	454.5	6.8	433	57	25.31	N/A
13SV06-48	0.61	0.023	0.0733	0.0013	0.11	13.64256	0.24196	0.0602	0.0021	0.31	483	15	455.8	7.6	618	85	15.48	N/A
13SV06-52	0.6	0.025	0.0734	0.0013	0.44	13.62398	0.2413	0.0603	0.0023	0.09	477	16	456.6	7.7	596	83	18.6	N/A
13SV06-69	0.608	0.032	0.07342	0.00084	0.29	13.62027	0.15583	0.0599	0.003	0.12	481	20	456.7	5	580	100	24.86	N/A
13SV06-68	0.768	0.031	0.0737	0.0014	0.31	13.56852	0.25775	0.0757	0.0031	0.26	577	18	458.4	8.4	1072	83	33.3	N/A
13SV06-09	0.594	0.029	0.0738	0.0012	0.01	13.55014	0.22033	0.0584	0.0031	0.25	472	18	458.9	7.1	520	110	10.11	N/A
13SV06-87	0.634	0.016	0.0739	0.0011	0.01	13.5318	0.20142	0.0627	0.0017	0.49	498.3	9.6	459.6	6.3	692	58	54.5	N/A
13SV06-73	0.768	0.095	0.0741	0.0018	0.29	13.49528	0.32782	0.0723	0.0069	0.14	569	50	461	11	920	170	28.1	N/A
13SV06-27	0.768	0.036	0.07431	0.00082	0.17	13.45714	0.1485	0.075	0.0036	0.12	577	21	462.1	4.9	1040	100	20.29	N/A

APPENDIX II

(continued)

Sample/grain	Data for Wetherill plot[1]					Data for Tera-Wasserburg plot[1]					Dates[1] (Ma)						Uppm[2]	% conc.[3]
	$^{207}Pb/^{235}U$	2σ abs	$^{206}Pb/^{238}U$	2σ abs	Rho	$^{238}U/^{206}Pb$	2σ abs	$^{207}Pb/^{206}Pb$	2σ abs	Rho	$^{207}Pb/^{235}U$	2σ abs	$^{206}Pb/^{238}U$	2σ abs	$^{207}Pb/^{206}Pb$	2σ abs		
13SV06																		
13SV06-06	0.641	0.055	0.0743	0.0013	0.39	13.45895	0.23549	0.0626	0.0044	0.24	499	33	462.2	7.7	650	140	15.7	N/A
13SV06-74	0.706	0.045	0.0744	0.0015	0.13	13.44086	0.27099	0.0699	0.0049	0.02	540	27	462.5	9	880	140	9.59	N/A
13SV06-44	0.613	0.042	0.0746	0.0032	0.24	13.40483	0.57501	0.0595	0.0043	0.21	490	29	463	19	570	160	8.84	N/A
13SV06-80	0.669	0.026	0.0745	0.0012	0.43	13.42282	0.21621	0.0656	0.002	0.16	519	16	463.4	7.2	783	67	29.13	N/A
13SV06-77	0.655	0.018	0.07468	0.00062	0.18	13.39047	0.11117	0.0637	0.0014	0.09	511	11	464.3	3.7	725	45	60.7	N/A
13SV06-32	0.584	0.032	0.0754	0.0028	0.53	13.2626	0.49251	0.0557	0.0026	0.02	465	20	469	17	420	100	20.8	N/A
13SV06-12	0.616	0.018	0.0757	0.0014	0.29	13.21004	0.24431	0.0581	0.0019	0.14	487	12	470.4	8.5	524	73	15.1	N/A
13SV06-76	0.583	0.033	0.0758	0.0014	0.34	13.19261	0.24366	0.0572	0.0027	0.03	465	21	470.7	8.4	480	100	14.48	N/A
13SV06-46	0.666	0.026	0.07578	0.0008	0.28	13.19609	0.13931	0.0624	0.002	0.06	520	16	470.9	4.8	708	68	15.58	N/A
13SV06-61	0.708	0.033	0.0761	0.0024	0.31	13.1406	0.41442	0.0664	0.0033	0.39	542	20	472	14	820	100	22.66	N/A
13SV06-71	0.674	0.051	0.07606	0.00099	0.51	13.14752	0.17113	0.0658	0.0044	0.34	520	30	472.5	6	760	130	21.5	N/A
13SV06-19	0.604	0.022	0.0762	0.0012	0.04	13.12336	0.20667	0.0577	0.0024	0.37	479	14	473.7	7.1	497	94	10.19	N/A
13SV06-34	0.646	0.035	0.077	0.0017	0.37	12.98701	0.28673	0.0617	0.0032	0.08	509	23	478	10	700	120	9.8	N/A
13SV06-65	0.708	0.022	0.07714	0.00088	0.51	12.96344	0.14788	0.0667	0.0016	0.1	551	14	479	5.3	822	51	63.47	N/A
13SV06-78	0.629	0.021	0.079	0.0012	0.14	12.65823	0.19228	0.0586	0.0019	0.25	495	13	490.1	7.2	559	61	36.7	N/A
13SV06-59	0.777	0.023	0.0803	0.0014	0.08	12.4533	0.21712	0.07	0.0025	0.5	583	13	497.6	8.2	928	77	20.82	N/A
13SV06-29	0.959	0.042	0.1019	0.0025	0.75	9.813543	0.24076	0.0666	0.0017	0.38	681	22	626	14	829	58	16.7	76
13SV06-10	1.334	0.052	0.1361	0.003	0.28	7.347539	0.16196	0.0708	0.0027	0.2	863	24	822	17	937	78	8.37	88
13SV06-38	1.41	0.032	0.137	0.0025	0.13	7.29927	0.1332	0.0759	0.0017	0.06	893	13	827	14	1089	44	11.56	76
13SV06-30	1.356	0.027	0.1386	0.0021	0.69	7.215007	0.10932	0.07126	0.00071	0.09	870	12	837	12	964	20	30.3	87
13SV06-75	1.541	0.026	0.1538	0.002	0.64	6.501951	0.08455	0.0727	0.0011	0.29	947	10	922	11	1004	30	37.84	92
13SV06-24	1.653	0.034	0.1544	0.0017	0.3	6.476684	0.07131	0.0783	0.0015	0.17	990	13	925.7	9.7	1152	38	35	80
13SV06-05	1.601	0.056	0.1572	0.0024	0.52	6.361323	0.09712	0.0762	0.0023	0.12	969	22	941	13	1090	59	16.29	86
13SV06-16	1.659	0.047	0.1618	0.0034	0.83	6.18047	0.12987	0.0748	0.0014	0.1	992	18	967	19	1061	37	23.63	91
13SV06-13	1.685	0.06	0.1631	0.0039	0.27	6.131208	0.14661	0.0739	0.0027	0.43	1001	23	974	22	1025	74	8.29	95
13SV06-82	1.662	0.041	0.1646	0.0026	0.71	6.075334	0.09597	0.0745	0.0013	0.19	993	16	982	14	1053	34	25.94	93
13SV06-15	1.679	0.059	0.1673	0.0032	0.24	5.977286	0.11433	0.0736	0.0027	0.42	999	22	997	18	1046	76	4.74	95
13SV06-85	1.671	0.061	0.1683	0.0024	0.27	5.941771	0.08473	0.0729	0.0024	0.17	995	23	1003	13	1000	66	6.78	100
13SV06-84	1.686	0.026	0.1686	0.0019	0.67	5.931198	0.06684	0.07395	0.00083	0.36	1003	9.8	1004	10	1039	23	26.78	97
13SV06-42	1.755	0.032	0.1697	0.0022	0.53	5.892752	0.07639	0.0744	0.0012	0.19	1028	12	1010	12	1050	31	28.65	96
13SV06-14	1.853	0.061	0.1844	0.0028	0.57	5.422993	0.08234	0.075	0.0017	0.18	1068	21	1091	15	1064	47	8.29	103
13SV06-31	1.916	0.061	0.1891	0.0027	0.66	5.288207	0.07551	0.0745	0.0016	0.06	1085	21	1117	14	1050	42	12.17	106
13SV06-18	2.497	0.065	0.1968	0.0045	0.83	5.081301	0.11619	0.0935	0.0016	0.2	1270	19	1158	24	1495	32	16.03	77
13SV06-02	2.684	0.044	0.2266	0.0021	0.74	4.413063	0.0409	0.0892	0.0013	0.22	1323	12	1316	11	1407	27	13.67	94

APPENDIX II

(continued)

Sample/grain	Data for Wetherill plot[1]					Data for Tera-Wasserburg plot[1]					Dates[1] (Ma)						Uppm[2]	% conc.[3]
	$^{207}Pb/^{235}U$	2σ abs	$^{206}Pb/^{238}U$	2σ abs	Rho	$^{238}U/^{206}Pb$	2σ abs	$^{207}Pb/^{206}Pb$	2σ abs	Rho	$^{207}Pb/^{235}U$	2σ abs	$^{206}Pb/^{238}U$	2σ abs	$^{207}Pb/^{206}Pb$	2σ abs		
13SV06																		
13SV06-23	3.394	0.071	0.2626	0.0044	0.89	3.808073	0.06381	0.0942	0.001	0.21	1502	17	1503	22	1511	20	45.04	99
13SV06-36	3.72	0.13	0.2643	0.008	0.82	3.783579	0.11452	0.1067	0.0023	0.64	1572	28	1511	41	1740	40	11.3	87
13SV06-22	3.909	0.093	0.281	0.0048	0.77	3.558719	0.06079	0.1021	0.0019	0.1	1618	20	1596	24	1660	34	15.7	96
13SV06-08	4.005	0.093	0.2864	0.0031	0.5	3.49162	0.03779	0.1019	0.0021	0.03	1634	19	1623	16	1655	38	12.23	98
13SV06-79	4.053	0.099	0.2908	0.0047	0.65	3.43879	0.05558	0.1029	0.0021	0.27	1643	20	1645	24	1673	37	14.25	98
13SV06-58	5.09	0.11	0.3294	0.0057	0.92	3.035823	0.05253	0.1129	0.0012	0.07	1833	19	1835	28	1846	19	32.69	99
13SV06-64	12.31	0.22	0.4659	0.0081	0.49	2.146383	0.03732	0.1892	0.0028	0.49	2627	17	2465	36	2734	25	17.79	90
13SV08																		
13SV08-32	0.638	0.022	0.06508	0.00083	0.32	15.3657	0.19597	0.0706	0.0023	0.06	500	14	406.4	5	954	60	68.8	N/A
13SV08-74	0.611	0.021	0.067	0.0013	0.15	14.92537	0.2896	0.065	0.0025	0.37	486	13	418.2	7.8	778	75	42.8	N/A
13SV08-09	0.5805	0.009	0.0673	0.0017	0.67	14.85884	0.37533	0.0622	0.0011	0.84	464.7	6	420	10	695	43	190.5	N/A
13SV08-44	0.564	0.019	0.0674	0.0018	0.21	14.8368	0.39623	0.0618	0.0025	0.27	454	12	420	11	648	84	36.4	N/A
13SV08-37	0.629	0.03	0.0677	0.0011	0.54	14.77105	0.24	0.0677	0.0034	0.26	494	18	422	6.9	837	91	28.2	N/A
13SV08-60	0.664	0.03	0.0679	0.0012	0.28	14.72754	0.26028	0.0713	0.0032	0.18	516	18	423.2	7.3	964	92	23.95	N/A
13SV08-25	0.593	0.016	0.06833	0.00077	0.16	14.63486	0.16492	0.063	0.0017	0.16	472.4	9.9	426.1	4.6	701	56	58.5	N/A
13SV08-06	0.55	0.017	0.0684	0.0013	0.25	14.61988	0.27786	0.0595	0.0018	0.37	449	11	426.2	7.9	573	68	28.5	N/A
13SV08-50	0.616	0.03	0.0693	0.0016	0.13	14.43001	0.33316	0.0648	0.0033	0.28	486	18	431.9	9.5	760	110	26.2	N/A
13SV08-49	0.614	0.014	0.0694	0.0013	0.44	14.40922	0.26991	0.0637	0.001	0.26	485.6	8.6	432.4	8	729	33	93.9	N/A
13SV08-105	0.624	0.012	0.06942	0.0009	0.02	14.40507	0.18676	0.06532	0.00096	0.48	493.9	7	432.6	5.4	782	31	115.8	N/A
13SV08-38	0.59	0.018	0.0697	0.0013	0.24	14.3472	0.26759	0.062	0.0015	0.27	470	12	434.6	7.8	680	59	31.3	N/A
13SV08-86	0.602	0.014	0.0698	0.0011	0.16	14.32665	0.22578	0.063	0.0016	0.44	480.3	9.3	434.8	6.6	699	53	54.6	N/A
13SV08-10	0.574	0.016	0.0701	0.0012	0.4	14.26534	0.2442	0.0594	0.0014	0.1	460	11	436.4	7.1	577	51	22.55	N/A
13SV08-65	0.582	0.019	0.0702	0.0017	0.13	14.24501	0.34496	0.0609	0.0024	0.5	465	12	437	10	620	84	24.6	N/A
13SV08-01	0.541	0.009	0.0703	0.0012	0.68	14.22475	0.24281	0.05648	0.00092	0.63	438.9	6	438.1	7.2	468	36	70	N/A
13SV08-47	0.649	0.027	0.0701	0.0015	0.09	14.26534	0.30525	0.0681	0.0033	0.2	507	16	438.2	8.4	851	87	32.92	N/A
13SV08-76	0.707	0.021	0.0706	0.002	0.39	14.16431	0.40126	0.0737	0.0028	0.34	542	13	440	12	1035	71	52.3	N/A
13SV08-28	0.691	0.019	0.0709	0.0012	0.43	14.10437	0.23872	0.0688	0.002	0.31	533	12	441.4	7.5	897	58	46.6	N/A
13SV08-90	0.729	0.05	0.0712	0.0026	0.45	14.04494	0.51288	0.0723	0.0037	0.02	553	29	443	16	970	110	39	N/A
13SV08-100	0.653	0.039	0.0712	0.0028	0.63	14.04494	0.55233	0.0673	0.0028	0.08	512	24	443	17	828	88	68.2	N/A
13SV08-66	0.633	0.033	0.0712	0.0015	0.25	14.04494	0.29589	0.0648	0.004	0.11	497	20	443.4	8.8	740	120	36.8	N/A
13SV08-73	0.652	0.038	0.07126	0.00099	0.05	14.03312	0.19496	0.0639	0.0031	0.17	508	23	443.7	6	740	110	63.5	N/A
13SV08-61	0.589	0.036	0.0714	0.0027	0.3	14.0056	0.52962	0.0574	0.0032	0.45	468	23	444	16	470	120	20.21	N/A
13SV08-62	0.554	0.018	0.0713	0.0017	0.55	14.02525	0.3344	0.0573	0.0016	0.29	450	11	444.2	9.9	504	61	67.4	N/A
13SV08-30	0.609	0.023	0.0716	0.0018	0.49	13.96648	0.35111	0.0613	0.0017	0.19	482	14	446	11	641	59	78	N/A

APPENDIX II

(continued)

Sample/grain	Data for Wetherill plot[1]					Data for Tera-Wasserburg plot[1]					Dates[1] (Ma)						Uppm[2]	% conc.[3]
	$^{207}Pb/^{235}U$	2σ abs	$^{206}Pb/^{238}U$	2σ abs	Rho	$^{238}U/^{206}Pb$	2σ abs	$^{207}Pb/^{206}Pb$	2σ abs	Rho	$^{207}Pb/^{235}U$	2σ abs	$^{206}Pb/^{238}U$	2σ abs	$^{207}Pb/^{206}Pb$	2σ abs		
13SV08																		
13SV08-54	0.636	0.037	0.0717	0.0027	0.66	13.947	0.5252	0.0663	0.0028	0.12	498	23	446	16	799	85	82.4	N/A
13SV08-68	0.71	0.036	0.0721	0.0014	0.35	13.86963	0.26931	0.0706	0.0031	0	543	21	448.7	8.4	963	87	28	N/A
13SV08-52	0.652	0.031	0.0721	0.0013	0.77	13.86963	0.25008	0.0662	0.0023	0.57	509	19	448.9	7.8	819	76	234.6	N/A
13SV08-57	0.57	0.01	0.0724	0.0015	0.92	13.81215	0.28616	0.0569	0.0006	0.32	458.2	6.6	450.4	9.2	486	23	135.4	N/A
13SV08-78	0.599	0.015	0.0725	0.002	0.7	13.7931	0.3805	0.0586	0.0013	0.25	476	9.3	451	12	565	47	82.5	N/A
13SV08-20	0.672	0.035	0.0726	0.0015	0.5	13.7741	0.28459	0.0676	0.0029	0.19	520	21	451.6	9.2	836	88	20.2	N/A
13SV08-56	0.732	0.07	0.0728	0.0051	0.28	13.73626	0.96229	0.074	0.0076	0.32	551	40	452	31	930	210	11.51	N/A
13SV08-107	0.601	0.014	0.0727	0.0011	0.12	13.75516	0.20812	0.0606	0.0013	0.44	477.6	8.8	452.1	6.5	632	51	43.74	N/A
13SV08-13	0.589	0.024	0.07279	0.00096	0.42	13.73815	0.18119	0.0588	0.0022	0.02	469	15	452.9	5.8	547	83	20.44	N/A
13SV08-31	0.682	0.036	0.0729	0.0015	0.07	13.71742	0.28225	0.0687	0.0039	0.35	531	23	453.8	8.9	850	110	44.5	N/A
13SV08-69	0.681	0.027	0.0736	0.0015	0.2	13.58696	0.27691	0.0662	0.0022	0.19	526	16	457.5	8.7	817	65	49.8	N/A
13SV08-67	0.705	0.042	0.0737	0.0014	0.31	13.56852	0.25775	0.0691	0.0039	0.06	539	25	458.2	8.3	870	110	39.8	N/A
13SV08-40	0.769	0.082	0.075	0.0031	0	13.33333	0.55111	0.0731	0.0069	0.26	572	44	466	18	940	190	38.4	N/A
13SV08-80	0.656	0.012	0.0753	0.0013	0.01	13.28021	0.22927	0.0631	0.0015	0.79	512.2	7.1	468.2	8	705	51	76	N/A
13SV08-77	0.7	0.04	0.0756	0.0019	0.78	13.22751	0.33244	0.0679	0.0026	0.49	537	23	470	11	850	75	85.9	N/A
13SV08-59	0.752	0.046	0.0759	0.0021	0.11	13.17523	0.36453	0.0701	0.0039	0.37	566	26	471	12	930	120	30.06	N/A
13SV08-82	0.787	0.041	0.0775	0.0033	0.12	12.90323	0.54943	0.0739	0.0047	0.54	588	23	481	20	1020	130	26.7	N/A
13SV08-48	0.666	0.019	0.0788	0.0015	0.73	12.69036	0.24157	0.0621	0.0011	0.33	518	11	489	9.1	673	38	47.1	N/A
13SV08-33	0.765	0.025	0.0828	0.0016	0.06	12.07729	0.23338	0.0659	0.0024	0.41	576	14	512.5	9.6	824	77	18.98	62
13SV08-96	0.748	0.028	0.0854	0.0018	0.37	11.7096	0.24681	0.0654	0.0025	0.1	566	16	528	11	771	78	16.44	68
13SV08-55	1.299	0.041	0.1274	0.0029	0.26	7.849294	0.17867	0.0732	0.002	0.5	844	18	773	16	1026	60	30.1	75
13SV08-79	1.294	0.041	0.1316	0.0033	0.28	7.598784	0.19055	0.0715	0.0016	0.45	842	18	797	19	965	48	17.35	83
13SV08-92	1.524	0.077	0.141	0.0056	0.64	7.092199	0.28168	0.0796	0.0028	0.09	936	30	850	31	1175	65	20.94	72
13SV08-91	1.498	0.051	0.1424	0.0037	0.58	7.022472	0.18247	0.0784	0.0025	0.35	928	21	858	21	1160	58	23.35	74
13SV08-08	1.555	0.025	0.1504	0.0031	0.87	6.648936	0.13705	0.07462	0.00067	0.63	952	10	903	18	1062	20	52.7	85
13SV08-71	1.925	0.066	0.1621	0.0055	0.53	6.169031	0.20931	0.0849	0.0032	0.32	1088	23	968	30	1313	70	9.5	74
13SV08-103	1.718	0.034	0.1643	0.0032	0.65	6.086427	0.11854	0.0765	0.0012	0.32	1015	13	980	18	1112	29	32.29	88
13SV08-93	2.043	0.056	0.1786	0.0046	0.32	5.599104	0.14421	0.0858	0.0028	0.44	1129	19	1059	25	1324	60	54	80
13SV08-03	1.979	0.071	0.179	0.0064	0.97	5.586592	0.19974	0.08131	0.00088	0.54	1106	25	1061	35	1228	21	47.5	86
13SV08-63	1.872	0.037	0.1807	0.0029	0.74	5.534034	0.08881	0.0762	0.001	0.3	1071	13	1070	16	1104	25	44.9	97
13SV08-98	2.975	0.059	0.2289	0.0044	0.61	4.36872	0.08398	0.0959	0.0017	0.49	1400	15	1328	23	1543	33	34	86
13SV08-88	3.185	0.088	0.2458	0.0056	0.85	4.068348	0.09269	0.0941	0.0015	0.1	1452	22	1416	29	1508	30	59.7	94
13SV08-58	3.951	0.08	0.2763	0.0061	0.96	3.619254	0.0799	0.10356	0.00074	0.58	1623	17	1572	31	1688	13	51.7	93
13SV08-72	4.794	0.09	0.283	0.0065	0.81	3.533569	0.08116	0.1224	0.0015	0.57	1783	16	1606	33	1991	22	39.8	81

APPENDIX II

(continued)

Sample/grain	Data for Wetherill plot[1]					Data for Tera-Wasserburg plot[1]					Dates[1] (Ma)						Uppm[2]	% conc.[3]
	$^{207}Pb/^{235}U$	2σ abs	$^{206}Pb/^{238}U$	2σ abs	Rho	$^{238}U/^{206}Pb$	2σ abs	$^{207}Pb/^{206}Pb$	2σ abs	Rho	$^{207}Pb/^{235}U$	2σ abs	$^{206}Pb/^{238}U$	2σ abs	$^{207}Pb/^{206}Pb$	2σ abs		
13SV08																		
13SV08-101	4.761	0.08	0.3032	0.0063	0.83	3.298153	0.06853	0.115	0.0013	0.37	1777	14	1707	31	1879	20	52.8	91
13SV08-102	4.93	0.11	0.3074	0.0058	0.82	3.25309	0.06138	0.1177	0.0017	0.12	1807	19	1727	29	1926	24	38.6	90
13SV08-99	9.86	0.24	0.3994	0.0094	0.94	2.503756	0.05893	0.1797	0.0014	0.05	2420	23	2165	43	2649	12	34.1	82
13SV08-97	11.4	0.29	0.443	0.011	0.92	2.257336	0.05605	0.1889	0.0018	0.28	2554	25	2363	49	2732	16	26.21	86
13SV05																		
13SV05-72-T	0.598	0.012	0.06732	0.00087	0.73	14.85443	0.19197	0.06479	0.00077	0	476	7.5	419.9	5.3	772	27	220	N/A
13SV05-86	0.591	0.018	0.0683	0.00073	0.19	14.64129	0.15649	0.0625	0.002	0.2	471	11	425.9	4.4	694	69	42.74	N/A
13SV05-82	0.618	0.011	0.0688	0.00082	0.09	14.53488	0.17324	0.0642	0.0014	0.24	488.6	6.9	428.9	4.9	743	45	60.7	N/A
13SV05-81	0.554	0.017	0.0692	0.0014	0.26	14.45087	0.29236	0.0575	0.0018	0.3	447	11	431.6	8.3	498	70	38.5	N/A
13SV05-34	0.615	0.021	0.0695	0.0015	0.31	14.38849	0.31054	0.0653	0.0023	0.43	486	13	433	8.9	773	72	50.6	N/A
13SV05-05	0.552	0.018	0.06963	0.00093	0.45	14.36163	0.19182	0.057	0.0015	0.02	446	12	433.9	5.6	495	62	34.14	N/A
13SV05-28	0.6	0.02	0.06977	0.00069	0.21	14.33281	0.14175	0.0627	0.002	0.14	477	13	434.8	4.2	704	64	36.2	N/A
13SV05-18	0.628	0.015	0.0702	0.0007	0.03	14.24501	0.14204	0.0655	0.0017	0.28	494.7	9.6	437.3	4.2	783	53	23.78	N/A
13SV05-74	0.68	0.017	0.07035	0.00066	0.42	14.21464	0.13336	0.0694	0.0017	0	526	10	438.3	4	906	50	51.64	N/A
13SV05-21	0.5542	0.009	0.0705	0.0011	0.58	14.1844	0.22132	0.05732	0.00092	0.5	448.8	6.1	439.3	6.6	507	36	99.5	N/A
13SV05-12	0.7	0.027	0.0705	0.0012	0.33	14.1844	0.24144	0.0725	0.002	0.29	538	16	439.4	7.2	992	57	24.42	N/A
13SV05-23	0.658	0.016	0.07042	0.0006	0.41	14.20051	0.12099	0.0689	0.0017	0.11	513	9.9	439.5	3.3	891	50	20.24	N/A
13SV05-08	0.601	0.017	0.07091	0.00084	0.09	14.10238	0.16706	0.0621	0.0012	0.18	477	11	441.6	5.1	674	40	134.3	N/A
13SV05-79	0.565	0.011	0.07111	0.00084	0.29	14.06272	0.16612	0.0575	0.001	0.37	454.7	7.3	442.8	5	508	39	111.2	N/A
13SV05-38	0.568	0.018	0.0711	0.0012	0.49	14.0647	0.23738	0.0586	0.0015	0.09	456	12	443	7.2	544	58	37.21	N/A
13SV05-76	0.732	0.025	0.07148	0.00069	0.73	13.98993	0.13505	0.0737	0.0024	0.61	557	14	445.1	4.2	1022	66	85.7	N/A
13SV05-14	0.617	0.013	0.07154	0.00082	0.16	13.97819	0.16022	0.0626	0.0014	0.27	487.5	8.1	445.4	4.9	690	49	37.93	N/A
13SV05-10	0.633	0.017	0.0718	0.0013	0.58	13.92758	0.25217	0.0636	0.0014	0.13	497	11	447.2	7.8	722	47	42.9	N/A
13SV05-53	0.583	0.01	0.07184	0.0007	0.23	13.91982	0.13563	0.0584	0.0011	0.34	466.1	6.5	447.2	4.2	539	42	54.81	N/A
13SV05-25	0.719	0.048	0.07191	0.00057	0.77	13.90627	0.11023	0.0734	0.0052	0.66	547	27	447.6	3.4	980	130	101.9	N/A
13SV05-17	0.5535	0.008	0.07213	0.0005	0.57	13.86386	0.0961	0.05587	0.00076	0.04	447.2	5.5	449	3	445	30	121.8	N/A
13SV05-35	0.747	0.019	0.0727	0.0012	0.4	13.75516	0.22705	0.0748	0.002	0.1	566	11	452.2	7.3	1055	56	31.9	N/A
13SV05-67	0.622	0.011	0.0734	0.001	0.43	13.62398	0.18561	0.0618	0.00098	0.31	490.9	7	456.9	6.2	685	36	89.2	N/A
13SV05-68	0.5833	0.007	0.07348	0.00046	0.23	13.60915	0.0852	0.05785	0.00081	0.3	467.5	4.1	457.1	2.8	522	31	92.13	N/A
13SV05-49	0.623	0.02	0.07357	0.00093	0.87	13.5925	0.17182	0.0617	0.0017	0.42	491	12	457.6	5.6	657	57	39.3	N/A
13SV05-20	0.5701	0.009	0.074	0.00099	0.62	13.51351	0.18079	0.05651	0.00059	0.29	458	6	460.2	6	471	23	110.5	N/A
13SV05-50	0.628	0.016	0.0747	0.0012	0.43	13.38688	0.21505	0.0613	0.0013	0.2	494.5	9.8	464.6	6.9	646	45	58.8	N/A
13SV05-11	0.649	0.015	0.07476	0.00083	0.61	13.37614	0.1485	0.0633	0.0011	0.1	507.4	9.3	464.7	5	716	37	98	N/A
13SV05-27	0.805	0.031	0.07515	0.00082	0.71	13.30672	0.1452	0.0781	0.0023	0.52	599	18	467.1	4.9	1163	58	85.8	N/A

APPENDIX II

(continued)

Sample/grain	Data for Wetherill plot[1]					Data for Tera-Wasserburg plot[1]					Dates[1] (Ma)						Uppm[2]	% conc.[3]
	$^{207}Pb/^{235}U$	2σ abs	$^{206}Pb/^{238}U$	2σ abs	Rho	$^{238}U/^{206}Pb$	2σ abs	$^{207}Pb/^{206}Pb$	2σ abs	Rho	$^{207}Pb/^{235}U$	2σ abs	$^{206}Pb/^{238}U$	2σ abs	$^{207}Pb/^{206}Pb$	2σ abs		
13SV05																		
13SV05-70	0.6314	0.009	0.07688	0.00062	0.35	13.00728	0.1049	0.06027	0.00078	0.17	496.9	5.6	477.5	3.7	611	28	67.2	N/A
13SV05-33	0.773	0.017	0.07726	0.0004	0.74	12.94331	0.06701	0.073	0.0012	0.54	581.4	9.5	479.7	2.4	1020	31	114.6	N/A
13SV05-56	0.726	0.038	0.0801	0.0032	0.52	12.48439	0.49875	0.0651	0.003	0.27	552	22	496	19	755	96	27.45	N/A
13SV05-88	0.803	0.059	0.0802	0.0032	0.46	12.46883	0.49751	0.0714	0.0043	0.01	595	32	497	19	930	120	35.1	N/A
13SV05-19	0.765	0.021	0.0813	0.0016	0.21	12.30012	0.24207	0.0689	0.0016	0.41	577	12	503.5	9.3	890	49	34.9	57
13SV05-57	0.81	0.021	0.0816	0.0012	0.04	12.2549	0.18022	0.0721	0.0019	0.53	602	12	505.4	7.2	982	52	37.47	51
13SV05-16	0.683	0.011	0.08256	0.00052	0.31	12.1124	0.07629	0.06037	0.00096	0.17	528.2	6.9	511.4	3.1	614	34	61.8	83
13SV05-40	0.827	0.04	0.0874	0.0023	0.79	11.44165	0.3011	0.0675	0.0023	0.27	610	22	540	13	841	70	33.01	64
13SV05-94	0.851	0.011	0.0897	0.0011	0.44	11.14827	0.13671	0.06882	0.00088	0.37	625.2	6.2	553.9	6.2	892	26	184	62
13SV05-105	0.734	0.016	0.0909	0.0011	0.13	11.0011	0.13313	0.0586	0.0014	0.49	558.4	9.5	561	6.2	559	49	25.76	100
13SV05-100	0.754	0.012	0.09421	0.0007	0.29	10.61458	0.07887	0.05834	0.00078	0.38	570.3	7	580.4	4.1	541	29	35.71	107
13SV05-97	0.816	0.052	0.0951	0.0019	0.08	10.51525	0.21008	0.0625	0.0043	0.11	603	29	586	11	640	150	4.741	92
13SV05-42	0.853	0.015	0.1014	0.001	0.67	9.861933	0.09726	0.06126	0.00078	0.11	627.5	7.7	622.6	6	647	27	106.9	96
13SV05-92	1.149	0.037	0.1196	0.0032	0.62	8.361204	0.22371	0.0692	0.0022	0.19	775	18	728	19	909	59	9.44	80
13SV05-108	1.072	0.025	0.1225	0.002	0.85	8.163265	0.13328	0.06429	0.00079	0.16	739	12	745	11	754	27	76.56	99
13SV05-73	1.329	0.055	0.131	0.0052	0.72	7.633588	0.30301	0.0733	0.0016	0.42	856	24	793	30	1031	50	22.3	77
13SV05-78	1.332	0.019	0.1351	0.0013	0.54	7.401925	0.07123	0.07087	0.00096	0.24	859.5	8.3	816.7	7.7	952	28	40.98	86
13SV05-15	1.367	0.037	0.1358	0.0018	0.73	7.36377	0.09761	0.073	0.0013	0.27	874	16	821	10	1012	36	40.24	81
13SV05-63	1.381	0.025	0.1367	0.0028	0.66	7.315289	0.14984	0.0731	0.0011	0.34	881	11	826	16	1015	32	36.1	81
13SV05-61	1.467	0.024	0.1391	0.0015	0.28	7.189073	0.07752	0.0771	0.0014	0.53	917	10	839.8	8.5	1120	37	39.7	75
13SV05-62	1.464	0.019	0.14622	0.00093	0.43	6.83901	0.0435	0.07311	0.00066	0.18	915.2	7.7	879.7	5.3	1016	18	52.48	87
13SV05-99	1.61	0.15	0.153	0.0071	0.14	6.535948	0.3033	0.0786	0.0054	0.1	962	58	917	40	1120	130	1.99	82
13SV05-72-C	1.66	0.051	0.1549	0.0041	0.58	6.455778	0.17088	0.0767	0.0019	0.36	992	20	928	23	1120	47	21.2	83
13SV05-77	1.676	0.02	0.1639	0.0017	0.5	6.101281	0.06328	0.07427	0.00088	0.36	999.2	7.5	978.4	9.7	1047	24	52.7	93
13SV05-91	1.932	0.055	0.1684	0.0021	0.79	5.938242	0.07405	0.0835	0.0018	0.54	1091	19	1003	12	1277	42	17.96	79
13SV05-95	1.749	0.024	0.1702	0.0021	0.72	5.875441	0.07249	0.07501	0.00077	0.19	1026.6	8.9	1013	12	1068	21	21.17	95
13SV05-06	2.006	0.069	0.1715	0.0024	0.25	5.830904	0.0816	0.0858	0.003	0.26	1121	24	1020	13	1338	70	4.771	76
13SV05-107	1.826	0.036	0.1723	0.0024	0.63	5.803831	0.08084	0.0776	0.0014	0.17	1054	13	1024	13	1134	35	17.97	90
13SV05-60	1.848	0.065	0.1736	0.002	0.45	5.760369	0.06636	0.0774	0.0023	0.05	1061	23	1032	11	1133	61	10.59	91
13SV05-114	1.803	0.039	0.176	0.0032	0.89	5.681818	0.10331	0.07381	0.00069	0.18	1046	14	1045	17	1035	19	150.5	101
13SV05-64	1.82	0.038	0.1764	0.0024	0.29	5.668934	0.07713	0.076	0.0016	0.4	1052	14	1047	13	1092	42	17.56	96
13SV05-104	2.272	0.02	0.1886	0.002	0.4	5.302227	0.05623	0.08828	0.00097	0.53	1203.4	6.3	1114	11	1388	21	69.6	80
13SV05-52	2.622	0.069	0.198	0.0039	0.93	5.050505	0.09948	0.09538	0.00082	0.33	1305	20	1164	21	1535	16	121.5	76
13SV05-90	2.264	0.045	0.2009	0.0031	0.65	4.977601	0.07681	0.0826	0.0013	0.04	1200	14	1180	16	1256	32	16.94	94

APPENDIX II

(continued)

Sample/grain	Data for Wetherill plot[1]					Data for Tera-Wasserburg plot[1]					Dates[1] (Ma)							
	$^{207}Pb/^{235}U$	2σ abs	$^{206}Pb/^{238}U$	2σ abs	Rho	$^{238}U/^{206}Pb$	2σ abs	$^{207}Pb/^{206}Pb$	2σ abs	Rho	$^{207}Pb/^{235}U$	2σ abs	$^{206}Pb/^{238}U$	2σ abs	$^{207}Pb/^{206}Pb$	2σ abs	Uppm[2]	% conc.[3]
13SV05																		
13SV05-03	2.331	0.036	0.2049	0.0023	0.73	4.880429	0.05478	0.08214	0.00067	0.17	1221	11	1201	12	1248	16	43.61	96
13SV05-103	2.634	0.051	0.2076	0.0051	0.96	4.816956	0.11834	0.0925	0.00073	0.33	1310	14	1215	27	1477	15	59.7	82
13SV05-80	2.501	0.026	0.2083	0.0014	0.51	4.800768	0.03227	0.08696	0.00076	0.22	1272	7.6	1219.7	7.3	1359	17	41.4	90
13SV05-04	2.587	0.049	0.2176	0.0041	0.85	4.595588	0.08659	0.08584	0.00087	0.43	1296	14	1269	22	1334	19	45.9	95
13SV05-30	2.621	0.034	0.2249	0.0033	0.82	4.446421	0.06524	0.08578	0.00084	0.43	1306.2	9.5	1308	17	1332	19	180	98
13SV05-115	3.58	0.17	0.2262	0.0083	0.95	4.420866	0.16222	0.1134	0.0017	0.39	1547	38	1314	43	1852	28	60.5	71
13SV05-55	3.268	0.092	0.2311	0.0051	0.88	4.327131	0.09549	0.1023	0.0012	0.35	1472	22	1340	27	1664	21	64.1	81
13SV05-93	3.069	0.042	0.2369	0.0034	0.84	4.22119	0.06058	0.09463	0.00076	0.29	1425	10	1370	17	1523	15	71.6	90
13SV05-106	3.381	0.052	0.2591	0.0029	0.67	3.859514	0.0432	0.0954	0.0011	0.08	1500	12	1485	15	1534	22	15.4	97
13SV05-113	3.685	0.082	0.2652	0.0039	0.49	3.770739	0.05545	0.1006	0.0014	0.09	1567	18	1516	20	1633	26	19.96	93
13SV05-119	3.504	0.068	0.266	0.0049	0.67	3.759398	0.06925	0.0966	0.0013	0.51	1527	15	1520	25	1558	24	19.93	98
13SV05-39	3.545	0.043	0.2671	0.0024	0.89	3.743916	0.03364	0.09643	0.00055	0.11	1537	9.7	1526	12	1556	11	215.4	98
13SV05-66	3.843	0.086	0.2722	0.0058	0.9	3.673769	0.07828	0.10144	0.00085	0.06	1601	18	1551	29	1650	16	28.12	94
13SV05-96	3.601	0.049	0.2738	0.0024	0.84	3.652301	0.03201	0.09537	0.00062	0.04	1549	11	1560	12	1535	12	53.6	102
13SV05-44	3.786	0.067	0.2745	0.0031	0.89	3.642987	0.04114	0.10186	0.00065	0.02	1589	14	1563	16	1658	12	44.66	94
13SV05-117	4.629	0.093	0.3148	0.0051	0.79	3.17662	0.05146	0.1061	0.0011	0.08	1754	17	1764	25	1733	19	32.47	102
13SV05-54	4.721	0.073	0.3181	0.0036	0.8	3.143666	0.03558	0.1079	0.00094	0.49	1770	13	1780	18	1764	16	43.4	101
13SV05-101	5.712	0.075	0.3402	0.004	0.65	2.939447	0.03456	0.1223	0.0011	0.09	1933	11	1887	19	1990	16	48.03	95
13SV05-102	11.22	0.17	0.4503	0.0093	0.91	2.220742	0.04586	0.1831	0.0014	0.64	2541	15	2396	42	2681	13	19.53	89
13SV05-36	13.62	0.18	0.4927	0.0054	0.88	2.029633	0.02224	0.2016	0.0013	0.04	2725	13	2586	22	2839	10	26.6	91
13SV05-116	15.92	0.28	0.5555	0.0082	0.82	1.80018	0.02657	0.2082	0.0022	0.29	2871	17	2847	34	2890	17	26.75	99
13SV05-118	15.75	0.26	0.565	0.01	0.95	1.769912	0.03133	0.2017	0.0012	0.59	2861	16	2887	42	2840	10	25.89	102
13SV04																		
13SV04-46	0.517	0.016	0.0677	0.0012	0.67	14.77105	0.26182	0.0574	0.0014	0.03	423	11	422.4	7.5	499	52	46.6	N/A
13SV04-37	0.592	0.014	0.068	0.0013	0.07	14.70588	0.28114	0.0632	0.0019	0.74	471.8	8.7	423.9	7.6	705	62	47.1	N/A
13SV04-20	0.531	0.016	0.0684	0.0018	0.79	14.61988	0.38473	0.056	0.001	0.2	432	11	426	11	450	40	57.4	N/A
13SV04-45	0.551	0.014	0.0684	0.00079	0.04	14.61988	0.16886	0.0592	0.0018	0.45	445.7	9.2	426.5	4.7	579	65	40.8	N/A
13SV04-22	0.585	0.023	0.0688	0.0016	0.65	14.53488	0.33802	0.0626	0.0016	0.01	467	15	428.7	9.4	685	57	30.2	N/A
13SV04-29	0.546	0.02	0.0697	0.0021	0.69	14.3472	0.43227	0.058	0.0015	0.05	442	13	434	13	521	57	32.4	N/A
13SV04-23	0.565	0.022	0.0699	0.0016	0.56	14.30615	0.32747	0.0573	0.0018	0.03	454	14	435.6	9.9	505	75	20.4	N/A
13SV04-63	0.5746	0.006	0.07202	0.00052	0.1	13.88503	0.10025	0.05779	0.00067	0.58	461	3.8	448.3	3.2	520	25	121.8	N/A
13SV04-16	0.579	0.023	0.0726	0.0018	0.63	13.7741	0.34151	0.0575	0.002	0.21	463	14	452	11	512	71	30.3	N/A
13SV04-84	0.715	0.012	0.07346	0.00072	0.01	13.61285	0.13342	0.0703	0.0012	0.55	547.4	7.2	456.9	4.3	934	35	54.9	N/A
13SV04-83	0.618	0.017	0.0741	0.002	0.74	13.49528	0.36425	0.0621	0.0012	0.02	488	11	460	12	683	45	57.2	N/A

APPENDIX II

(continued)

Sample/grain	Data for Wetherill plot[1]					Data for Tera-Wasserburg plot[1]					Dates[1] (Ma)						Uppm[2]	% conc.[3]
	$\frac{^{207}Pb}{^{235}U}$	2σ abs	$\frac{^{206}Pb}{^{238}U}$	2σ abs	Rho	$\frac{^{238}U}{^{206}Pb}$	2σ abs	$\frac{^{207}Pb}{^{206}Pb}$	2σ abs	Rho	$\frac{^{207}Pb}{^{235}U}$	2σ abs	$\frac{^{206}Pb}{^{238}U}$	2σ abs	$\frac{^{207}Pb}{^{206}Pb}$	2σ abs		
13SV04																		
13SV04- 44	0.591	0.019	0.0741	0.0024	0.31	13.49528	0.43709	0.0587	0.0022	0.49	471	12	461	14	540	83	26.5	N/A
13SV04-87	0.741	0.019	0.07431	0.00079	0.25	13.45714	0.14306	0.0712	0.0016	0.29	563	11	462.1	4.7	957	45	58.8	N/A
13SV04-41	0.649	0.038	0.0748	0.0018	0.3	13.36898	0.32171	0.0613	0.0034	0.11	506	23	465	11	690	110	11	N/A
13SV04-61	0.582	0.021	0.0758	0.0021	0.6	13.19261	0.36549	0.0563	0.002	0.24	465	14	471	13	449	77	21.3	N/A
13SV04-68	0.634	0.016	0.0769	0.0021	0.54	13.0039	0.35511	0.0593	0.0014	0.42	498	9.7	477	12	583	48	23.9	N/A
13SV04-72	0.613	0.018	0.0771	0.0015	0.19	12.97017	0.25234	0.0586	0.0018	0.44	487	11	478.8	8.7	542	64	19.3	N/A
13SV04-53	0.773	0.033	0.0826	0.0047	0.83	12.10654	0.68887	0.0668	0.0016	0.53	580	19	511	28	826	51	30.48	62
13SV04-112	0.898	0.039	0.0869	0.0033	0.88	11.50748	0.43699	0.0751	0.0013	0.07	649	21	537	20	1074	34	52.9	50
13SV04-39	0.841	0.038	0.0882	0.0041	0.92	11.33787	0.52704	0.0697	0.0012	0.41	618	21	544	24	923	37	112	59
13SV04-95	0.806	0.041	0.0918	0.0034	0.16	10.89325	0.40345	0.0643	0.0036	0.33	598	23	566	20	720	110	8.02	79
13SV04-49	0.83	0.021	0.0952	0.0023	0.66	10.5042	0.25378	0.0639	0.0016	0.26	616	13	586	14	733	50	41.1	80
13SV04-64	1.45	0.15	0.129	0.011	0.99	7.751938	0.66102	0.0817	0.0023	0.66	901	65	777	61	1238	54	47.35	63
13SV04-74	1.245	0.067	0.1295	0.0062	0.96	7.722008	0.3697	0.0698	0.0011	0.06	817	31	784	35	929	29	38	84
13SV04-38	1.28	0.051	0.1304	0.0044	0.96	7.668712	0.25876	0.07021	0.00081	0.15	835	23	790	25	933	24	82.2	85
13SV04-57	1.354	0.058	0.1349	0.0065	0.92	7.412898	0.35718	0.0714	0.0015	0.43	867	26	815	37	976	37	18.5	84
13SV04-47	1.438	0.06	0.1439	0.0046	0.64	6.94927	0.22214	0.0747	0.0021	0.09	903	25	867	26	1052	57	13.51	82
13SV04-98	1.64	0.11	0.146	0.01	0.23	6.849315	0.46913	0.0825	0.0062	0.21	980	42	879	58	1240	140	6.99	71
13SV04-09	1.478	0.058	0.1491	0.0042	0.9	6.706908	0.18893	0.0726	0.0012	0.21	923	23	896	24	1000	32	40	90
13SV04-66	1.786	0.034	0.1498	0.0022	0.09	6.675567	0.09804	0.0867	0.0026	0.6	1040	12	900	12	1348	58	27.13	67
13SV04-08	1.476	0.082	0.1521	0.0038	0.19	6.574622	0.16426	0.0694	0.0033	0.16	916	34	912	21	880	100	2.658	104
13SV04-06	1.537	0.089	0.1525	0.0074	0.81	6.557377	0.31819	0.0735	0.0013	0.01	948	35	914	42	1023	37	30.16	89
13SV04-54	1.57	0.1	0.1535	0.0093	0.47	6.514658	0.3947	0.0738	0.004	0.48	961	41	919	52	1010	110	7.91	91
13SV04-76	1.557	0.078	0.1538	0.0064	0.74	6.501951	0.27056	0.0747	0.0029	0.32	949	32	921	36	1074	73	23.4	86
13SV04-50	1.46	0.046	0.1551	0.0035	0.59	6.447453	0.14549	0.0708	0.0017	0.39	913	19	929	20	946	50	12.83	98
13SV04-67	1.717	0.07	0.1556	0.0053	0.1	6.426735	0.21891	0.0789	0.004	0.54	1012	26	932	30	1140	100	5.3	82
13SV04-81	1.545	0.057	0.1566	0.004	0.53	6.385696	0.16311	0.0717	0.0022	0.25	947	23	938	22	970	60	6.86	97
13SV04-27	2.136	0.06	0.159	0.003	0.43	6.289308	0.11867	0.099	0.003	0.38	1159	20	951	16	1606	54	11.65	59
13SV04-77	1.618	0.029	0.1597	0.0029	0.78	6.261741	0.11371	0.07445	0.00081	0.65	977	11	955	16	1052	22	59.1	91
13SV04-93	1.723	0.076	0.1598	0.0054	0.53	6.257822	0.21147	0.0791	0.0027	0.27	1019	30	955	30	1179	72	5.78	81
13SV04-52	1.75	0.16	0.159	0.012	0.99	6.289308	0.47466	0.0796	0.0017	0.77	1022	61	962	67	1191	41	30.37	81
13SV04-106	1.713	0.071	0.1616	0.0051	0.55	6.188119	0.19529	0.0777	0.0031	0	1011	27	965	28	1144	74	4.04	84
13SV04-97	1.656	0.037	0.1617	0.0037	0.63	6.184292	0.14151	0.0758	0.0016	0.42	991	14	966	21	1093	45	16.13	88
13SV04-94	1.654	0.098	0.1625	0.0062	0.5	6.153846	0.23479	0.0768	0.0026	0.06	996	35	970	34	1105	69	8.94	88
13SV04-96	2	0.13	0.1614	0.0071	0.59	6.195787	0.27255	0.0896	0.0044	0.01	1108	45	971	38	1428	93	2.76	68

APPENDIX II

(continued)

Sample/grain	Data for Wetherill plot[1]					Data for Tera-Wasserburg plot[1]					Dates[1] (Ma)						Uppm[2]	% conc.[3]
	$^{207}Pb/^{235}U$	2σ abs	$^{206}Pb/^{238}U$	2σ abs	Rho	$^{238}U/^{206}Pb$	2σ abs	$^{207}Pb/^{206}Pb$	2σ abs	Rho	$^{207}Pb/^{235}U$	2σ abs	$^{206}Pb/^{238}U$	2σ abs	$^{207}Pb/^{206}Pb$	2σ abs		
13SV04																		
13SV04-28	1.664	0.046	0.1632	0.0045	0.81	6.127451	0.16896	0.0748	0.0013	0.27	994	17	974	25	1073	32	19.5	91
13SV04-75	1.708	0.074	0.1641	0.007	0.65	6.093845	0.25994	0.0763	0.0023	0.4	1008	28	979	39	1109	52	31.6	88
13SV04-56	1.737	0.057	0.1643	0.004	0.67	6.086427	0.14818	0.0771	0.0021	0.35	1021	21	980	22	1124	56	14.51	87
13SV04-43	1.642	0.029	0.1645	0.0029	0.82	6.079027	0.10717	0.07322	0.00091	0.1	989	12	982	16	1023	26	33.5	96
13SV04-82	1.678	0.032	0.1656	0.0034	0.8	6.038647	0.12398	0.0735	0.0011	0.55	1002	13	988	19	1026	29	36.18	96
13SV04-104	1.789	0.056	0.1668	0.0039	0.54	5.995204	0.14018	0.0784	0.0028	0.41	1045	22	994	22	1143	71	8.46	87
13SV04-03	1.741	0.046	0.1674	0.0051	0.78	5.973716	0.18199	0.074	0.0014	0.44	1023	17	997	28	1037	38	18.7	96
13SV04-34	1.917	0.076	0.1675	0.0064	0.1	5.970149	0.22811	0.0831	0.004	0.54	1084	26	998	36	1292	94	6.08	77
13SV04-107	1.84	0.11	0.1677	0.0071	0.29	5.963029	0.25246	0.0784	0.0038	0.02	1053	36	999	39	1135	97	3.73	88
13SV04-14	1.685	0.067	0.1681	0.0054	0.71	5.94884	0.1911	0.0739	0.002	0.34	1005	25	1001	30	1032	54	12.48	97
13SV04-113	1.758	0.042	0.1685	0.0033	0.43	5.934718	0.11623	0.0766	0.0017	0.35	1032	15	1004	18	1106	45	15.65	91
13SV04-04	1.749	0.055	0.1701	0.0046	0.79	5.878895	0.15898	0.0743	0.0015	0.21	1025	20	1012	26	1060	41	17.67	95
13SV04-108	1.721	0.072	0.1715	0.0085	0.68	5.830904	0.289	0.0753	0.0031	0.8	1013	28	1019	47	1073	81	26	95
13SV04-116	1.797	0.048	0.1722	0.0034	0.77	5.807201	0.11466	0.0761	0.0012	0	1043	18	1024	19	1096	32	28.16	93
13SV04-33	1.826	0.054	0.1732	0.004	0.64	5.773672	0.13334	0.0783	0.0019	0.3	1053	19	1030	22	1159	47	12.62	89
13SV04-19	1.834	0.057	0.1741	0.005	0.34	5.743825	0.16496	0.0771	0.0028	0.61	1056	21	1034	28	1124	70	6.42	92
13SV04-80	1.785	0.043	0.1739	0.0027	0.36	5.750431	0.08928	0.0746	0.0017	0.31	1043	14	1034	15	1053	47	13.55	98
13SV04-62	1.847	0.08	0.1744	0.003	0.45	5.733945	0.09863	0.0775	0.0028	0.42	1064	27	1036	16	1120	74	3.85	93
13SV04-31	1.807	0.082	0.1752	0.0068	0.87	5.707763	0.22153	0.0755	0.0019	0.07	1044	30	1040	38	1084	48	13.9	96
13SV04-70	1.788	0.079	0.1754	0.0074	0.93	5.701254	0.24053	0.0747	0.0011	0.02	1043	30	1041	41	1066	29	19.1	98
13SV04-05	1.757	0.069	0.1762	0.0053	0.76	5.675369	0.17071	0.0733	0.0017	0.04	1032	24	1046	29	1016	47	8.11	103
13SV04-92	1.896	0.066	0.1767	0.0047	0.6	5.65931	0.15053	0.0796	0.0019	0.23	1077	23	1049	26	1182	48	13.2	89
13SV04--11	1.894	0.077	0.178	0.0058	0.67	5.617978	0.18306	0.0755	0.0025	0.09	1082	26	1055	32	1084	64	9	97
13SV04-36	1.917	0.059	0.1781	0.0049	0.54	5.614823	0.15448	0.0777	0.0023	0.58	1085	21	1056	27	1154	59	14.8	92
13SV04-15	1.83	0.058	0.1783	0.0048	0.8	5.608525	0.15099	0.0743	0.0016	0.42	1058	20	1057	26	1052	41	14	100
13SV04-26	1.897	0.059	0.1797	0.0053	0.71	5.56483	0.16413	0.0778	0.0018	0.45	1078	21	1065	29	1135	46	14.1	94
13SV04-07	1.862	0.081	0.1798	0.0045	0.66	5.561735	0.1392	0.0768	0.0028	0.23	1065	29	1066	25	1133	66	6.22	94
13SV04-79	2.06	0.15	0.185	0.01	0.99	5.405405	0.29218	0.0814	0.0016	0.84	1125	53	1095	55	1228	40	44	89
13SV04-21	1.896	0.053	0.1859	0.0046	0.59	5.379236	0.13311	0.075	0.002	0.6	1078	19	1099	25	1062	53	11.6	103
13SV04-109	2.02	0.094	0.1866	0.0075	0.77	5.359057	0.2154	0.0783	0.0022	0.27	1118	32	1102	41	1147	56	14.19	96
13SV04-91	2.149	0.078	0.1875	0.0063	0.86	5.333333	0.1792	0.0832	0.0015	0.24	1167	26	1107	34	1271	36	11.61	87
13SV04-55	2.15	0.049	0.1893	0.0041	0.84	5.28262	0.11441	0.0832	0.0012	0.33	1168	17	1117	22	1272	27	30.1	88
13SV04-24	2.266	0.074	0.1902	0.0051	0.94	5.257624	0.14098	0.0865	0.0012	0.4	1200	23	1122	28	1348	26	27.5	83
13SV04-58	2.222	0.076	0.1904	0.0057	0.66	5.252101	0.15723	0.0852	0.0017	0.2	1191	23	1123	31	1317	39	8.95	85

APPENDIX II

(continued)

Sample/grain	Data for Wetherill plot[1]					Data for Tera-Wasserburg plot[1]					Dates[1] (Ma)						Uppm[2]	% conc.[3]
	$\frac{^{207}Pb}{^{235}U}$	2σ abs	$\frac{^{206}Pb}{^{238}U}$	2σ abs	Rho	$\frac{^{238}U}{^{206}Pb}$	2σ abs	$\frac{^{207}Pb}{^{206}Pb}$	2σ abs	Rho	$\frac{^{207}Pb}{^{235}U}$	2σ abs	$\frac{^{206}Pb}{^{238}U}$	2σ abs	$\frac{^{207}Pb}{^{206}Pb}$	2σ abs		
13SV04																		
13SV04-12	2.38	0.22	0.197	0.015	0.97	5.076142	0.38651	0.0894	0.002	0.32	1231	70	1176	78	1408	43	11.02	84
13SV04-115	2.16	0.05	0.2004	0.0042	0.93	4.99002	0.10458	0.0784	0.0007	0.2	1167	17	1177	22	1156	18	57.1	102
13SV04-73	2.345	0.053	0.2012	0.0043	0.95	4.970179	0.10622	0.08532	0.0006	0.13	1225	16	1181	23	1322	14	93.4	89
13SV04-40	2.57	0.12	0.2099	0.0079	0.79	4.764173	0.17931	0.0889	0.0023	0.1	1289	34	1227	42	1395	49	8.83	88
13SV04-89	2.742	0.093	0.2103	0.0058	0.96	4.755112	0.13114	0.0941	0.0012	0.23	1338	26	1230	31	1514	26	55.19	81
13SV04-105	2.867	0.08	0.2273	0.0057	0.95	4.399472	0.11033	0.09053	0.00094	0.13	1371	22	1320	30	1436	20	34.1	92
13SV04-100	3.31	0.15	0.2394	0.0097	0.89	4.177109	0.16925	0.0989	0.0019	0.07	1485	35	1382	51	1600	36	24.6	86
13SV04-118	3.034	0.061	0.2415	0.005	0.82	4.140787	0.08573	0.0903	0.001	0.53	1415	16	1394	26	1431	22	36.35	97
13SV04-65	3.53	0.078	0.2574	0.0058	0.94	3.885004	0.08754	0.09935	0.00083	0.32	1533	18	1476	30	1611	16	66.4	92
13SV04-110	5.45	0.39	0.307	0.018	0.72	3.257329	0.19098	0.1223	0.0061	0.3	1889	59	1723	88	1968	90	10	88
13SV04-35	5.01	0.2	0.314	0.0069	0.8	3.184713	0.06998	0.1188	0.0028	0.25	1835	35	1760	34	1934	43	5.82	91
13SV04-32	5.42	0.15	0.3322	0.0086	0.93	3.010235	0.07793	0.12003	0.00098	0.27	1886	24	1848	42	1956	15	31.3	94
13SV04-25	10.77	0.63	0.434	0.023	0.99	2.304147	0.12211	0.179	0.002	0.53	2521	47	2320	110	2642	19	20.51	88
13SV04-114	12.65	0.23	0.4922	0.0092	0.97	2.031694	0.03798	0.18729	0.00086	0.24	2653	17	2579	40	2720	8	38.8	95
13SV04-101	12.94	0.24	0.5017	0.0083	0.91	1.993223	0.03298	0.1886	0.0019	0.42	2674	18	2620	36	2733	15	14.8	96
13SV04-117	18.4	1.3	0.54	0.013	0.98	1.851852	0.04458	0.245	0.011	0.91	2995	57	2780	54	3142	60	20.52	88
13SV04-30	13.83	0.32	0.541	0.014	0.97	1.848429	0.04783	0.1866	0.0012	0.04	2736	22	2786	61	2712	11	33.4	103
13SV03																		
13SV03-92	0.531	0.012	0.06449	0.0004	0.33	15.50628	0.09618	0.0594	0.0013	0.05	431.3	8.1	403	2.4	569	47	62	N/A
13SV03-101	0.522	0.011	0.06484	0.00041	0.54	15.42258	0.09752	0.0584	0.0012	0.3	424	7	405	2.5	501	41	86.28	N/A
13SV03-119	0.516	0.013	0.0654	0.00043	0.06	15.29052	0.10053	0.0571	0.0014	0.19	421.1	8.6	408.5	2.6	463	52	47.69	N/A
13SV03-32	0.524	0.025	0.06555	0.00064	0.13	15.25553	0.14895	0.0586	0.0029	0.1	426	17	409.2	3.9	486	94	17.2	N/A
13SV03-129	0.542	0.014	0.06631	0.00051	0.57	15.08068	0.11599	0.0595	0.0014	0.38	435.5	8.4	413.8	3.1	529	46	64.2	N/A
13SV03-131	0.54	0.018	0.06627	0.0007	0.15	15.08978	0.15939	0.0593	0.002	0.13	436	12	413.9	4.2	525	71	65.8	N/A
13SV03-99	0.534	0.012	0.06634	0.00043	0.26	15.07386	0.09771	0.058	0.0013	0.02	432.2	8.2	414	2.6	500	48	61.2	N/A
13SV03-111	0.557	0.022	0.06675	0.00058	0.39	14.98127	0.13017	0.0609	0.0024	0.2	442	14	416.4	3.5	534	74	28.1	N/A
13SV03-91	0.539	0.013	0.06678	0.0004	0.25	14.97454	0.08969	0.0583	0.0014	0	436.9	8.5	416.7	2.4	534	50	61	N/A
13SV03-110	0.519	0.013	0.06685	0.00044	0.29	14.95886	0.09846	0.0563	0.0013	0.04	421.3	8.2	417.1	2.7	435	49	57.4	N/A
13SV03-80	0.604	0.021	0.06689	0.00065	0.5	14.94992	0.14528	0.0655	0.0021	0.25	471	12	417.3	3.9	701	62	58.2	N/A
13SV03-61	0.5263	0.009	0.06707	0.0004	0.14	14.9098	0.08892	0.0571	0.001	0.23	429.6	6.1	418.4	2.4	476	39	84.8	N/A
13SV03-121	0.54	0.017	0.0671	0.00054	0.23	14.90313	0.11994	0.0585	0.0018	0.04	439	11	418.6	3.3	509	65	27.7	N/A
13SV03-109	0.533	0.014	0.0672	0.00043	0.06	14.88095	0.09522	0.0572	0.0014	0.19	432.2	8.9	419.2	2.6	461	53	53.2	N/A

APPENDIX II

(continued)

Sample/grain	Data for Wetherill plot[1]					Data for Tera-Wasserburg plot[1]					Dates[1] (Ma)							
	$^{207}Pb/^{235}U$	2σ abs	$^{206}Pb/^{238}U$	2σ abs	Rho	$^{238}U/^{206}Pb$	2σ abs	$^{207}Pb/^{206}Pb$	2σ abs	Rho	$^{207}Pb/^{235}U$	2σ abs	$^{206}Pb/^{238}U$	2σ abs	$^{207}Pb/^{206}Pb$	2σ abs	Uppm[2]	% conc.[3]
13SV03																		
13SV03-22	0.609	0.018	0.06718	0.0005	0.43	14.88538	0.11079	0.0665	0.0019	0.2	475	11	419.3	3	738	58	58.6	N/A
13SV03-71	0.54	0.013	0.06829	0.00054	0.52	14.64343	0.11579	0.0575	0.0014	0.28	434.8	8.3	425.8	3.3	470	47	63	N/A
13SV03-124	0.611	0.025	0.0684	0.00072	0.37	14.61988	0.15389	0.0645	0.0024	0.18	479	15	426.4	4.3	712	75	65.6	N/A

[1] data not corrected for common-Pb.
[2] concentration uncertainty c.20%.
[3] Concordance calculated as (206Pb-238U age/207Pb-206Pb age)*100.
#N/A = not available.
Uncertainties quoted without components related to systematic error.

APPENDIX III

ID-TIMS U-Pb zircon data for rocks of the Saint-Victor Formation of the Magog Group (samples 13SV03, 13SV04, 13SV08)

Sample # grain(s)	Poids (mg)	U (ppm)	Pbrad (ppm)	Pbcom (pg)	Th/U	$^{207}Pb/^{204}Pb$	$^{207}Pb/^{235}U$	1 s %	$^{206}Pb/^{238}U$	1 s %	r	$^{207}Pb/^{206}Pb$	1 s %	$^{206}Pb/^{238}U$	2 σ	$^{207}Pb/^{235}U$	2 σ	$^{207}Pb/^{206}Pb$	2 σ	Disc.
														Dates (Ma)						
SV03																				
32	0.001	715	59	38.1	0.992	19.882	0.530	0.91	0.0694	0.15	0.53	0.05546	0.84	432.2	1.2	432.0	6.4	430.9	37.2	-0.3
101	0.001	92	8	12.5	1.007	17.369	0.591	2.59	0.0759	0.38	0.55	0.05642	2.40	471.7	3.4	471.3	19.4	469.0	104.7	-0.6
30,60	0.001	418	32	4.1	0.698	66.056	0.539	0.17	0.0702	0.11	0.67	0.05574	0.12	437.2	0.9	438.0	1.2	441.9	5.5	1.1
SV04																				
29	0.001	229	20	2.6	1.067	37.149	0.555	0.23	0.0723	0.16	0.75	0.05575	0.15	449.8	1.4	448.5	1.7	442.3	6.8	-1.8
SV08																				
25	0.001	62	5	1.3	0.701	27.405	0.556	0.95	0.0735	0.48	0.57	0.05486	0.78	457.0	4.3	448.7	6.9	406.5	34.8	-12.9

REFERENCES

Aleinikoff, J. N., Ratcliffe, N. M., and Walsh, G. J., 2011, Provisional zircon and monazite uranium-lead geochronology for selected rocks from Vermont: US Geological Survey, Open-File Report 2011-1309, 46 p.

Armstrong, T. R., Tracy, R. J., and Hames, W. E., 1992, Contrasting styles of Taconian, eastern Acadian and western Acadian metamorphism, central and western New England: Journal of Metamorphic Geology, v. 10, n. 3, p. 415–426, https://doi.org/10.1111/j.1525-1314.1992.tb00093.x

Berry, W. B., 1962, On the Magog, Quebec, graptolites: American Journal of Science, v. 260, n. 2, p. 142–148, https://doi.org/10.2475/ajs.260.2.142

Bourque, P.-A., Malo, M., and Kirkwood, D., 2000, Paleogeography and tectono-sedimentary history at the margin of Laurentia during Silurian to earliest Devonian time: The Gaspé Belt, Québec: Geological Society of America Bulletin, v. 112, n. 1, p. 4–20, https://doi.org/10.1130/0016-7606(2000)112<4:PATHAT>2.0.CO;2

Bradley, D. C., and O'Sullivan, P., 2016, Detrital zircon geochronology of pre- and syn-collisional strata, Acadian orogen, Maine Appalachians: Basin Research, v. 29, n. 5, p. 571–590, https://doi.org/10.1111/bre.12188

Chiarenzelli, J., Kratzmann, D., Selleck, B., and deLorraine, W., 2015, Age and provenance of Grenville supergroup rocks, Trans-Adirondack Basin, constrained by detrital zircons: Geology, v. 43, n. 2, p. 183–186, https://doi.org/10.1130/G36372.1

Cohen, K. M., Finney, S. C., Gibbard, P. L., and Fan, J.-X., 2013, The ICS international chronostratigraphic chart: Episodes, v. 36, n. 3, p. 199–204.

Cousineau, P. A., 1990, Le Groupe de Caldwell et le domaine océanique entre St-Joseph-de-Beauce et Sainte-Sabine: Ministère de l'Énergie et des Ressources du Québec, MM 87-02, 165 p.

Cousineau, P. A., and St-Julien, P., 1994, Stratigraphie et paléogéographie d'un bassin d'avant-arc ordovicien, Estrie-Beauce, Appalaches du Québec: Canadian Journal of Earth Sciences, v. 31, n. 2, p. 435–446, https://doi.org/10.1139/e94-040

Cousineau, P. A., and Tremblay, A., 1993, Acadian deformations in the southwestern Quebec Appalachians: Geological Society of America Special Papers, v. 275, p. 85–100, https://doi.org/10.1130/SPE275-p85

David, J., and Gariépy, C., 1990, Early Silurian orogenic andesites from the central Quebec Appalachians: Canadian Journal of Earth Sciences, v. 27, n. 5, p. 632–643, https://doi.org/10.1139/e90-060

David, J., and Marquis, R., 1994, Géochronologie U-Pb dans les Appalaches du Québec. Application aux roches de la zone de Dunnage: La Revue géologique du Québec, v. 1, p. 16–20.

David, J., Chabot, N., Marcotte, C., Lajoie, J., and Lesperance, P., 1985, Stratigraphy and sedimentology of the Cabano, Pointe aux Trembles, and Lac Raymond formations, Témiscouata and Rimouski counties, Québec: Current Research, Part B, Geological Survey of Canada, Paper n. 85-1B, p. 481–497, https://doi.org/10.4095/120280

David, J., Marquis, R., and Tremblay, A., 1993, U-Pb geochronology of the Dunnage zone in the southern Québec Appalachians: Geological Society of America Abstract with Programs, v. 25, A-485.

De Broucker, G., 1987, Stratigraphie, pétrographie et structure de la boutonnière de Maquereau-Mictaw (Région de Port-Daniel, Gaspésie): Ministère de l'énergie et des ressources de Québec, MM-8603, 160 p.

De Rômer, H. S., 1985, Géologie des Monts Stokes: Québec, Ministére de l'énergie et des ressources, Direction générale de l'exploration géologique et minérale, Direction de la recherche géologie, Cartes 2011A et 2011B (échelles 1/20 000), 3 microfiches, MM 85-03, 62 p.

de Souza, S., Tremblay, A., and Ruffet, G., 2014, Taconian orogenesis, sedimentation and magmatism in the southern Quebec–northern Vermont Appalachians: Stratigraphic and detrital mineral record of Iapetan suturing: American Journal of Science, v. 314, n. 7, p. 1065–1103, https://doi.org/10.2475/07.2014.01

Dewey, J., and Mange, M., 1999, Petrography of Ordovician and Silurian sediments in the western Irish Caledonides: Tracers of a short-lived Ordovician continent-arc collision orogeny and the evolution of the Laurentian Appalachian-Caledonian margin: Geological Society, London, Special Publications, v. 164, p. 55–107, https://doi.org/10.1144/GSL.SP.1999.164.01.05

Dewey, J. F., and Ryan, P. D., 1990, The Ordovician evolution of the South Mayo Trough, western Ireland: Tectonics, v. 9, n. 4, p. 887–901, https://doi.org/10.1029/TC009i004p00887

Dickinson, W. R., and Gehrels, G. E., 2009, Use of U–Pb ages of detrital zircons to infer maximum depositional ages of strata: A test against a Colorado Plateau Mesozoic database: Earth and Planetary Science Letters, v. 288, n. 1–2, p. 115–125, https://doi.org/10.1016/j.epsl.2009.09.013

Dupuis, C., Malo, M., Bédard, J., Davis, B., and Villeneuve, M., 2009, A lost arc–back-arc terrane of the Dunnage oceanic tract recorded in clasts from the Garin Formation and McCrea mélange in the Gaspé Appalachians of Québec: Geological Society of America Bulletin, v. 121, n. 1–2, p. 17–38, https://doi.org/10.1130/B26251.1

Gauthier, M., Auclair, M., Bardoux, M., Blain, M., Boisvert, D., Brassard, B., Chartrand, F., Datimont, A., Dupuis, L., Durocher, M., Gariépy, C., Godue, R., Jébrak, M., and Trottier, J., 1989, Synthèse gîtologique de l'Estrie et de la Beauce: Québec, Canada, Ministère de l'Energie et des Resources, MB 89-20, 681 p.

Gehrels, G. E., 2010, Age Pick Program: Tucson, Arizona, University of Arizona Laserchron Center.

Gehrels, G. E., Blakey, R., Karlstrom, K. E., Timmons, J. M., Dickinson, B., and Pecha, M., 2011, Detrital zircon U-Pb geochronology of Paleozoic strata in the Grand Canyon, Arizona: Lithosphere, v. 3, n. 3, p. 183–200, https://doi.org/10.1130/L121.1

Gerbi, C. C., Johnson, S. E., Aleinikoff, J. N., Bédard, J. H., Dunning, G. R., and Fanning, C. M., 2006, Early Paleozoic development of the Maine-Quebec Boundary Mountains region: Canadian Journal of Earth Sciences, v. 43, n. 3, p. 367–389, https://doi.org/10.1139/e05-113

Goldman, D., Leslie, S. A., Nõlvak, J., Young, S., Bergström, S. M., and Huff, W. D., 2007, The global

stratotype section and point (GSSP) for the base of the Katian Stage of the Upper Ordovician Series at Black Knob Ridge, Southeastern Oklahoma, USA: Episodes, v. 30, p. 258–270.
Hatch, N. L., and Stanley, R. S., 1988, Post-Taconian structural geology of the Rowe-Hawley zone and the Connecticut Valley belt west of the Mesozoic basins: US Geological survey professional paper, 1366-C.
Hibbard, J., Van Staal, C., Rankin, D., and Williams, H., 2006, Lithotectonic map of the Appalachian Orogen: Canada–United States of America: Geological Survey of Canada Map A, v. 2096, p. 2.
Hodych, J. P., and Cox, R. A., 2007, Ediacaran U-Pb zircon dates for the Lac Matapédia and Mt. St.-Anselme basalts of the Quebec Appalachians: Support for a long-lived mantle plume during the rifting phase of Iapetus opening: Canadian Journal of Earth Sciences, v. 44, n. 4, p. 565–581, https://doi.org/10.1139/e06-112
Horstwood, M. S. A., Košler, J., Gehrels, G., Jackson, S. E., McLean, N. M., Paton, C., Pearson, N. J., Sircombe, K., Sylvester, P., Vermeesch, P., Bowring, J. F., Condon, D. J., and Schoene, B., 2016, Community-Derived Standards for LA-ICP-MS U-(Th-) Pb Geochronology–Uncertainty Propagation, Age Interpretation and Data Reporting: Geostandards and Geoanalytical Research, v. 40, n. 3, p. 311–332, https://doi.org/10.1111/j.1751-908X.2016.00379.x
Jasra, A., Stephens, D. A., Gallagher, K., and Holmes, C. C., 2006, Bayesian mixture modelling in geochronology via Markov chain Monte Carlo: Mathematical Geology, v. 38, n. 3, p. 269–300, https://doi.org/10.1007/s11004-005-9019-3
Karabinos, P., and Hepburn, J., 2001, Geochronology and geochemistry of the Shelburne Falls arc: The Taconic Orogeny in western New England: Guidebook to Geological Field Trips in New England: Boulder, Colorado, Geological Society of America, p. H1–H20.
Karabinos, P., Samson, S. D., Hepburn, J. C., and Stoll, H. M., 1998, Taconian orogeny in the New England Appalachians: Collision between Laurentia and the Shelburne Falls arc: Geology, v. 26, n. 3, p. 215–218, https://doi.org/10.1130/0091-7613(1998)026<0215:TOITNE>2.3.CO;2
Krogh, T. E., 1973, A low-contamination method for hydrothermal decomposition of zircon and extraction of U and Pb for isotopic age determinations: Geochimica et Cosmochimica Acta, v. 37, n. 3, p. 485–494, https://doi.org/10.1016/0016-7037(73)90213-5
Kröner, A., Wan, Y., Liu, X., and Liu, D., 2014, Dating of zircon from high-grade rocks: Which is the most reliable method?: Geoscience Frontiers, v. 5, n. 4, p. 515–523, https://doi.org/10.1016/j.gsf.2014.03.012
Labbé, J.-Y., and St-Julien, P., 1989, Failles de chevauchement acadiennes dans la région de Weedon, Estrie, Québec: Canadian Journal of Earth Sciences, v. 26, n. 11, p. 2268–2277, https://doi.org/10.1139/e89-193
Ludwig, K. R., 2012, Isoplot 3.75, A Geochronological Toolkit for Microsoft Excel: Berkeley, California, University of California at Berkeley, Berkeley Geochronology Center Special Publication No. 5.
Lyons, J. B., Aleinikoff, J. N., and Zartman, R. E., 1986, Uranium-thorium-lead ages of the Highlandcroft Plutonic Suite, northern New England: American Journal of Science, v. 286, n. 6, p. 489–509, https://doi.org/10.2475/ajs.286.6.489
Macdonald, F. A., Ryan-Davis, J., Coish, R. A., Crowley, J. L., and Karabinos, P., 2014, A newly identified Gondwanan terrane in the northern Appalachian Mountains: Implications for the Taconic orogeny and closure of the Iapetus Ocean: Geology, v. 42, n. 6, 539–542, https://doi.org/10.1130/G35659.1
Malo, M., 1988, Stratigraphy of the Aroostook-Percé anticlinorium in the Gaspé Peninsula, Québec: Canadian Journal of Earth Sciences, v. 25, n. 6, p. 893–908, https://doi.org/10.1139/e88-086
——— 2004, Paleogeography of the Matapédia basin in the Gaspé Appalachians: Initiation of the Gaspé Belt successor basin: Canadian Journal of Earth Sciences, v. 41, n. 5, p. 553–570, https://doi.org/10.1139/e03-100
Malo, M., and Bourque, P.-A., 1993, Timing of the deformation events from Late Ordovician to Mid-Devonian in the Gaspé Peninsula: Geological Society of America Special Papers, v. 275, p. 101–122, https://doi.org/10.1130/SPE275-p101
Mange, M., Idleman, B., Yin, Q.-Z., Hidaka, H., and Dewey, J., 2010, Detrital heavy minerals, white mica and zircon geochronology in the Ordovician South Mayo Trough, western Ireland: Signatures of the Laurentian basement and the Grampian orogeny: Journal of the Geological Society, v. 167, n. 6, p. 1147–1160, https://doi.org/10.1144/0016-76492009-091
Marquis, R., Figueiredo, M., Dion, D. J., Gauthier, M., David, J., and Hubert, J., 2001, Étude structurale des minéralisations aurifères du Groupe de Magog: Ministère des ressources naturelles du Québec, ET 99-03, 38 p.
Mattinson, J. M., 2005, U-Pb chemical abrasion ("CA–TIMS") method: Combined annealing and multi-step partial dissolution analysis for improved precision and accuracy of zircon ages: Chemical Geology, v. 220, n. 1–2, p. 47–66, https://doi.org/10.1016/j.chemgeo.2005.03.011
Mercier, P. E., ms, 2013, Analyse stratigraphique et structurale du Groupe de Magog et de la ceinture de Gaspé, région des Mont Stoke, Appalaches du Québec: Montréal, Canada, Université du Québec à Montréal, M. Sc. Thesis, 95 p.
Moench, R., 1993, Highlights of metamorphic stratigraphy and tectonics in western Maine to northeastern Vermont: GSA Annual Meeting, Field trip guidebook for the northeastern United States, v. 2, p. 01–32.
Moench, R. H., and Aleinikoff, J. N., 2003, Stratigraphy, geochronology, and accretionary terrane settings of two Bronson Hill arc sequences, northern New England: Physics and Chemistry of the Earth, Parts A/B/C, v. 28, n. 1–3, p. 113–160, https://doi.org/10.1016/S1474-7065(03)00012-3
Moench, R. H., Boone, G. M., Bothner, W. A., Boudette, E. L., Hatch, N. L., Jr., Hussey, A. J., III, and Marvinney, R. G., 1995, Geologic Map of the Sherbrooke-Lewiston Area, Maine, New Hampshire, and Vermont, United States, and Quebec, Canada: US Geological Survey, IMap 1898-D, scale 1:250,000.
Moore, G. F., Boston, B. B., Strasser, M., Underwood, M. B., and Ratliff, R. A., 2015, Evolution of tectono-sedimentary systems in the Kumano Basin, Nankai Trough forearc: Marine and Petroleum Geology, v. 67, p. 604–616, https://doi.org/10.1016/j.marpetgeo.2015.05.032

Osberg, P. H., 1978, Synthesis of the geology of the northeastern Appalachians, USA: IGCP project, v. 27, p. 78–13.
Osberg, P. H., Tull, J. F., Robinson, P., Hon, R., Butler, J. R. , 1989, The Acadian orogen, *in* America, Hatcher, R. D., Thomas, W. A., and Viele, G. W., editors, The Appalachian–Ouachita Orogen in the United States: Geological Society of America, The Geology of North America, v. F-2, p. 179–232.
Paton, C., Hellstrom, J., Paul, B., Woodhead, J., and Hergt, J., 2011, Iolite: Freeware for the visualisation and processing of mass spectrometric data: Journal of Analytical Atomic Spectrometry, v. 26, p. 2508–2518, https://doi.org/10.1039/c1ja10172b
Percival, J. A., 2007, Geology and metallogeny of the Superior Province, Canada, *in* Goodfellow, W. D., editor, Mineral Deposits of Canada: A Synthesis of Major Deposit-Types, District Metallogeny, the Evolution of Geological Provinces, and Exploration Methods: Geological Association of Canada, Mineral Deposits Division, Special Publication n. 5, p. 903–928.
Perrot, M., ms, 2014, Étude structurale et microstructurale de la faille St-Joseph et de la ligne Baie Verte-Brompton dans les Appalaches du sud du Québec: Montréal, Canada, Université du Québec à Montréal, M. Sc. Thesis, 77 p.
Perrot, M., and Tremblay, A., 2013, Compilation géologique de la région du Bas-Saint-Laurent, MRC de Kamouraska, du Témiscouata et de Rivière-Du-Loup: Ministère Des Ressources Naturelles, Québec Affiche G42, DV 2014-03, p. 72.
——— 2017, Compilation et révision géologique des régions de Drummonville, Richmond, Mont-Orford, Grandby, Cowansville et du Lac-Memphrémagog: Ministère de l'Énergie et des Ressources Naturelles, Québec CG31H-01, CG31H-02, CG31H-07, CG31H-08, CG31H-09, CG31H-16, scale 1/50 000.
Pinet, N., Tremblay, A., and Sosson, M., 1996, Extension versus shortening models for hinterland-directed motions in the southern Québec Appalachians: Tectonophysics, v. 267, n. 1–4, p. 239–256, https://doi.org/10.1016/S0040-1951(96)00096-0
Riva, J., 1974, A revision of some Ordovician graptolites of eastern North America: Palaeontology, v. 17, p. 1–40.
Rivers, T., 1997, Lithotectonic elements of the Grenville Province: Review and tectonic implications: Precambrian Research, v. 86, n. 3–4, p. 117–154, https://doi.org/10.1016/S0301-9268(97)00038-7
Robinson, P., Tucker, R. D., Bradley, D., Berry, H. N., IV, and Osberg, P. H., 1998, Paleozoic orogens in New England, USA: GFF, v. 120, n. 2, p. 119–148, https://doi.org/10.1080/11035899801202119
Roy, D. C., 1989, The Depot Mountain Formation: Transition from syn-to post-Taconian basin along the Baie Verte-Brompton line in northwestern Maine: Studies in Maine Geology, v. 2, p. 85–99.
Schroetter, J.-M., Tremblay, A., Bédard, J. H., and Villeneuve, M. E., 2006, Syncollisional basin development in the Appalachian orogen—The Saint-Daniel Mélange, southern Québec, Canada: Geological Society of America Bulletin, v. 118, n. 1–2, p. 109–125, https://doi.org/10.1130/B25779.1
St-Julien, P., ms, 1963, Géologie de la région d'Orford-Sherbrooke, Québec: Québec, Canada, Université Laval, Ph. D. Thesis, 368 p.
——— 1970, Région d'Orford-Sherbrooke: Ministère des Richesses Naturelles du Québec Map no. 1619, scale 1:50,000.
——— 1987, Géologie des régions de Saint-Victor et de Thetford-Mines (moitié est): Ministère des ressources naturelles du Québec, MM 86-01, 66 p.
Stacey, J. T., and Kramers, J., 1975, Approximation of terrestrial lead isotope evolution by a two-stage model: Earth and Planetary Science Letters, v. 26, n. 2, p. 207–221, https://doi.org/10.1016/0012-821X(75)90088-6
Stanley, R. S., and Ratcliffe, N. M., 1985, Tectonic synthesis of the Taconian orogeny in western New England: Geological Society of America Bulletin, v. 96, n. 10, p. 1227–1250, https://doi.org/10.1130/0016-7606(1985)96<1227:TSOTTO>2.0.CO;2
Tremblay, A., 1992a, Tectonic and accretionary history of Taconian oceanic rocks of the Quebec Appalachians: American Journal of Science, v. 292, n. 4, p. 229–252, https://doi.org/10.2475/ajs.292.4.229
——— 1992b, Géologie de la région de Sherbrooke (Estrie): Ministère de L'Énergie et des Resources, Geological Report, ET 90-02, 81 p.
Tremblay, A., and Castonguay, S., 2002, Structural evolution of the Laurentian margin revisited (southern Quebec Appalachians): Implications for the Salinian orogeny and successor basins: Geology, v. 30, n. 1, p. 79–82, https://doi.org/10.1130/0091-7613(2002)030<0079:SEOTLM>2.0.CO;2
Tremblay, A., and Pinet, N., 2005, Diachronous supracrustal extension in an intraplate setting and the origin of the Connecticut Valley–Gaspé and Merrimack troughs, northern Appalachians: Geological Magazine, v. 142, n. 1, p. 7–22, https://doi.org/10.1017/S001675680400038X
——— 2016, Late Neoproterozoic to Permian tectonic evolution of the Quebec Appalachians, Canada: Earth-Science Reviews, v. 160, p. 131–170, https://doi.org/10.1016/j.earscirev.2016.06.015
Tremblay, A., and St-Julien, P., 1990, Structural style and evolution of a segment of the Dunnage Zone from the Quebec Appalachians and its tectonic implications: Geological Society of America Bulletin, v. 102, n. 2, p. 1218–1229, https://doi.org/10.1130/0016-7606(1990)102<1218:SSAEOA>2.3.CO;2
Tremblay, A., Hébert, R., and Bergeron, M., 1989, Le Complexe d'Ascot des Appalaches du sud du Québec: Pétrologie et géochimie: Canadian Journal of Earth Sciences, v. 26, n. 12, p. 2407–2420, https://doi.org/10.1139/e89-206
Tremblay, A., Malo, M., and St-Julien, P., 1995, Dunnage zone Québec, *in* Williams, H., editor, Geology of the Appalachian–Caledonian Orogen in Canada and Greenland: Geological Survey of Canada, Geology of Canada, v. 6, p. 179–197.
Tremblay, A., Ruffet, G., and Castonguay, S., 2000, Acadian metamorphism in the Dunnage zone of southern Québec, northern Appalachians: $^{40}Ar/^{39}Ar$ evidence for collision diachronism: Geological Society of America Bulletin, v. 112, n. 1, p. 136–146, https://doi.org/10.1130/0016-7606(2000)112<136:AMITDZ>2.0.CO;2

Tremblay, A., Ruffet, G., and Bédard, J. H., 2011, Obduction of Tethyan-type ophiolites—A case-study from the Thetford-Mines ophiolitic Complex, Quebec Appalachians, Canada: Lithos, v. 125, n. 1–2, p. 10–26, https://doi.org/10.1016/j.lithos.2011.01.003

Tremblay, A., De Souza, S., Perrot, M., and Theriault, R., 2015, Géologie des Appalaches du Québec, Feuillet Sud-Ouest, regions de Montérégie, Cantons de l'Est, Centre-du-Québec et Chaudière-Appalaches: Ministère des Ressources Naturelles du Québec, MB 2015-11, scale 1:300,000.

Tucker, R. D., and Robinson, P., 1990, Age and setting of the Bronson Hill magmatic arc: A re-evaluation based on U-Pb zircon ages in southern New England: Geological Society of America Bulletin, v. 102, n. 10, p. 1404–1419, https://doi.org/10.1130/0016-7606(1990)102<1404:AASOTB>2.3.CO;2

van Staal, C. R., and Barr, S. M., 2012, Lithospheric architecture and tectonic evolution of the Canadian Appalachians and associated Atlantic margin, *in* Percival, J. A., Cook, F. A., and Clowes, R. M., editors, Tectonic Styles in Canada: The Lithoprobe Perspective: Geological Association of Canada, Special Paper 49, p. 41–95.

van Staal, C., Dewey, J. F., Mac Niocaill, C., and McKerrow, W. S., 1998, The Cambrian-Silurian tectonic evolution of the northern Appalachians and British Caledonides: History of a complex, west and southwest Pacific-type segment of Iapetus: Geological Society, London, Special Publications, v. 143, p. 197–242, https://doi.org/10.1144/GSL.SP.1998.143.01.17

van Staal, C. R., Zagorevski, A., McNicoll, V. J., and Rogers, N., 2014, Time-transgressive Salinic and Acadian orogenesis, magmatism and Old Red Sandstone sedimentation in Newfoundland: Geoscience Canada, v. 41, n. 2, p. 138–164, https://doi.org/10.12789/geocanj.2014.41.031

Walsh, G. J., and Aleinikoff, J. N., 1999, U-Pb zircon age of metafelsite from the Pinney Hollow Formation: Implications for the development of the Vermont Appalachians: American Journal of Science, v. 299, n. 2, p. 157–170, https://doi.org/10.2475/ajs.299.2.157

Wathen, B., Helou, C., Wintsch, R. P., Deasy, R. T., Yi, K., McAleer, R., and Matthews, J., 2015, Deformation spanning 200 million years along the peri-Laurentian (Pumpkin Ground Orthogneiss) Buttress and the East Derby Shear Zone, South-central Connecticut, *in* Gilmore, M. S., and Resor, P. G., editors, Guidebook to field trips in Connecticut and Massachusetts: Middletown, Connecticut, Wesleyan University, p. 153–172.

Whitehead, J., Dunning, G. R., and Spray, J. G., 2000, U-Pb geochronology and origin of granitoid rocks in the Thetford Mines ophiolite, Canadian Appalachians: Geological Society of America Bulletin, v. 112, n. 6, p. 915–928, https://doi.org/10.1130/0016-7606(2000)112<915:UGAOOG>2.0.CO;2

Williams, H., 1979, Appalachian orogen in Canada: Canadian Journal of Earth Sciences, v. 16, n. 3, p. 792–807, https://doi.org/10.1139/e79-070

Williams, H., and St-Julien, P., 1982, The Baie Verte-Brompton line: Early Paleozoic continent-ocean interface in the Canadian Appalachians: Major structural zones and faults of the northern Appalachians: Geological Association of Canada Special Paper, v. 24, p. 177–208.

Yin, Q. Z., Wimpenny, J., Tollstrup, D. L., Mange, M., Dewey, J. F., Zhou, Q., Li, X.-H., Wu, F.-Y., Li, Q.-L., Liu,Y., and Tang, G.-Q., 2012, Crustal evolution of the South Mayo Trough, western Ireland, based on U–Pb ages and Hf–O isotopes in detrital zircons: Journal of the Geological Society, v. 169, n. 6, p. 681–689, https://doi.org/10.1144/jgs2011-164